Evaluation and Optimization of Recent Analytical Approaches for In-Vivo Measurements with Near-Infrared Spectroscopy

vorgelegt von
Diplom-Ingenieur
Jan Mehnert
aus Berlin

von der Fakultät IV - Elektrotechnik und Informatik
der Technischen Universität Berlin
zur Erlangung des akademischen Grades

Doktor der Naturwissenschaften
- Dr. rer. nat. -

genehmigte Dissertation

Promotionsausschuss:

Vorsitzender:	Prof. Dr. B. Blankertz
Berichter:	Prof. Dr. K.-R. Müller
Berichter:	Prof. Dr. A. Villringer
Berichter:	Dr. J. Steinbrink

Tag der wissenschaftlichen Aussprache: 3.12.2012

Berlin 2012
D 83

Acknowledgment

This work would not have been possible without the infinite support from my friends, family and colleagues. My first and warmest thanks go to Tine Maikowski who stayed by my side all these long years of up and downs and significantly influenced this dissertation. I also have to thank my brother Hannes for his beautiful nature and long proof-reading periods. And of course I have to mentioned my parents Annette and Michael who supported me throughout my whole live with never ending calmness and energy. Further thanks to my grandparents Gottfried and Anneliese!

I am really happy that the supervisors of this thesis are also my respected mentors. Jens Steinbrink, Arno Villringer and Klaus-Robert Müller supported me with fruitful discussion about my work (and other stuff) and opened the possibility to conduct my experiments whatever they where about and wherever I wanted. Especially their openness to new collaborations impressed me.

Special thanks go to Christoph Schmitz and Jens Steinbrink (again) who introduced me to Near-Infrared Spectroscopy and wake my interest to learn more and more about its advantages and disadvantage and how to overcome the limitations. They also frame the cozy and open atmosphere of the optical group (and its extended surrounding) at the Charité Berlin where I could work most of my time. Nothing would be done without the motivation given by Hellmuth Obrig, Stephan Paul Koch, Riad Bourayou, Isabell Wartenburger, Silke Telkemeyer, Sonja Rossi, Thomas Betz, Arne Ewald, Sabrina Thiel, Till Nierhaus, Florian Siebörger, Franziska Preusse, Susanne Holtze and Birol Taskin. Special thanks to Christina Habermehl, Sophie Piper and Arne Krüger who motivated me during the last days in Berlin and to Angelika Borkowksi who is always a great help!

This thesis is not my work alone but numerous people were engaged in all the experiments (whether the results were significant or not, we learned a lot). I will try a complete list slightly sorted in time but it is hard to not forget anybody.

So I am sorry for those who do not appear. Be forgiving! My earliest work rely on a collaboration with Susanne Neufang who currently works in Munich (but soon in Würzburg). It was a hard time with all these kids (and parents) but I really enjoyed to work with you! My next step lead me to Arno Villringer's lab at the Max Planck Institute in Leipzig. There were so many interesting people and stimulating research areas, not only in Arno's but also in the other departments. It is hard work to mention everybody. Daniel Margulies had a big influence on me by introducing me to resting-state analysis. Karsten Müller and Harald Möller helped me with my simultaneous NIRS-fMRI studies. I had a nice time in Prague with Śtefan Holiga during our visit of Robert Jech. Hadas Okon-Singer gave a big boost in my interest in blood pressure. Tobias Grossmann allowed me to compare several NIRS systems. Stefan Kiebel explained me Dynamic Causal Modeling. Marco Taubert, Derek Ott, Birgit Mittag and Ramona Menger made my life at the Max Planck nice and comfortable! And it was very helpful to discuss NIRS with Matthias Schroeter.

I enjoyed the fruitful work in the Bernstein Focus Neurotechnology Berlin network which connected me deeply with Klaus-Robert Müller's lab at the Institute of Technology in Berlin. With Siamac Fazli we made very productive work on multimodal BCI. New plans emerged with Sven Dähne, Matthias Treder and Stefan Haufe. Benjamin Blankertz and Gabriel Curio have my full respect. It was nice to meet Vadim Nikulin and Tommaso Fedele and work on strange oscillations! One day we will be able to explain them! Mirror illusion was performed with Maddalena Brunetti an Christian Dohle. During the research with Carsten Bogler from John-Dylan Haynes' lab he became a close friend of mine.

My stay in Brazil in 2011 connected me with Roberto Covolan and Fernando Cendes where I learned a lot about epilepsy. Also Louis Lemieux could teach me a lot about this interesting illness. Thank you for my nice time in Brazil, it was just too short! Andreas Wunder helped me to get in touch with the interesting field of near-infrared fluorescence imaging. Our cooperation with the physics department of Free University, i.e. with Cristina Stanca-Kaposta and Matthieu Lalanne, helped me to understand the limitations of this technique. Now I have to thank the great people in Korea where the last parts of my thesis were written: Seong-Whan Lee who made it possible for us to come and his lovely and interested students. I am

looking forward to numerous nice studies!

Least but not last all my dearest friends make my life so wonderful: Oliver and Jochen, Melanie, Moritz and Gali (congrats for your second adorable child!), Martin and Vaneska (love to be in your full house!), Christian Schneider and Dagmar (see you soon!), Daniel (welcome in Berlin!), Mischa, Manu, Stefan Felder, Alexis, Daphne and Christos, Anna Salami, Michalis, Aicha, Benni und Nadja, Matthieu, Mirjam, Helene, Jeehye and Justin, and Agata!

Zusammenfassung

Nah-Infrarot Spektroskopie (NIRS) ist eine nicht-invasive Technik im Bereich der neurowissenschaftlichen Bildgebung um hämodynamische Effekte zu messen, die neuronalen Ereignissen folgen. NIRS verwendet nah-infrarotes Licht um über den Farbunterschied von oxygeniertem und deoxygeniertem Hämoglobin die Konzentrationsdynamiken derselben zu ermitteln. Allerdings existieren Einschränkung für diese Technik: NIRS hat eine geringe Eindringtiefe in das Gewebe und eine hohe Empfindlichkeit gegenüber Artefakten, die von ruckartigen Bewegung oder kardiovaskulären Oszillationen stammen. Des Weiteren ist die hämodynamische Antwort relativ langsam und überlappt sich bei schnellen Stimulationen. In der vorliegenden Arbeit stelle ich drei Analysekonzepte vor, die versuchen artefaktbedingte Defizite von NIRS überwinden. Diese sind: Allgemeines Lineare Model (GLM), maschinelles Lernen (ML) und funktionelle Konnektivität im Ruhezustand (RS-FC). Für die GLM-Analyse wird ein Model der erwarteten hämodynamischen Antwort generiert und mit gemessenen Daten verglichen. Ich zeige die Machbarkeit einer solchen Analyse für NIRS anhand einer Studie über Spiegelillusionen und einer Studie zur Entwicklung von Inhibition. In zuletzt genannter Studie werden schnelle Stimuluspräsentationen verwendet, weswegen die hämodynamischen Antworten überlappen. Diese können jedoch mit Hilfe des GLM entfaltet werden. Eine ähnliche Analyse wurde durchgeführt um den gemittelten und entfalteten Verlauf der hämodynamischen Antwort zu bestimmen. Beim maschinellen Lernen wird versucht die maximale Trennbarkeit zwischen zwei Konditionen mit Hilfe der gemessenen Daten zu bestimmen. ML-Analyse macht es zudem möglich Daten in Echtzeit zu interpretieren, wie hier am Beispiel von Gehirn-Computer Schnittstellen gezeigt wird. Eine weitere Anwendungsmöglichkeit von ML-Analysen ist die kontinuierliche Vorhersage des Aufmerksamkeitsstadiums eines Menschen. RS-FC hat das Ziel funktionelle, neuronale Netzwerke aus Ruhedaten zu extrahieren. Dies ist insbesondere sinnvoll um Menschen zu untersuchen die Konzentrationsschwie-

rigkeiten haben, wie zum Beispiel Kinder oder Patienten mit schweren Schädigungen. Die RS-FC-Analyse korreliert langsame, spontane Oszillationen zwischen Bereichen des Gehirns die funktionelle Netzwerke bilden. In meiner Arbeit werden Netzwerke vorgestellt, die über weite Distanzen miteinander verbunden sind. Dies ist durch die Abdeckung des gesamten Kopfes mit Sensoren des NIRS möglich. Des Weiteren wird die Entwicklung von funktionellen Netzwerken von Kindern zu Erwachsenen dargestellt. Die RS-FC-Anaylse von NIRS-Daten wird zudem anhand von simultanen Messungen mit dem fMRT überprüft für welches RS-FC eigentlich entwickelt wurde. Alle drei vorgestellten Analysewerkzeuge können für NIRS verwendet werden. Jede Routine hat dabei spezifischen Anwendungsmöglichkeiten in den Neurowissenschaften. Daher öffnen sich viele neue Forschungsgebiete in denen es sinnvoll ist mit NIRS Daten zu erheben.

Abstract

Near-Infrared Spectroscopy (NIRS) is a non-invasive neuroimaging technology. It measures hemodynamic responses after local neuronal activity with near-infrared light. NIRS depends on the different colors of oxygenated and deoxygenated hemoglobin and measures their change of concentration over time. This technique suffers from several limitations as there is its low depth penetration depth and its sensibility to movement and cardio-vascular artifacts. Furthermore, the hemodynamic response is relative slow and tends to overlap in fast experimental design. In this work I present three recent analytical tools to overcome artifact related shortcomings of NIRS. The analyzing tools introduced here are General Linear Model analysis (GLM), Machine Learning tools (ML) and Resting-State Functional Connectivity analysis (RS-FC). For GLM analysis one creates a model of the expected hemodynamic response to stimuli and compares it to the actual measured data. I show the feasibility of GLM analysis for NIRS data in an experiment on mirror illusion and a developmental study on inhibition. The later contains overlapping hemodynamics which can be deconvolved by the GLM analysis. Further work on GLM-like approaches is done to yield a deconvolution of the average hemodynamic responses. ML tools maximize the separability between experimental conditions in the data and are capable of real-time data analysis. I show an example where we use ML techniques for Brain-Computer Interfaces. A second study shows the ability of ML routines to continuously predict the subject's attentional state. RS-FC aims to analyze functional networks between brain areas using resting-state data. This is useful for subjects that are not able to concentrate, like severely ill patients or young children. RS-FC analyzes slow, spontaneous oscillations which are correlated within areas forming a functional network. Here I present functional networks derived by RS-FC analysis in an experiment where the whole-head of the subjects was covered by NIRS sensors allowing also the estimation of long-distance connection between parietal and frontal brain areas. Further results are

presented for developmental effects within resting-state networks. This approach is also validated against the *golden standard* of fMRI where RS-FC analysis stems from. All three introduced analyzing techniques are feasible for NIRS data and have their specific applications in neuroscientific research which opens new fields of research for using NIRS.

Vita and Publications

Vita

1980	born in Herdecke near Dortmund, Germany
2000	*Abitur* (A-levels) in Berlin, Germany
2000-2003	Student of Environmental Engeneering at Berlin Institute of Technology, Germany
2003-2005	Student of Philosophy and Political Science at RWTH Aachen, Germany
2005-2007	Student of Environmental Engeneering at Berlin Institute of Technology, Germany
2007	Degree as *Diplom Ingenieur* at Berlin Institute of Technology, Germany
2007-2008	Assistant scientist at Department of Neurology, Charité University Medicine, Berlin, Germany
2008-2011	PhD student at Department of Neurology, Max Planck Institute for Human Cognitive and Brain Sciences, Leipzig, Germany
2011	Guest scientist at Grupo de Neurofísica, Universidade Estadual de Campinas, São Paulo, Brazil
2011-2012	PhD student at Department of Neurology, Charité University Medicine, Berlin, Germany
since 2012	Guest scientist at the Department of Brain and Cognitive Engineering, Korea University, Seoul, Republic of Korea

Prizes and Scholarships

2008 3-year PhD scholarship from Max Planck Society
2010 Student Travel Award from Organization of Human Brain Mapping
2011 Scholarship from Berlin Focus Neurotechnology to start a cooperation with Universidade Estadual de Campinas, São Paulo, Brazil

Journal Articles

Mehnert, J., Habermehl, C., Köhler, S., Steinbrink, J., and Villringer, A. (2012): Principles of Near-Infrared Spectroscopy of the human brain - a video lecture. In preparation.

Mehnert, J., Okon-Singer, H., and Villringer, A. (2012): Modeling event-related blood pressure responses. In preparation.

Nikulin, V.*, Fedele, F.*, Mehnert, J., Noack, C., Lipp, A., Steinbrink, J., and Curio, G. (2012): Monochromatic ultra slow oscillations in the human electroencephalogram. In preparation.

Okon-Singer, H., Mehnert, J., Hoyer, J., Hellrung, L., Dukart, J., and Villringer, A. (2012): Attention modulates the neural control of blood pressure emotional reactions: simultaneous fMRI and continuous blood pressure study. In preparation.

Bogler, C.*, Mehnert, J.*, Steinbrink, J., and Haynes J.-D. (2012): Decoding vigilance with NIRS. In preparation.

Mehnert, J.*, Brunetti, M.*, Steinbrink, J., Dohle, C. (2012): Effect of the mirror illusion on M1 and the precuneus measured with near-infrared spectroscopy. In preparation.

Piper, S.*, Betz, T.*, Gosmann, J., Mehnert, J., Ebert, B., and Steinbrink, J. (2012): Sounding the depth of fluorescent targets for fluorescence reflectance imaging. Journal of Biomedical Optics, submitted.

Mehnert, J., Akhrif, A., Telkemeyer, S., Rossi, S., Schmitz, C., Steinbrink, J., Wartenburger, I., Obrig, H., and Neufang, S. (2012): Developmental changes in function and coherence during response inhibition in the early childhood brain. Brain & Development, submitted.

Mehnert, J.*, Piper, S.*, Habermehl, C., Wunder, A., Schmitz, C.H., Obrig, H., and Steinbrink, J. (2012): Whole body fluorescence imaging in humans. Optics Express, submitted.

Dähne, S., Bießmann, F., Meinecke, F.C., Mehnert, J., Fazli, S., and Müller, K.-R. (2012): Integration of Multivariate Data Streams with Bandpower Signals. IEEE Transactions on Multimedia, submitted.

Stemmer, N., Mehnert, J., Steinbrink, J., and Wunder, A. (2012): Noninvasive fluorescence imaging in animal models of stroke. Current Medicinal Chemistry, accepted.

Fazli, S.*, Mehnert, J.*, Curio, G., Villringer, A., Müller, K.-R., Steinbrink, J., and Blankertz, B. (2012): Enhanced performance by a Hybrid NIRS-EEG Brain Computer Interface. NeuroImage, volume 59, issue 1, pages 519:529.

Habermehl, C., Holtze, S., Steinbrink, J., Koch, S.P., Obrig, H., Mehnert, J., and Schmitz, C.H. (2012): Somatosensory activation of two fingers can be discriminated with ultrahigh-density diffuse optical tomography. NeuroImage, Volume 59(4), pages 3201:11

Koch, S.P., Habermehl, C., Mehnert, J., Schmitz, C.H., Holtze, S., Villringer, A., Steinbrink, J., and Obrig, H. (2010): High-resolution optical functional mapping of the human somatosensory cortex. Frontiers in Neuroenergetics, Volume 2, page 12ff.

**These authors contributed equally to the work.*

Conference Abstracts

Fazli, S., Mehnert, J., Steinbrink, J., and Blankertz, B. (2012): Using NIRS as a predictor for EEG-based BCI performance. 34th Annual International IEEE EMBS Conference, San Diego, USA

Okon-Singer, H., Mehnert, J., Hoyer, J., Hellrung, L., Dukart, J., and Villringer, A. (2012): Behavioral, neural and cardiovascular responses to emotional stimuli: simultaneous recording of fMRI and continuous blood pressure reactions. Annual Meeting of the European Society for Cognitive and Affective Neuroscience, Marseille, France.

Krüger, A., Koch, S.P., Mehnert, J., Habermehl, C., Piper, S., Steinbrink, J., Obrig, H., and Schmitz, C.H. (2012): Imaging of Motor Activity in Freely Moving Subjects Using a Wearable NIRS Imaging System. Biomedical Optics (Biomed), Miami, USA.

Habermehl, C., Schmitz, C.H., Koch, S.P., Mehnert, J., and Steinbrink, J. (2012): Depth sensitivity in multi-distance NIRS measurements in humans. Biomedical Optics (Biomed), Miami, USA.

Habermehl, C., Schmitz, C., Koch, S.P., Mehnert, J., and Steinbrink, J. (2012): Investigating hemodynamics in scalp and brain using high-resolution diffuse optical tomography in humans. Biomedical Optics (Biomed), Miami, USA.

Barbour, R.L., Mehnert, J., Xu, Y., Graber, H.L., Nichols, J.D., Ossadtchi, A., and Pflieger, M.E. (2011): Software for Integrated Analysis of NIRS-EEG Data. 7th NIH Inter-Institute Workshop on Optical Diagnostic and Biophotonic Methods from Bench to Bedside, National Institutes of Health, Bethesda, Maryland, USA.

Fazli, S., Mehnert, J., Villringer, A., Steinbrink, J., Curio, G., and Blankertz, B. (2010): Functional near-infrared spectroscopy supports Brain Computer Interface performance in EEG. Annual Meeting of the Organization of Human Brain Mapping, Barcelona, Spain.

Mehnert, J., Preusse, F., Margulies, D.S., Villringer, A., van der Meer, E., and Wartenburger, I. (2010): Intelligence modulates deactivation of the default-mode network. Annual Meeting of the Organization of Human Brain Mapping, Barcelona, Spain.

Mehnert, J., Schmitz, C., Möller, H., Villringer, A., Obrig, H., and Müller, K. (2010): Functional connectivity analysis is reliable in whole-head near-infrared Spectroscopy. Annual Meeting of the Organization of Human Brain Mapping, Barcelona, Spain.

Mehnert, J., Schmitz, C., Möller, H.E., Obrig, H., and Müller, K. (2010): Simultaneous Optical Tomography (OT) and fMRI with and without Task Activation. Annual Meeting of the International Society for Magnetic Resonance in Medicine, Stockholm, Sweden.

Fazli, S., Mehnert, J., Steinbrink, J., Curio, G., and Blankertz, B. (2010): NIRS signals predict SMR-based performance in EEG. 4th International BCI meeting, Asilomar, USA.

Fazli, S., Mehnert, J., Steinbrink, J., Curio, G., and Blankertz, B. (2010): Combined NIRS-EEG measurement enhances Brain-Computer Interface performance. Integrating Brain-Computer Interfaces with Conventional Assistive Technology - Tools for Brain-Computer Interfaces (TOBI), Graz, Austria.

Mehnert, J., Schmitz, C.H., Möller, H.E., Obrig, H., and Müller, K. (2009): Simultaneous NIRS-fMRI measurements proves resting state analysis for optical data. Optical Imaging of Brain Function, Heraeus Foundation, Bad Honnef, Germany.

Mehnert, J., Holtze, S., Koch, S.P., Habermehl, C., Schmitz, C.H., Villringer, A., and Steinbrink, J. (2009): Optical tomographic mapping of the human somatosensory cortex. Inter-Institute Workshop on Optical Diagnostic and Biophotonic Methods from Bench to Bedside, National Institutes of Health, Bethesda, Maryland, USA.

Fazli, S., Mehnert, J., Rausch, M., Villringer, A., Curio, G., Müller, K.-R., Steinbrink, J., and Blankertz, B. (2009): Combined NIRS-EEG measurement enhances Brain Computer Interface performance. Berlin Brain-Computer Interface Workshop, Berlin Institute of Technology, Germany.

Mehnert, J., Margulies, D.S., Schmitz, C., Steinbrink, J., Obrig, H., Villringer, A. (2009): Resting-state networks revealed with whole-head Near-Infrared Spectroscopy. Annual Meeting of the Organization of Human Brain Mapping, San Francisco, USA.

Mehnert, J., Kozlowski, B., Telkemeyer, S., Schmitz, C.H., Steinbrink, J., Obrig, H., and Wartenburger, I. (2009): Differential processing of sounds with varying spectral and temporal complexity in bilateral temporal cortex. Annual Meeting of the Organization of Human Brain Mapping, San Francisco, USA.

Mehnert, J., and Pesch, M. (2007): Locating the mixing layer: algorithms to identify the mixing layer height using LIDAR signals. SPIE Remote Sensing Conference, Florence, Italy.

Talks

Whole body fluorescence imaging in humans. Biomedical Optics (Biomed) Conference, Miami, USA, in May 2012.

Enhanced performance by a hybrid NIRS-EEG Brain Computer Interface. Universidade Estadual de Campinas, Sao Paulo, Brazil, in May 2011.

Current and future clinical applications of Near-Infrared Spectroscopy. Universidade Estadual de Campinas, Sao Paulo, Brazil, in May 2011.

Functional connectivity analysis is reliable in whole-head Near-Infrared Spectroscopy. Annual Meeting of the Organization of Human Brain Mapping in Barcelona, Spain, in July 2010.

Non-invasive Near-Infrared Spectroscopy - method, possibilities and current enhancement. Child Study Center, New York University, USA, in September 2009.

Locating the mixing layer: algorithms to identify the mixing layer height using LIDAR signals. SPIE Remote Sensing Conference, Florence, Italy, in September 2007.

Contents

1. Introduction

The development of functional magnetic resonance imaging (fMRI) in the 1990s by Ogawa and colleagues [Ogawa et al., 1990] led to a boom in in the non-invasive branch of neurosciences. The underlying effect of the fMRI contrast, i.e. the focal changes in perfusion following neuronal activity in brain regions, had already been discovered in the 19th century by Roy and Sherrington [Roy and Sherrington, 1890]. FMRI measures changes in local magnetic fields caused by concentration changes of the oxygen-transport molecule, hemoglobin. Because of its non-invasive nature and rather high spatial resolution (around 1 mm^3), fMRI facilitated new insights into the brain's neuro-vascular dynamics and allowed the field of functional brain imaging to emerge, affording the study of diverse areas encompassing cognitive processes as well as neurological and psychological diseases. For all its advantages, fMRI still suffers from some limitations: 1) the usage of strong magnetic fields, whose biological effects are not fully understood and which poses limits on the possible target populations, 2) high costs, large size, and technical complexity, 3) the fixation of the subjects' head inside a confined space, 4) its stationary nature, and 5) the subjects exposure to a high level of acoustic noise during measurements. These limitations prevent the usage of fMRI measurements for certain subjects, such as very young children, patients with anxiety or attention deficit disorders, and patients with implanted electronic devices. Furthermore, fMRI studies are often not feasible for bedside monitoring of patients and applications outside of the clinical environment like Brain-Computer Interfacing, and not affordable for the monitoring of therapeutic intervention outside of big hospitals. Some of these limitations can be overcome by Near-Infrared Spectroscopy. While fMRI is based on the magnetic properties of deoxygenated hemoglobin, NIRS depends on its optical properties: The optical extinction coefficient has large spectral differences for deoxygenated and oxygenated hemoglobin.

Using light in the near-infrared spectrum to indirectly determine neuronal activ-

ity leads to several advantages over strong magnetic fields: 1) NIRS is completely harmless and can be used for any subject of any age without any cumulative adverse effects. 2) The head has not to be fixated and the subjects are able to move around as the sensors are fixated in a cap. 3) Due to recent developments of low-cost optoelectronic sensors and sources, NIRS is inexpensive. 4) The technology readily lends itself to miniaturization, making it feasible for applications outside of the laboratories and suitable for long-term bedside measurement. 5) Lastly, it does not produce any sound or other artifacts disturbing the subjects' concentration during the measurements. Despite these advantages, which make NIRS a promising tool in neuroimaging, the method also has shortcomings that limit its scope of applicability. 1) Optical radiation is severely attenuated in tissue, which limits the penetration depth and allows NIRS study only of the most superficial brain regions (cortical activation). 2) NIRS is very sensitive to physiological noise stemming from extra-cerebral tissue. 3) Because of light-scattering, the resolution of NIRS imaging is fairly low (∼10-30 mm). Whereas the first of these major drawbacks, the penetration limits of NIRS is dictated by physical limits and it cannot be expected to be improved in a principle way, the other two shortcomings can be enhanced by more sophisticated instrumental designs and analysis methods. Some studies have already shown that the spatial resolution of NIRS can be enhanced up to a sub-centimeter range [Zeff et al., 2007, Koch et al., 2010, Habermehl et al., 2012]. The present work focuses on improving the third - the most severe limitation: The understanding of extra-cerebral noise, its sources, impact on the signal, and possible ways of removing, correcting, or otherwise ameliorating its effects.

1.1. Scientific Proposal

The purpose of this work twofold: 1) the evaluation and optimization of analysis tools for NIRS data and 2) the usage of these tools to enhance the current applications of NIRS. In this dissertation the term *analyzing tools* is used to describe mathematical approaches to analyze NIRS data. Which analyzing strategy is useful depends on the current issue for what NIRS is applied. Each analyzing tool has advantages and disadvantages over the other. Nevertheless, all of them have to deal with the high extra-cerebral noise content in NIRS data, which is magnitudes

higher then the actual signal of interest (i.e. the hemodynamic response to neuronal activation). By developing and applying improved analysis tools the present thesis aims to promote NIRS as a new neuroimaging tool for clinical applications outside of the laboratory previously not amenable to the advantages of NIRS over fMRI. To this end, we first conducted studies dedicated to improve the reliability and signal quality of the used NIRS instruments. Following this, we evaluated three different signal analysis strategies addressing challenges in different types of studies:

- The general linear model (GLM) is the analytical basis for most fMRI results, which we here applied to NIRS. GLM can be applied, when the neuroscientist defines his hypothetical biological model of how the data should be and compares this with the actual data to gain statistical significant results. This analyzing tool is capable of separating the hemodynamic response from the extra-cerebral noise and analyzing overlapping hemodynamic responses, which frequently occurs due to the sluggish behavior of the response (with peaks around 5-30 s, depending on the length of the stimulus).

- Machine Learning (ML) summarizes self-learning algorithms which adapt to subject specific data. Multiple applications for NIRS outside the laboratory like neuronal-guided therapy, Brain Computer Interfaces (e.g. to control a robotic arm), monitoring of subjects attentional state or neuronal-assisted learning demand for single trial analysis in real-time. ML algorithms are capable of single trial and real-time analysis, regardless of the high noise content in the NIRS data by combining information of several measurement channels. Thereby, ML is necessary to exploit the mobility of NIRS instrumentations in natural environments. In this work we evaluate machine learning algorithm for NIRS.

- Functional Connectivity Analysis (FC) overcomes the dependency on tasks, which is necessary for bedside imaging and useful for studies with children. This method is based on simultaneous oscillations in the brains' networks and allows to analyze their connectivity. FC concentrates on specific frequencies in the data and, thereby, addresses the issue of noise.

The second aim of this work is to apply the above mentioned analysis tools in the fields where NIRS can be a useful device. This means 1) in clinical setups, 2) for developmental studies, 3) by monitoring of attentional states and diseases, and 3) in brain-computer interfaces. We will exemplary study specific questions in each of these research areas to show the future possibilities for the application of near-infrared spectroscopy.

Thus, we address the following hypotheses:

- NIRS data analysis is feasible with general linear model approaches, machine learning tools and functional connectivity analysis.
- NIRS can be used in clinical setups, for development studies, to monitor attentional states, and for brain-computer interfaces.

1.2. Outline of the Thesis

The challenge of disturbing extra-cerebral signal contamination is explained by introducing the basic principles of NIRS, which is done in **Chapter 2**.

Chapters 3, 4 and 5 contain the core methodological contributions of this thesis. Each chapter describes one analyzing tool and is structured as follows: First, the theoretical background is given, then the data analysis and experimental results are discussed, and lastly the obtained results are discussed in the context of the applied analysis tool. To this end, a multitude of physiological experiments were conducted, which are introduced along with the analyzing tools used.

Chapter 3 sheds light on use of general linear model, probably the most common approach to NIRS analysis. First the biological foundations of the hemodynamic response is discussed, which is the basis of the physiological models used in GLM as introduced by Friston in 1994 [Friston et al., 1994] for fMRI analysis. We outline the underlying math and describe the performed experiments and our GLM NIRS data analysis. GLM is then applied to an experiment on mirror illusion, which demonstrates the application of GLM for monitoring therapeutic process in situations where fMRI is not available, specifically in mirror therapy to recover traumatized limbs after e.g. a stroke. The second experiment evaluates the capacity of GLM to recover overlapping hemodynamic responses, a common

problem in NIRS experiments because of the sluggish hemodynamic response function, which peaks only after around 5 seconds following neuronal activation. This advantage together with the applicability of NIRS for developmental studies was used to research the neuronal background of inhibition in an experiment comparing adults and children of the age between 3 and 6 years. A fourth experiment uses a GLM-like approach, which does not rely on a model of the hemodynamic response: Finite Impulse Response (FIR). Here, we analyzed data gained during an attentive task and can show the predictive information content of the shape of the hemodynamic response for the reaction time of the subjects.

The application of machine learning tools is presented in **Chapter 4**. These algorithms are used for Brain-Computer Interfaces (BCI) paving the path for experiments outside of the laboratories. We start with a description of the theoretical background followed by an experiment testing the application of NIRS for BCIs. Here we performed an experiment using the imagination of hand movements to control a visual feedback analyzed with machine learning tools. This study was performed simultaneously with electroencephalography (EEG), most often used for non-invasive BCIs, allowing direct comparison of results from instruments and, furthermore, the evaluation of a multimodal approach using information of both instruments for the visual feedback.

In **Chapter 5** we present functional connectivity analyses by means of experiments on the connectivity of several regions in the brain during the subjects' rest. Before going into the details of the actual experiments we introduce several mathematical algorithms for the analysis of NIRS data. Resting-state networks are signified by oscillation pattern in low frequencies (<0.1 Hz) and studies with fMRI show that their analysis can lead to fruitful insights into numerous diseases. Here, we were able to show that NIRS is also feasible with functional connectivity analysis. The possibility of using NIRS to detect resting-state networks raises hope for future applications like bedside monitoring in the clinics. In a first experiment we used sensors on the whole head to gain insights into larger networks. Positive results from this experiment inspired us to analyze differences in the development from 3-6 years olds to adults by using data from the developmental study already presented in Chapter 3. We furthermore performed simultaneous measurements of NIRS and fMRI in the somato-motoric regions of the brain to evaluate the

reliability of NIRS in finding resting-state networks.

This work concludes with a discussion on the used analyses and an outlook of their future application areas in **Chapter 6**.

2. Principles of Near-Infrared Spectroscopy

This chapter describes the basic principles of Near-Infrared Spectroscopy (NIRS) in the human brain. In Section 2.1 we first introduce how neuronal activity through neurovascular coupling leads to hemodynamic responses. Following this, we describe the propagation of near infrared light through the brain's tissue (Section 2.2) and the formation of the optical hemodynamic contrast. Finally, we discuss the time-frequency characteristics of NIRS signals in Section 2.3.

After describing the characteristics of the NIRS signal, we elaborate on the preprocessing of the data in Section 2.4. An example of a simple analysis by averaging of event-related, focal hemodynamical changes is shown in Section 2.5.

NIRS, as a functional imaging method, by itself is not capable of measuring anatomical brain structures. We will therefore include a short discussion on proper methods of statistical mapping functional signals onto anatomical brain models in Section 2.6.

This is followed by a section describing the instruments used in this dissertation in Section 2.7. One of the advantages of NIRS is its artifact-free use in concurrent measurements with several electro physiological (EEG) and peripheral measurements, which will be introduced in Section 2.8. This chapter concludes with a discussion about the advantages and the limitations of NIRS for neuroscientific research and application (Section 2.9).

2.1. From Neuronal Activity to the Hemodynamic Response

Information transport in the brain is dominated by electric current exchanges of neurons and neuronal populations. Neuroscientific research, therefore, focuses on

the understanding how and why changes in the environment leads to changes in the electric activity. Usually, one uses controlled paradigms or stimuli to enforce neuronal activity changes which then are measured to support or contradict a hypothesis. Because direct measures of neuronal activation require invasive measures, one often has to resort to indirect measures of the electric or magnetic changes caused by brain activity (e.g. electroencephalography and magnetoencephalography). Relatively early, in 1890, Roy [Roy and Sherrington, 1890] detected that the energy demand of neuronal activity also leads to changes in the local blood supply (*hemodynamics*). The link between neuronal activity and changes in the vascular system is called *neurovascular coupling*, which opened the research field on hemodynamics. FMRI and NIRS use local blood flow changes as an indirect measure of neuronal activity.

Figure 2.1 illustrates the example of a visual stimulus (e.g., a flickering *checkerboard* pattern) leading to neuronal activity followed by a response of the vascular system, which causes local changes in the cerebral blood flow and volume. This results in concentration changes of the blood-borne cells and molecules in the capillaries surrounding the neurons. Non-invasive measures of concentration changes in the microvascular system are feasible by either functional magnetic resonance imaging (fMRI) or NIRS. Both methods are sensitive to focal concentration changes of the reduced and the oxygenated form of the oxygen transport molecule hemoglobin, i.e., HbO (oxygenated hemoglobin) and HbR (deoxygenated hemoglobin), respectively. While fMRI depends mostly on the magnetic dipole moment of HbR, NIRS measures the shift in the near-infrared absorption spectrum of blood (i.e., its color) depending on the relative amount of HbO and HbR.

2.2. Photon Transport in the Human Brain

To detect hemodynamic changes with NIRS, a deeper understanding of how light spreads in the human brain is needed as well as the mathematical background of NIRS measurements. Both is presented in the following subsections.

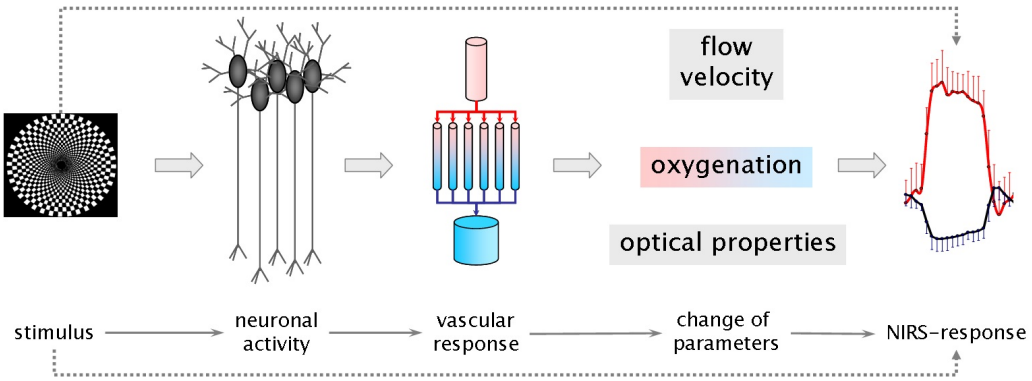

Figure 2.1.: Neuronal activity leads to changes in the tissue's optical properties

2.2.1. Optical Window of Near-Infrared Light in Biological Tissue

NIRS is based on the differential absorption spectra of the two chromophores of hemoglobin, shown in Figure 2.2, as a function of wavelength of the illuminating light.

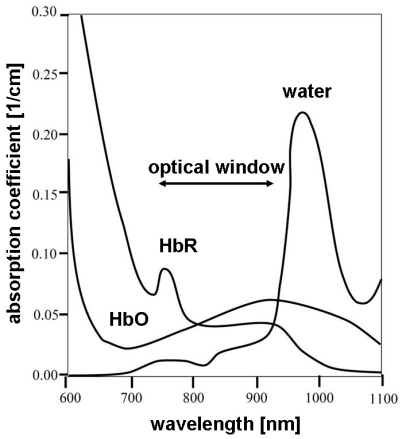

Figure 2.2.: Absorption coefficients of water, HbO and HbR in part of the visible and near-infrared spectrum

Near-infrared radiation in the 700-900 nm region is optimally suited for probing dynamic changes of the hemoglobin concentration, because in this region, hemoglobin is the main absorber, and light penetration into biological tissue is maximal.

Outside of the so-called *optical window*, light show either high absorption for

water (in higher wavelengths) or high absorption for hemoglobin. Both sides of this optical window prevent the light from penetrating the head deep enough to reach the cortex [Cope et al., 1988] because most photons will be absorbed in the first millimeters. Commercially available NIRS instruments use two or more distinct wavelengths for tissue illumination, to allow the separation of the concentration changes of HbO and HbR (further explained in Section 2.2.3).

2.2.2. Non-invasive Measures of Near-Infrared Spectroscopy

The measurement of intra-cranial changes in hemoglobin concentration requires the placement of a light source and a detector on the subject's head at a separation distance of about 2-4 cm. The light travels into the brain undergoing scattering and absorption by the tissue. A small fraction of photons escapes the head and reaches the detector. These photons have a path whose probability can be described as a *banana-shaped* volume in which the measurement of hemoglobin concentration changes takes place as illustrated in Figure 2.3.

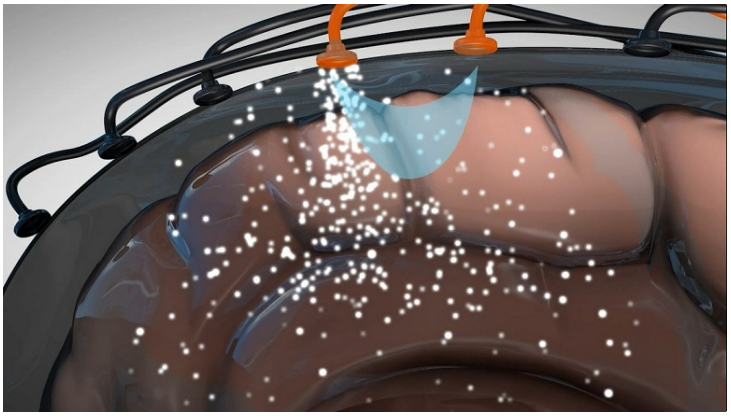

Figure 2.3.: Photon propagation in the brain. Photons (white dots) propagate from the source to the detector with a *banana-shaped* probability (light blue).

2.2.3. Absorption and Scattering of Light in Tissue

Both wavelengths used by the NIRS instrumentation are absorbed by either of the two chromophores (see Figure 2.2) to different degrees, and their different

contributions may be separated using an analytical approach which estimates the concentration changes of HbO from HbR: the *modified Beer-Lambert law*. It is based on the simple law formulated by Bouguer in 1729 which states that the amount of photons transmitted through a solution of dye in an aqueous medium is logarithmical dependent on the concentration of the dye and the length d of the penetrated medium (see Figure 2.4 A). The attenuation A of the light is defined

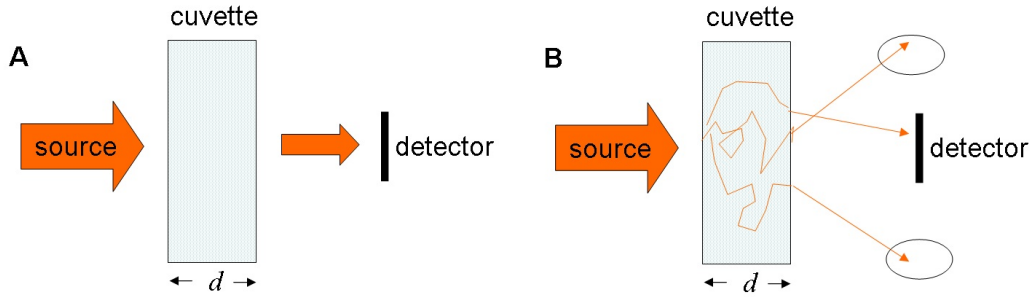

Figure 2.4.: A) Schema of photons traveling through a cuvette of dye soluted in water. B) Schema of photons traveling through a cuvette with scattering media.

as follows:

$$A = -log(I_{det}/I_{emit})d \tag{2.1}$$

where I_{emit} is the light intensity emitted by the source, and I_{det} is the transmitted intensity measured by the detector. This relation, usually termed the Beer-Lambert law, can also be formulated in terms of the absorption coefficient μ_a

$$A = -\mu_a d \tag{2.2}$$

In general, $\mu_a(\lambda)$ is a medium-specific, wavelength-dependent quantity. The combined wavelength dependent absorption coefficient of a mixture of chromophores may be stated as:

$$\mu_a(\lambda) = \sum_i e_i(\lambda)c_i \tag{2.3}$$

where λ is a specific wavelength and $e_i(\lambda)$ signifies the wavelength dependent extinction coefficients of each chromophore i interacting with the light, and c_i their respective concentrations.

In turbid media, such as tissue, matters get more complicated because the photons are not only absorbed but also scattered (see Figure 2.4 B). Therefore, one can no longer regard straight light paths. The mean free path length L takes this into account and describes the most probable path of photons reaching the detector, as defined by Beer in 1852 [Beer, 1852].

In 1998 Cope and Delpy [Delpy et al., 1988, Cope and Delpy, 1988] took also additional losses caused by scattering into account. Assuming a constant scattering, these losses are expressed by the summand G in Equation 2.4.

$$A = -\mu_a L + G \tag{2.4}$$

In NIRS measurements the scattering in the measured volume is unknown which prevents us from a quantifying the concentration of the hemoglobin chromophores. Nevertheless, functional measurements are feasible because calculating the changes of hemoglobin concentration between two time points is independent from the scattering. This only holds for the assumption of constant scattering and a constant path length L over time [Obrig and Villringer, 2003], which can be held in the case of brain tissue. We can formulate, with Δ signifying a difference between two points in time:

$$\Delta A = \Delta\mu_a L \tag{2.5}$$

Using Equation 2.1 this can be re-written for two time points (t_0 and t_1 as:

$$\Delta A = -log(I_{t_0}/I_0) + log(I_{t_1}/I_0) = log(I_{t_1}/I_{t_0}) \tag{2.6}$$

where the emitted light intensity I drops out. By choosing I_{t_0} as a reference light intensity represented, e.g., by an initial baseline measurement, or a temporal mean value. We are now able to calculate intensity changes for each time point of a measurement.

Our aim is now two separate the concentration change of two chromophores (HbO and HbR) from the actual measured attenuation change of two wavelengths of light. For two chromophores (HbO and HbR) $\Delta\mu_a$ and can be expressed with Equation 2.3 as a dependency of the wavelength λ, the concentration c of each

chromophore and the specific extinction coefficient e.

$$\Delta\mu_a = e_{\lambda,HbO}\Delta c_{HbO} + e_{\lambda,HbR}\Delta c_{HbR} \tag{2.7}$$

For two wavelengths (λ_1 and λ_2) this results in the following relation for the concentration change of HbO [Kocsis et al., 2006], known as the *modified Beer-Lambert law* defined by [Cope and Delpy, 1988].:

$$\Delta c_{HbO} = \frac{e_{HbR,\lambda_1}\frac{\Delta A_{\lambda_2}}{L_{\lambda_2}} - e_{HbR,\lambda_2}\frac{\Delta A_{\lambda_1}}{L_{\lambda_1}}}{e_{HbR,\lambda_1}e_{HbO,\lambda_2} - e_{HbR,\lambda_2}e_{HbO,\lambda_1}}, \tag{2.8}$$

and for HbR:

$$\Delta c_{HbR} = \frac{e_{HbO,\lambda_1}\frac{\Delta A_{\lambda_2}}{L_{\lambda_2}} - e_{HbO,\lambda_2}\frac{\Delta A_{\lambda_1}}{L_{\lambda_1}}}{e_{HbO,\lambda_1}e_{HbR,\lambda_2} - e_{HbO,\lambda_2}e_{HbR,\lambda_1}}. \tag{2.9}$$

The accuracy of determining the concentration changes of the different chromophores' is limited by two major effects, termed *cross-talk* (stemming from the simplified assumption of homogeneous change) and *separability* (influenced by different noise levels of the used wavelengths), the concept of which is nicely reviewed in [Kocsis et al., 2006]. These errors depend on the wavelengths used and can be estimated using Monte-Carlo simulations (e.g. the simulation of a high number of photons traveling through media) as shown by [Uludağ et al., 2004]. This means the existence of optimal combinations of wavelengths for NIRS instrumentation (see also Section 2.7).

2.3. Time-Frequency Characteristics of the Signals

Although NIRS aims to measure changes in the micro-vascular hemodynamics in the brain, it is also influenced by other, so called *extra-cerebral*, changes of the cardio-vascular system. This is due to the fact that all measured photons have to cross the skin of the head twice: directly at the sources output and before entering the detector (see Figure 2.3). Therefore, global concentration changes of hemoglobin, such as caused by the heartbeat or breathing, have a strong potential of poisoning NIRS measurements.

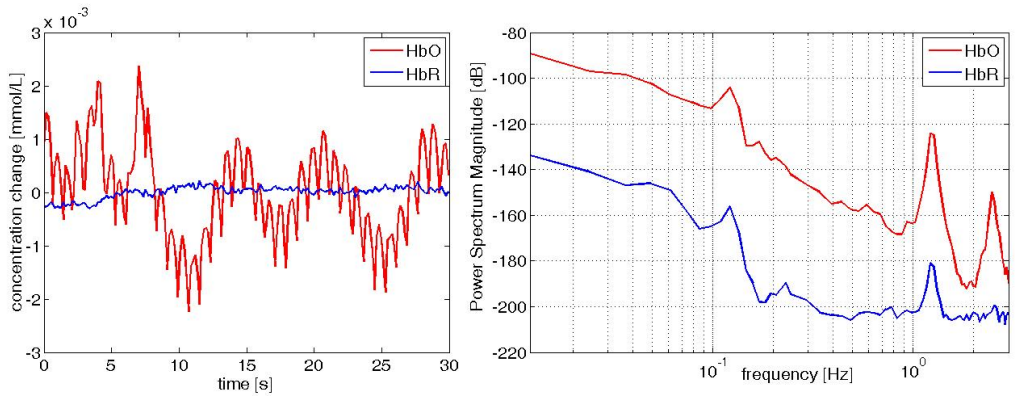

Figure 2.5.: Time course and frequencies in one sample NIRS channel during rest. Left: Time course of one NIRS channel for 30 s measurement time and both chromophores. HbO (red) has a higher variance than HbR (blue) and contains a larger fraction of heartbeat (fast oscillations) and slower (around 0.1 Hz) oscillations. Right: Frequency spectra for HbO and HbR. Most prominent are the heartbeat around 1.2 Hz and its first harmonic (2.4 Hz) in HbO. The respiratory activity (around 0.22 Hz, HbR) is only a minor component, while between 0.1 and 0.2 Hz there is a huge peak in the spectrum. Overall, these global physiological signatures are much less pronounced in the HbR signal.

The frequency characteristics of a typical NIRS channel (Figure 2.5), shows peaks stemming from the heart beat around 1 Hz (and its higher harmonics) and the breathing at around 0.3 Hz. A further peak is visible around 0.1 Hz, which might be raised by auto-regulations of the brains' vascular system or, at least partly, stems from extra-cerebral blood pressure changes [Nikulin et al., 2012].

Extra-cerebral artifacts are more prominent in HbO. This is most likely because the skin contains mainly HbO while HbR is most prominent in the arterioles and capillary bed of the brain. This is an indicator that HbR might the more reliable chromophore when studying brain's activity.

The heartbeat is the fastest observed signal. As the heartbeat is extra-cerebral noise and, thereby, a physiological artifact it has to be sampled with an adequate sampling frequency to get rid of it. This means that, according to the *Nyquist theorem* [Nyquist, 1928], the sampling rate of NIRS should not fall below ∼2.5 Hz (e.g. the double of the highest frequency band of interest).

Current NIRS instruments sample in a range of 3-20 Hz. This is a quite high sampling rate, keeping in mind that the hemodynamic response peaks around 5 s (0.2 Hz) and, especially, considering the low sampling rate of fMRI (mostly around 0.5 Hz). This causes a clearer signal (more information per time) but is mostly needed to filter out extra-cerebral noise.

In contrast to the sampling rate, the duration of the measurements is not limited. As there is no need for a patient or subject to lie down, or to keep high magnetic fields constant, NIRS is suited to measure people all day long, which might be useful for bedside measurements in the clinic (e.g. [Obrig and Steinbrink, 2011]) but also opens the field to brain computer interfacing (e.g. [Fazli et al., 2012b]).

2.4. Preprocessing of Data from Near-Infrared Spectroscopy

2.4.1. Filtering

Given the extra-cerebral origin of some components in our data, there is need for a proper filtering. To attenuate high frequency artifacts caused by heartbeat and breathing all data shown in this work is low-pass filtered between 0.4 and 0.2 Hz. To choose the appropriate low-pass filter frequency we consider the stimulus length and the inter-trial interval to prevent the removal of task-induced hemodynamics. Short stimulus length and fast inter-trial intervals suggest a low-pass filter below 0.2 Hz. Here, the HRF will peak at 0.2 Hz and lower filter would remove the expected hemodynamic response and leave us with noise only.

For longer stimuli the HRF will peak later (i.e. the frequency of the expected hemodynamics decreases) and long inter-trial intervals also cause a lower frequency of the hemodynamic responses. In this case we have the possibility to filter in lower frequency ranges. In the work presented we use a Butterworth 3^{rd} order filter.

To attenuate drifts and very slow oscillation an additional high pass filter is necessary. If not stated otherwise, we use a discrete cosine transform (DCT) [Ashburner and Friston, 1999] approach to remove these frequencies from the data. This approach uses a matrix of cosines with different frequencies which assumes more an oscillatory than a spontaneous occurrence of the low frequency noise.

Removing oscillation around 0.1 Hz is a very sensitive problem. Assuming an

occurrence in the whole head, the regression of a global mean is one way to reduce these artifacts. This approach is also frequently used for preprocessing fMRI data. If there is a possibility of measuring local skin hemodynamics by short source-detector distances (the banana reaches only the skin) a favorable approach would be nearest-neighbor correction used e.g. in [Gregg et al., 2010].

2.4.2. Applying the Modified Beer-Lambert Law

As a next step in the NIRS data processing we apply the modified Beer-Lambert law to transform the actual measured attenuation (absorption) changes into concentration changes of HbO and HbR. The division of the actual measured intensity by a reference intensity (Equation 2.6) causes the signal to vary around zero. It is also the reason of minor errors as already discussed in Section 2.2.3.

2.4.3. Removing Artifacts Caused by Movement

In addition to physiological artifacts caused by the cardio-vascular system, the movement of the subjects also causes frequently artifacts. These artifacts are dependent on the subject's nervousness and ability to concentrate. Especially children are not able to control their movements during experimental situations. These artifacts cause spikes with a length between 1 and 10 s in the data but mostly the attenuation changes goes back to the channel's individual baseline. This return to baseline is essential for some of the ways to analyze data presented in this dissertation (esp. general linear model analysis, Chapter 3). As there is no standardized way to remove movement artifacts we mostly use, if necessary, a semi-automated approach. We interpolate artifact loaded sequences of the data with a simple line. Some analyses are still valid when data surrounding the artifact is cut, as frequently done in EEG. For the analysis of correlation (Chapter 5) we cut the artifacts out of the data, because movement artifacts and also interpolation would induce a higher correlation.

2.5. Statistics for Hemodynamic Responses: the Difference Approach

After previously described preprocessing, results for experiments with long inter-stimulus intervals and clearly defined tasks can be analyzed in epochs of the time course around each repetition of a stimulus in each measurement channel. To calculate the effect of a stimulus for a single subject the baseline activity given at a time point before the stimulus onset t_0 in data X is subtracted from a point in time where one expects the peak of the hemodynamic response t_1. In this work we refer to this analysis as the *difference method*.

$$\Delta X_{i,j} = X_{i,j}(t_1) - X_{i,j}(t_0) \tag{2.10}$$

Where $\Delta X_{i,j}$ is the result for each stimulus i and measurement channel j of the data. This approach gains one value for each channel, stimulus and subject. Statistics can now be calculated for the individuals and the group. Individual results are processed by a *(Students') t-test* where each single trial difference ΔX_j is tested against zero (the *null hypothesis*) or the result for another stimulus. For group level statistics we use averages of the differences $\Delta X_{i,j}$ in each subject and calculate the t-test in a group level. In both cases one has to adjust the statistical results for the number of measurement channels to prevent an over fitting e.g. by a Bonferroni correction [Bonferroni, 1935].

2.6. Mapping of Statistical Results

NIRS itself does not recognize the brain structures underlying a measurement channel which is required to reference statistical results to brain areas. There are several approaches to coregister the channels to single subjects brains' or, as a rougher estimation, to a brain atlas (which is a standardized brain given by an average over numerous individuals anatomical MRI scans such as the *MNI brain* [Evans et al., 1992] or structural analysis of a post-mortem brain as the Talairach atlas [Talairach and Tournoux, 1988]).

Though anatomical MRI-scans of the individuals are not always available (and further decreases the advantages of NIRS - like low costs and portability) another

way to link channel positions to the underlying brain structure is necessary. 3D coordinates of the channels can be referenced to standardized locations of EEG electrode position (e.g. the EEG 10-20 system [Jasper, 1958, Niedermeyer and Da Silva, 2005]) for whom the underlying brain structure is (roughly) known [Koessler et al., 2009].

The acquisition of the 3D coordinates for this approach can either be done on a single subject basis with instrument like electromagnetic field based 3D digitizing systems as the Polhemus system (www.polhemus.com), the Zebris 3D digitizing system (www.zebris.de) based on ultrasound, Photomodeler software (www.photomodeler.com) based on 3D reconstruction of photos from several perspectives, or infrared stereo cameras (e.g. www.nexstim.com).

Because all afore mentioned instrumentations have shown an error >0.5 mm (these results have not been published) and the EEG-caps we use (www.easycap.de) have a further uncertainty of ∼0.5 cm, we argue that a single subject measurement of optode position is not precise enough and additionally time consuming (ca. 20 minutes until 1 hour per subject).

In this dissertation we use a EEG cap to fix the optodes inside (see Section 2.7.1) which automatically references the optode positions to the EEG 10-20 system and provides us with information about the underlying brain areas for each measurement channel.

For visual inspection and demonstration of the results on a 3D brain we use the freeware MATLAB toolbox NFRI (www.jichi.ac.jp/brainlab/tools.html) described by [Singh et al., 2005], which estimates brain regions underlying the channel and the EEG 10-20 position. This toolbox also allows to sketch experimental results as colored circles at the channels locations on a 3 dimensional head surface but prevents an interpolation between actual measurement channels e.g. as used in NIRS-SPM (bisp.kaist.ac.kr/NIRS-SPM.html) [Ye et al., 2009]. This interpolation is not favorable because it leads to the imagination of higher spatial sampling than actually measured and drops the focal nature of NIRS measurements.

2.7. Instrumentation

Since the upcoming of NIRS technology [Villringer et al., 1993] the instrumentation has dramatically improved. Nowadays the instruments have enough channels

to cover the whole head with light sources and detectors (together called *optodes*).

2.7.1. Attachment of Optodes onto the Head

For a NIRS measurement there have to be sources and detectors. Glass fibers can be used to transmit the light to and from the head. Thereby an electric contact between the actual instrument and the head is prevented and allows artifact-free simultaneous measurements with e.g. EEG or fMRI. For other measurements sources and detectors can be attached directly on the head (without the glass fiber as transmitter) [Krüger et al., 2012]. The advantage is that the weight and bulk of glass fiber bundles are avoided and movement artifact become less pronounced.

There are several ways to attach NIRS probes on a subjects head. As already stated earlier, one solution is to include them into an EEG-cap. Therefore, the glass fibers are bent by 90° as shown in Figure 2.6 A in a plastic form, which is also provides as an adapter for EEG electrode holders which are integrated into the cap. With this arrangement one has the ability to put an optode and an EEG ring-electrode at the same position of the head.

Classical EEG caps with 128 holders provide a distance between holders reaching from 2.5 till 3.5 cm and are therefore well suited for NIRS measurements. This distance is the favorable inter-optode-distance, because the *banana shaped* volume is then deep enough to reach the upper layer of the cortex. Longer distances than 4 cm between source and detector cannot be employed because then too few photons will reach the detector. A bandage can press the optodes slightly onto the skin to guarantee optimal contact.

2.7.2. Whole-Head Coverage

Recent instruments have up to 64 optodes which cover nearly the whole head when spread with an inter-optode distance of 3 cm over the head. Such an arrangement is shown in Figure 2.7, covering frontal, temporal, central and parietal parts of the brain. Only the visual cortex is not covered. With such an approach it is feasible to measure functional neuronal networks spreading not only in a small part of the brain but connecting several areas spread all over the brains surface (e.g. a connection of parietal and frontal regions).

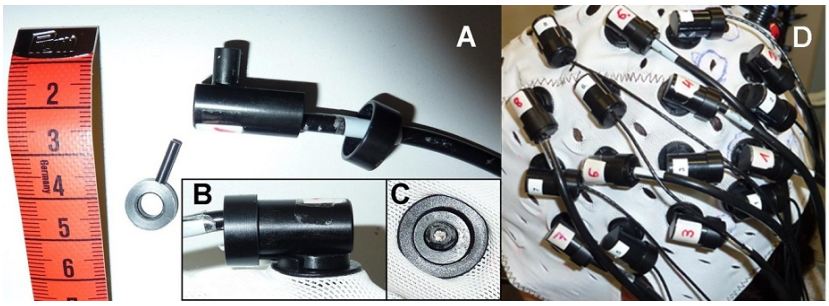

Figure 2.6.: Integration the optodes into an EEG-cap. A) A black plastic adapter ring is inserted into the electrode holder of a standard EEG-cap. The optode (top) is then placed into the hole of the adapter. A retaining ring is used to secure the optode on the adapter. B) Optode in position. C) Bottom view of the optode (underside of the cap).

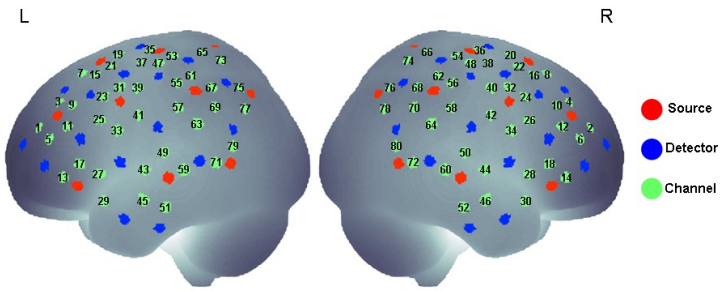

Figure 2.7.: Setup of whole-head coverage as used in [Mehnert et al., 2012a] and [Mehnert et al., 2009] superimposed onto a brain surface. Red dots: Laser emitter positions; blue: detector positions; green: actual NIRS measurement channel positions with channel number. Note the use of even / odd numbers for the right / left hemisphere and small / large numbers for frontal / parietal areas

2.8. Combination of NIRS with other Modalities

A major advantage of NIRS is its possibility for artifact-free simultaneous measurements with other neuroimaging devices such as EEG and fMRI, and also with peripheral measurements to measure e.g. blood pressure, heart beat and/or skin conductance. Multimodal imaging studies open wide fields of possible research. A favorable combination is the simultaneous acquisition of electrophysiology and hemodynamics. The signals of both devices contain complementary information. Simultaneous NIRS and EEG measurements are, for example, used in order to research language processing [Wartenburger et al., 2007,Ehlis et al., 2009,Telkemeyer et al., 2009,Rossi et al., 2011,Grossmann et al., 2010] the visual cortex [Obrig et al., 2002,Herrmann et al., 2008]. Multimodal approaches will enhance our knowledge about the complexity of the human cortex and its cognitive functions [Bießmann et al., 2011].

2.9. Advantages and Disadvantages of Near-Infrared Spectroscopy

The major limitation of NIRS is its low penetration depth and physical restrictions prevent from enhancing it. The spatial resolution can be enhanced by sufficient data analysis and experimental setup as shown in [Zeff et al., 2007, Koch et al., 2010,Habermehl et al., 2012]. What remains as benefits of NIRS are the mobility of this device, its low cost and harmless nature. NIRS has also the advantage of artifact-free simultaneous multimodal measurements, which then provides us with information from both instruments.

Further technical improvement in miniaturizing NIRS devices enables neuroscientific research outside the laboratory environment. This makes applications in real environments, for children and neonates possible but is also of interest for long-term bedside monitoring in the clinics.

NIRS data requires sufficient data analysis to separate extra-cerebral noise from the brains' hemodynamics. In the next chapters we describe several ways to analyze NIRS data.

3. General Linear Model Analysis

The hemodynamic responses are quite slow. Therefore, the break after each stimulus has to be at least 15 seconds long to avoid overlapping responses and allow an analysis by averaging. Experimental settings with faster stimulus presentation are not analyzable without deconvolving the overlapping responses. General linear model (GLM) analysis is a stable way to deconvolve overlapping hemodynamic response for fast stimulus presentation. Here, a researcher models the overlapping hemodynamics and estimates statistical results by comparing, i.e. *regressing*, his model with the actual measured data. GLM, thereby, needs sensitive knowledge about the hemodynamic response and a strong hypothesis about its behavior during overlapping. Nevertheless, since the vascular response is quite well studied and the onset of each stimulus is given by the experimental setup, GLM analysis provides results which are statistically easy to prove and quite stable against extra-cerebral and other artifacts. GLM is the only tool which is able to analyze overlapping hemodynamic responses and allows relative short inter-trial-intervals (ITI). This method was first applied to fMRI data and has been shown to be a robust and reliable analysis method for NIRS [Cohen-Adad et al., 2007]. GLM has been for example frequently used for NIRS data analysis in recent developmental studies [Wartenburger et al., 2007, Telkemeyer et al., 2009, Minagawa-Kawai et al., 2011, Rossi et al., 2011, Telkemeyer et al., 2011] though young children demand attentive and relative fast stimuli presentations to stay concentrated.

This chapter discusses the reliability of the HRF approach and gives a brief introduction into the math behind GLM analysis in Section 3.1. A first impression of its advantages is given in Section 3.2 by analyzing data from a study on the effect of mirror illusion in the precuneus brain area where the hemodynamics do not overlap. An experiment with faster stimulus presentation and the analysis of overlapping hemodynamic responses is shown in Section 3.3 in a study comparing the underlying neuronal structure of response inhibition between children and

adults. Furthermore, other GLM-like analyzing approaches do not depend on a specific model of the HRF. Finite impulse response (FIR) analysis has the average hemodynamic responses as output, also the case when the responses overlap. It also provides the possibility to test whether the subjects behavior on a single trial has an influence on the height and shape of the HRF (similar approaches can be used for classical GLM analysis). An example where we asses the effect of subjects' reaction time on the hemodynamic response is given in Section 3.4. This chapter concludes with an outlook on further analytical improvement in Section 3.5

3.1. Theory

3.1.1. Models of Hemodynamic Response

The occurrence of hemodynamic responses to neuronal activity [Fox and Raichle, 1986] led to models of it [Boynton et al., 1996, Friston et al., 2000, Buxton et al., 2004]. This hemodynamic response function (HRF) is generated by a model including the neuronal response and its vascular coupling described by [Friston et al., 2000]. Recent implementation of the HRF uses a linear combination of two gamma functions, originally introduced to blood oxygenation level dependent (BOLD) fMRI [Friston et al., 2007] but also used for NIRS analysis. Note that the HRF is quite slow: e.g. for a short stimulus and neuronal event it peaks around 4-8 seconds afterwards and reaches baseline again after around 20 until 30 seconds. Further properties of the hemodynamics show that its behavior is linear and, thereby, also predictable for different lengths of stimuli and when HRFs are overlapping [Boynton et al., 1996, Friston et al., 2000, Buxton et al., 2004]. Given this information it was shown that a good mathematical estimate of the hemodynamics is a convolution of the HRF and a boxcar function of the stimulus onset and length. With this idea, GLM analysis became popular and simple, and dominates the fMRI community nowadays while it is also very frequently used for NIRS analysis.

3.1.2. Mathematical Background

The general linear model (GLM) is a statistical linear model where the data X is compared to a model of the researchers expectations M, which is also called

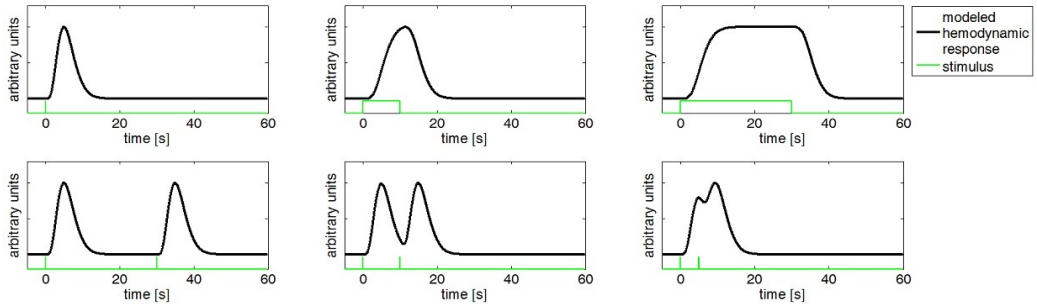

Figure 3.1.: Models of the hemodynamics as response to different stimuli (black lines). The green line signifies a boxcar function of stimulus onset and length. Top, left hand: Convolution of a single pulse with Hemodynamic Response Function (HRF) at time point 0 reveals the used HRF (from [Boynton et al., 1996]) itself. Top, center: Hemodynamic response to a stimulus with 10 s length with later peak and decay. Top, right hand: Hemodynamic response for a stimulus with 30 s length. Here, a plateau evolves. Bottom, left hand: Hemodynamic response to 2 stimuli with short length and 30 s inter-trial-interval. Bottom, center: Hemodynamic response to 2 stimuli with short length and 10 s inter-trial-interval. The hemodynamic responses start to overlap. Bottom, right hand side: Further decrease of the inter-trial-interval leads to a strong overlap of the hemodynamic responses.

design matrix. There is some (white) noise ϵ which cannot be explained by the experiment, referred also as *unexplained variance*.

$$X = \beta M + \epsilon \tag{3.1}$$

The aim is now to fit the model M to the data X by minimizing the unexplained variance (i.e. the error) in ϵ and, thereby, maximizing the values in β. The minimizing procedure is usually done by least-square algorithms. β is a vector with one entry for each regressor (model) and used for further statistical analysis. This procedure was introduced to the NIRS community by [Cohen-Adad et al., 2007].

Least square fitting is, in case of outliers, sensitive to over fitting. The number of regressors used should therefore be much lower than the data points acquired and outliers should be removed in the artifact correction before the fitting. The

model M is, hereby, created by a convolution of a boxcar function s (representing stimulus onset and lengths) with a model of the hemodynamic response (i.e., the HRF). This can mathematically described by

$$M = s * HRF \tag{3.2}$$

where $*$ signifies the convolution. Results for this approach can be seen in Figure 3.1 for several examples of differing stimulus length and inter-trial-intervals.

3.1.3. Finite Impulse Response Analysis

Finite Impulse Response (FIR) does not take a strong biophysical model like the HRF into account but uses one regressor for each time point of the hemodynamic response. This regressor is a simple stick function. The βs in FIR are standing thereby for the height of an amplitude in a time point after stimulus onset. The model M from Equation 3.1 consists of impulse functions I. Each of these regressors stands for a certain time point after stimulus onset and for every stimulus an impulse is set. The number N of regressors, thereby, defines the resolution of the result. The mathematical notation is:

$$M = I_{1...N} \tag{3.3}$$

This analyzing technique is schematized in Figure 3.2 for non-overlapping and overlapping responses.

Using a second set of the regressors and a multiplication for the signal trials with behavioral results gives the parametric modulation of the hemodynamic response.

3.2. General Linear Model Analysis in a Study on Mirror Illusion

We applied the GLM approach in a study where overlapping hemodynamic responses are prevented by long inter-trial intervals to show its reliability. This opens the possibility to compare the *difference analysis*, already presented in Section 2.5, with the GLM approach. This study was further designed to investigate the neuronal basis for mirror illusion [Mehnert et al., 2012b]. In recent years, the

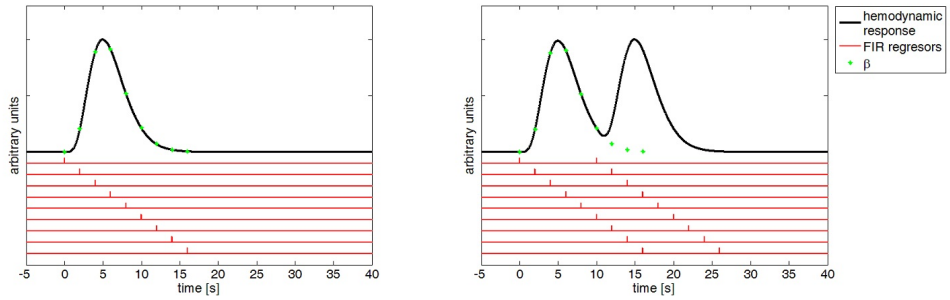

Figure 3.2.: Schema of Finite Impulse Response (FIR) analysis. The black line is the hemodynamic response for one (left hand)/two (right hand) short stimuli. Red lines show the regressors of the FIR for 9 time points after stimulus onset. In case of the overlapping hemodynamics (right hand) each regressor consist of 2 impulses because there are 2 stimuli given. The green stars show the resulting β, deconvolving the overlapping hemodynamics (right side).

use of mirror illusion has become increasingly popular to treat limbs affected by phantom pain [Ramachandran et al., 1995] or stroke [Ezendam et al., 2009, Rothgangel et al., 2011]. Mirror therapy works in patients with one sided affected limbs. Here, the unaffected side is trained while the patients look into a mirror image of the unaffected side, giving the illusion of training the affected side.

Experimental Procedure in Mirror Illusion Experiment
Tasks: 20 trials per condition (normal finger movements, mirrored finger movements, static observation of the normal hand and static observation of the mirrored hand)
Subjects: 20 healthy, right-handed volunteers (aged 21 to 40)
Instrumentation: NIRS: 16 sources, 16 detectors, 38 measurement channels
See Appendix A.1 for a detailed description of the experimental setup

Textbox: Experimental Procedure in Mirror Illusion Experiment

3.2.1. Methods

To compare the effect of mirror illusion with and without movement we designed an experiment consisting of four stimuli for each hand: (1) Finger movements, normal (movement, NOR), (2) Finger movements, mirrored (movement, MIR), (3) no movements, normal (static, NOR), and (4) no movements, mirrored (static, MIR). For a direct comparison of the difference analysis with the GLM, movement related trials (NOR and MIR) were pooled and analyzed with both methods. Using the difference method we subtracted the temporal average between 5 s before until trial onset $\overline{X_{i,j}(t_0)}$ from the effect assumed to be within 5-15 s after trial onset $\overline{X_{i,j}(t_1)}$ for each channel j, trial i, chromophore and subject in the preprocessed (and band-pass filtered) data (see also Section 2.4.1). Recalling Equation 2.10 this results in:

$$\Delta X_{i,j} = \overline{X_{i,j}(t_1)} - \overline{X_{i,j}(t_0)}, \tag{3.4}$$

with $t_1 \in [5...15]$ and $t_0 \in [-5...0]$ seconds in relation to the stimulus onset. Single trial results $\Delta X_{i,j}$ where then averaged within each subject, gaining one value for each subject and channel, and used for further statistical comparison.

For the GLM analysis regressors were composed by a convolution of a boxcar function, representing stimulus onset and length, with a hemodynamic response function [Boynton et al., 1996]. Additional regressors are composed by a discrete cosine transform (DCT) [Ashburner and Friston, 1999] working as high pass filter (see also Section 2.4.1). All regressors were fitted to the preprocessed and low-pass filtered data by a least square approach. For each subject, condition and channel, the GLM provided two β values (for HbO and HbR, respectively), indicating the strength of the modulation of the hemodynamic response. Furthermore, we tested the assumption of white noise content for the error ϵ in the GLM (Equation 3.1) by averaging the power spectral density for the residual (i.e. unexplained variance) in the motor related channels. Please note, that stronger activity in both methods is indicated by positive values for HbO and negative values for HbR [Fox and Raichle, 1986, Logothetis and Wandell, 2004].

For the effect estimation of the mirror illusion, we further performed a GLM analysis taking all four conditions into account. For visual inspection and demonstration we used the approach described in Section 2.6. The two imaging studies by Dohle and colleagues [Dohle et al., 2004, Dohle et al., 2011], which also analyzed

the mirror effect, indicated that comparable foci in the region of the precuneus were activated (Figure A.1 B). Regions of interest (ROI) were defined corresponding to the activation foci of the above-mentioned studies in the precuneus as the three channels displayed in Figure A.1 C (further referred to as *Precuneus-ROI*) for both hemispheres. ROIs in somato-motoric area (MA) were defined as the four midsagittal channels on either hemisphere as these positions are known to cover somato-motoric areas (see [Koessler et al., 2009]) (further referred to as (*MA-ROIs*) (see Figure A.1 C).

3.2.2. Results

Results for the direct comparison of the difference and GLM analysis are shown for left hand movements in Figure 3.3. Both methods lead to very similar topographies in an average over the subjects. HbO and HbR reveal maximal effects on the right somato-motoric area. As expected HbO increases and has about the double value of concentration change than HbR, which decreases after stimulation (Figure 3.3). Furthermore, the effect in HbO spreads also on the left hemisphere indicating a more focal nature of the HbR signal (Figure 3.3 A).

Although GLM reveals higher significance for both chromophores, comparing the average of somato-motoric channels against the null-hypothesis of no effect (Figure 3.3 B), there is no significant difference neither between the HbO nor the HbR results of both methods. Note that the significance for HbR is far higher in both methods than for HbO (i.e. p-values are lower). The comparison of GLM and difference method in single subjects (Figure 3.3 B) reveals similar results for both methods as their results are highly correlated between subjects.

Further analysis on the residual ϵ of the GLM approach, namely the average frequency spectrum over subject in the somato-motoric channels, reveals a rejection of the white noise assumption made in Section 3.1.2 as can be seen in Figure 3.4. There is still $1/f$-noise (also called *pink*-noise) present in the residual which signifies a physiological origin of the noise. Effects in the frequency ranges of the extra-cerebral noise (heartbeat ($\sim$1 Hz), breathing ($\sim$0.3 Hz) and blood pressure ($\sim$0.1 Hz); see Section 2.3) are not visible. Also the variance is not increased in these frequency bands.

To estimate the effects of the mirror illusion, baseline-corrected time courses for

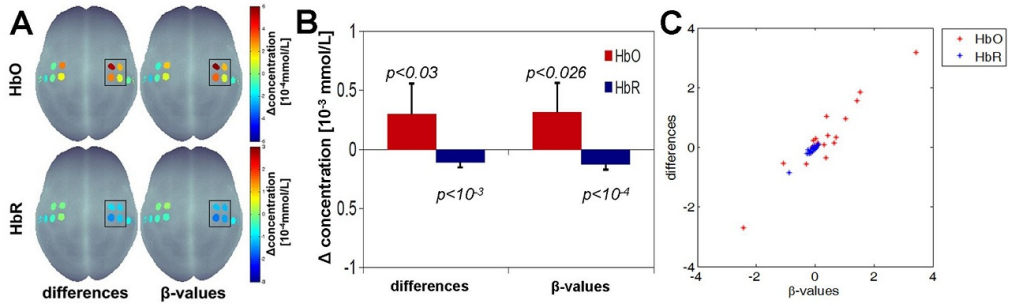

Figure 3.3.: Comparison of the *difference* and *general linear model* analysis for non-overlapping hemodynamics. A) Resulting differences (left hand side) and β-values (right hand side) for HbO (top) and HbR (bottom) during left hand movements plotted on a schematic brain (top = frontal). Note that the scale for HbO results is double the height than for HbR results. As expected HbO shows positive values in the right somatomotoric-areas while HbR becomes negative. The black rectangle marks the channels used for the analysis shown in B). Regional averages for both methods are shown in B) and tested against the null-hypothesis of no effect (t-test). p marks the resulting significance and the error bars the standard error of the mean over the group. C) Comparison of β-values and differences for single subjects. The correlation between results for GLM and difference method are 0.96 for HbO and 0.97 for HbR, both highly significant ($p < 10_1 0$ and $p < 10_1 1$).

the Precuneus-ROIs were averaged across subjects and smoothed (moving window of 10 s) for MIR and NOR conditions (shown in Figure 3.5, top). As expected, we observed less concentration change for both chromophores in the contralateral hemisphere (Figure 3.5, right hand side) when comparing MIR with in the NOR condition. This difference peaks at about 10 s after stimulus onset in both chromophores. In contrast, in the ipsilateral hemisphere (Figure 3.5, left hand side), there is less concentration change in the NOR compared with the one in MIR condition for both chromophores, with this difference peaking slightly later at about 12 s after stimulus onset.

Baseline-corrected time courses for the MA-ROIs (Figure 3.5, bottom) show as expected only a slight change of concentration in the ipsilateral and contralat-

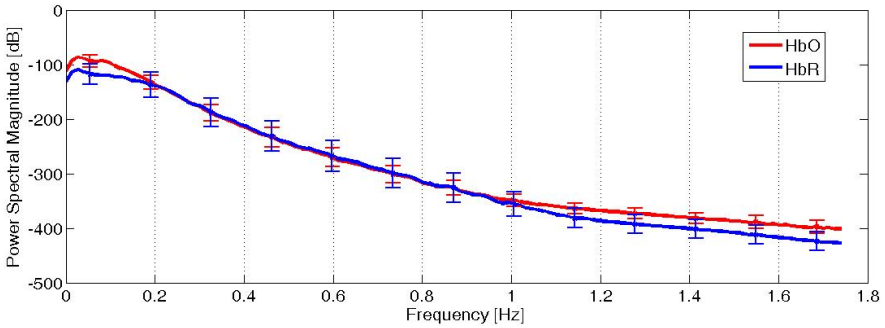

Figure 3.4.: Power spectral density for the residual ϵ of the general linear model analysis for HbO (red) and HbR (blue) shown as an average of the frequency spectra in the right somato-motoric area of all subjects. The error bars signify the standard deviation over subjects.

eral hemisphere for the MIR compared with in the NOR condition (Figure 3.5, bottom).

The four-way repeated measures ANOVA over the beta values show a significant main effect of the factor movement ($F(19)=4.92$; $p<0.05$, $\eta^2=0.21$) for HbO. Furthermore, there is a significant two-way interaction of the factors mirror and hemisphere ($F(19)=4.59$; $p<0.05$, $\eta^2=0.20$) for HbO, although post-hoc analysis of this two-way interaction revealed no significant effect in the paired t-tests. The two-way interaction of the factors mirror and hemisphere failed to reach significance for HbR ($F(19)=1.71$; $p=0.21$, $\eta^2=0.08$).

In the somato-motoric ROIs the four-way ANOVA over the beta values show, as expected, a significant main effect of the factor movement for HbO ($F(19)=5.06$; $p<0.05$, $\eta^2=0.21$) and also for HbR ($F(19)=5.51$; $p<0.05$, $\eta^2=0.23$). Because there was more activation in movement conditions then in static conditions, a further three-way repeated measures ANOVA with the factors mirror (MIR / NOR), hand (left / right) and hemisphere (ipsilateral / contralateral) was applied on the beta values of the MA-ROI. This was done for the trials with movement to confirm our hypothesis of minor influence of mirror illusion on the somato-motoric area. This three-way ANOVA showed a main effect of hemisphere ($F(19)=4.65$, $p<0.05$, $\eta^2=0.20$) for HbR. The beta value for the hemisphere contralateral to the moving hand was -0.11 and -0.04 for ipsilateral, which indicates more activation contralateral than ipsilateral for the trials with movement. The same effect was

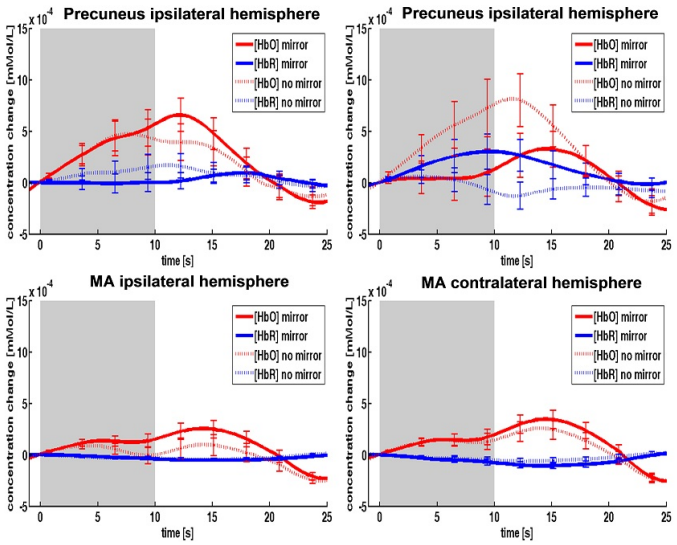

Figure 3.5.: Averaged time courses of the MA- and Precuneus-ROIs, contra- and ipsilateral to the moving hand. The duration of stimulus presentation is shaded in gray. HbO is presented in red while HbR is coded in blue. Time courses have error bars with standard error of the mean.

observed for HbO, but failed to reach significance ($F(19)=3.71$ $p=0.069$, $\eta^2=0.16$; mean beta value contralateral: 0.33; mean beta value ipsilateral: 0.19). No other effects reached significance for the three-way ANOVA validating our hypothesis of minor influence of mirror illusion on MA.

3.2.3. Discussion

The comparison of the difference approach and the GLM analysis revealed similar results for both methods. This suggests that, in the case of non-overlapping hemodynamics, an equivalent usage of GLM is feasible. Both methods show a higher reliability and localization for the HbR chromophore. HbO is naturally more poised by extra-cerebral artifacts which stem from the skin, where the HbR concentration is negligible. We can show that the model of the hemodynamic response is realistic, which serves the basis for analyzing overlapping hemodynamics, as done in the next section. The frequency spectrum of the residual from the GLM reveals a rejection of the assumption that the residual consists only of white noise. The $1/f$ distribution over the frequencies suggest a physiological origin.

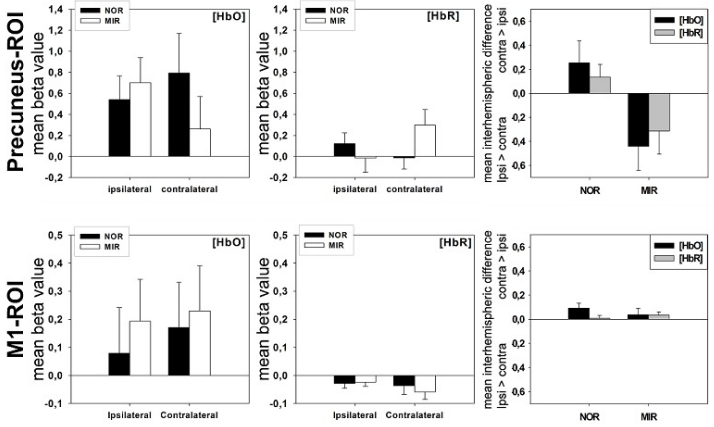

Figure 3.6.: Mean beta values and differences and their corresponding standard deviations at the Precuneus-ROI (top row) and MA-ROI (bottom row). Left column: mean beta values for HbO of the ipsi- and contralateral hemisphere for the MIR and NOR conditions; middle column: mean beta values for HbR of the ipsi- and contralateral hemisphere for the MIR and NOR condition; right column: mean inter-hemispheric differences in the MIR and NOR conditions for HbO and HbR (later multiplied by -1 for direct comparison). Note that in the figures of the right column values > 0 indicate higher activation in the ipsilateral than in the contralateral hemisphere and values < 0 indicate higher activation in the contralateral than in the ipsilateral hemisphere, respectively.

This indicates that the DCT approach, used to model low-frequency oscillation of physiological origin, is not capable to regress the low frequencies occurring in the brain. This might be due to the oscillatory nature of the DCT approach while the low-frequency content in the brain is from spontaneous origin. Nevertheless, extra-cerebral artifacts from cardio-vascular mechanisms are not visible in their typical frequency bands and seem, therefore, captured by the GLM.

Neural correlates of the mirror illusion were found ipsilateral to the moving hand for the precuneus-ROI for HbO, but not in the primary motor cortex. This is in line with previous studies [Dohle et al., 2004, Matthys et al., 2009, Michielsen et al., 2011, Dohle et al., 2011]. The effect for the precuneus-ROI for HbR was similar, but failed to reach statistical significance. However, in extension to previous findings our results showed that the mirror illusion does not simply induce

increased activation ipsilateral to the moving hand. Rather, the presentation of a right or left hand elicits a hemispheric lateralization in the precuneus opposite to the seen hand - irrespective of the hand that is actually moved. This lateralization is inverted by the mirror illusion. In contrast to the activation pattern of the precuneus, activity in MA is only modulated by the side of the hand which is actually moved, but not by the visually perceived hand. In summary, we demonstrated bilateral activation in MA- and Precuneus-ROI with dissociated lateralization patterns: While motor cortex activity is lateralized opposite to the moving hand, the precuneus activity is lateralized opposite to the visually perceived hand. These patterns seem to be independent of each other.

These findings are not only important to understand the neuronal origin of mirror illusion, but they might also help to understand and optimize the effect of the mirror therapy. Our findings indicate that activity in the precuneus does not depend on the hand that is actually used. This would imply that the effect of mirror therapy would not differ from training with direct view on the affected limb. This was confirmed by a recent systematic review, which found a significant effect of mirror therapy only compared to therapies without view, but not with unrestricted view on the affected limb [Thieme et al., 2012].

The physiological aim was to systematically examine the neural correlates of the mirror illusion with near-infrared spectroscopy. As described in previous studies [Dohle et al., 2004, Matthys et al., 2009, Michielsen et al., 2011, Dohle et al., 2011], we found increased activation ipsilateral to the moving hand for the Precuneus-ROI for HbO, but not in the primary motor cortex. The effect for the Precuneus-ROI for HbR was similar, but failed to reach statistical significance. Rather, the presentation of a right or left hand elicits a hemispheric lateralization in the Precuneus opposite to the seen hand - irrespective of the hand that is actually moved. This lateralization is inverted by the mirror illusion. In contrast to the activation pattern of the Precuneus, activity in somato-motoric areas was only modulated by the side of the hand that is actually moved, but not by the visually perceived hand. In summary, our findings indicate that the mirror illusion should not be regarded as an isolated phenomenon. Rather, at least at the level of the Precuneus, inversion of the visual feedback seems to be integrated into visuomotor behavior in the same way as processing of regular, non-mirrored movements.

Furthermore, the inversion of the visual feedback has no direct effect on MA.

3.3. Overlapping Hemodynamic Responses in a Developmental Study on Inhibition

In the experiment described in the section above we used quite long inter-trial intervals (15 s) and one therefore would also gain results by simple averaging (as shown in Figure 3.5) or calculating the difference in amplitude before and after stimulus onset (see Figure 3.3 and Section 2.5). This is not the case when the inter-trial interval is short and the hemodynamic responses will overlap and add up. Here, the GLM approach is one method to deconvolute the signal taking a model of the HRFs behavior into account. Here, we present an experiment with overlapping HRFs in the field of developmental research. With the GLM analysis we study age-related differences in the ability and the neurophysiological background of response inhibition between children at the age of 4-6 and adults [Mehnert et al., 2012a].

Experimental Procedure in Development of Inhibition Experiment

Tasks: 108 trials with 75% go trials and 25% no-go trials (mean inter-trial interval 5500 ms, jittered, ranging from 3750 to 12000 ms)

Subjects: 51 healthy, right-handed volunteers (21 adults, ranging from 21 to 36; 30 children, ranging from 3-6 years)

Instrumentation: NIRS: 20 sources, 32 detectors, 80 measurement channels

See Appendix A.2 for a detailed description of the experimental setup

Textbox: Experimental Procedure in Development of Inhibition Experiment

3.3.1. Methods

Volunteers were asked to respond to frequent, visually presented targets by pressing a button with the right hand (go condition) and to avoid the response to rare non-targets (no-go condition), i.e. to inhibit a reaction. The subjects were

instructed to respond to the targets as fast as possible. We presented cartoon images of *Bob the builder* and *Wendy* characters for go and no-go stimuli. Task versions were balanced with respect to the stimulus material (i.e., which of the characters was used as the go or no-go condition) and sex of participants for both subject groups. The task consisted of two runs, each of which lasted 250 s and contained of 54 trials with 75% go trials and 25% no-go trials. The order of the presentation was randomized. The stimulus duration was 800 ms and the average inter-trial interval was 5500 ms (jittered, ranging from 3750 to 12000 ms).

To estimate the effect of motoric activation within overlapping circumstances, inhibition, and the differences between adults and children, we generated a hemodynamic model, i.e. regressors, by convolving the temporal stimulus profile with a canonical hemodynamic response function (HRF). We applied a GLM analysis, separately for both hemoglobin chromophores (HbO and HbR), for each condition, and for each subject. The so obtain parameter estimates (i.e. β-values) are a measure of the stimulus-related relative change of tissue hemoglobin concentration and the basis of all our further statistical analysis. To analyze differences in brain activation between children and adults we applied a repeated measures ANOVA model on the GLM analysis results including group (children vs. adults) as a between-subject factor and condition (go v.s no-go) as within-subject factor. Significant motor related changes (go-condition) in the adult group were post-hoc analyzed within a region of interest. Here, we additionally applied a difference analysis (using -1 until 0 s as baseline and 4 until 6 s as the time of effect) to compare both analysis methods. See Section A.2 in the appendix for further information of the data processing.

3.3.2. Results

The ANOVA revealed 7 significant channels for the within subject factor condition (i.e. movement of the right hand during the go-condition) in the expected motor-related areas of the left hemisphere. Figure 3.7 (left hand side) shows the results of the channel-wise average over subjects for GLM and difference analysis. As expected, the difference method did not reveal any significant changes (Figure 3.7 (right hand side)) within this region comparing the go-condition to the null hypothesis due to the overlap of hemodynamics.

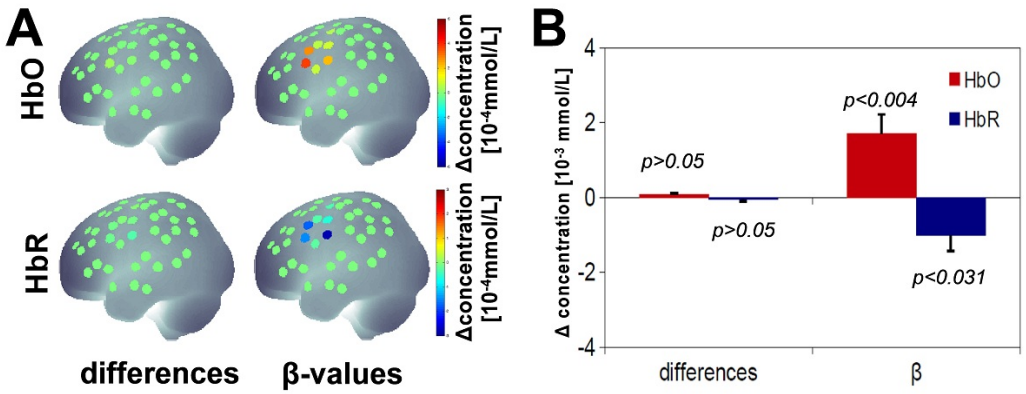

Figure 3.7.: Comparison of the *difference* and *general linear model* (GLM) analysis for overlapping hemodynamics. A) Resulting differences (left hand side) and β-values (right hand side) for HbO (top) and HbR (bottom) during the go-condition, which includes a button press with the right hand, in the somato-motoric region of the brain. Note that the scale for HbO results is double the height than for HbR results. As expected,the difference analysis is not capable to analyze overlapping hemodynamics. HbO shows positive values fro the GLM analysis, while HbR becomes negative. Regional averages for both methods are shown in B) and tested against the null-hypothesis of no effect (t-test). p marks the resulting significance and the error bars the standard error.

Nevertheless, the GLM approach shows significant activation in the somato-motoric region for the go-condition, reflecting its ability to take the overlapping hemodynamics for fast motoric stimulations into account.

The effect of inhibition was estimated by a 2x2 (group and condition) ANOVAs. This analysis revealed significant interactions in the channels over the right frontal and right parietal cortices (see also Figure 3.8), when using the HbR values as dependent variable and controlling for accuracy (AC) and reaction time (RT). In the frontal regions, a group by condition interaction is based on a strong decrease in the values of HbR (i.e. activation) for the no-go compared to go trials in adults. This stands in contrast to children, who activated stronger frontal regions during the go trials compared to the no-go trials. We observed the same qualitative behavior in the parietal areas: considering the absolute magnitudes, we found comparable activation magnitudes for the go and the no-go trials in the adult

group. Although children showed a similar absolute activation strength of the parietal areas in the go condition compared to adults, the activation during the no-go-trials remained weak. In addition to the interaction effect, we found a significant change in the HbR signals in the left motor areas when testing them for the condition effect (go > no-go), which reflected the motor response with the right hand.

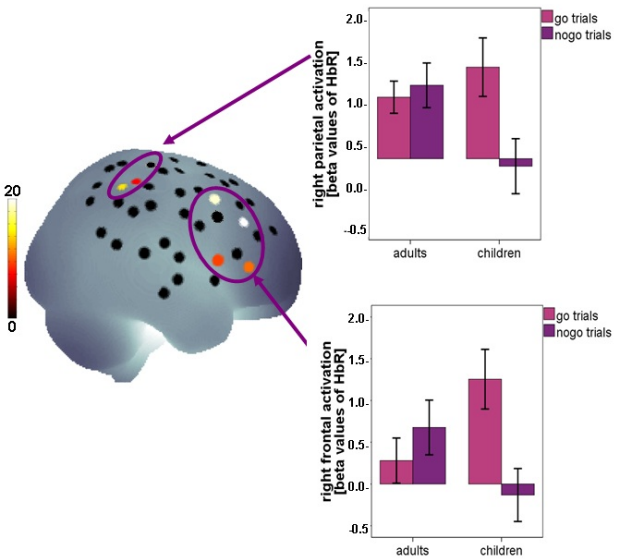

Figure 3.8.: Group x condition interaction. F-scores of NIRS signal changes are superimposed onto a brain surface. Bar plots represent group-specific and condition-specific mean beta value of HbR. The left bar plot is based on the average beta value of the two significant parietal channels, the right bar plot is based the average beta value of the four significant frontal channels. Error bars represent ± 1 standard error.

The HbO signal showed significant changes of the GLM-derived values only in the motor areas when considering the contrast condition go > no-go, signifying the expected primary motor activation. However, there was no significant group and condition interaction effect in the HbO signal (for a comparison of the NIRS signal components HbR and HbO see above).

Due to significant correlation between age and both behavioral parameters (RT and AC) we performed multiple regression analyses to reveal developmental effects on brain parameters. Out of 80 channels, we identified a significant effect of task-

induced brain activation change with age: In channel 30, located in the right frontal lobe, age correlated significantly with the HbR values, ($r = -.82$, $p<.05$).

3.3.3. Discussion

In task-induced brain activation patterns during the go condition, we identified a left-lateralized central activation across both groups, reflecting the motor activation during the go trials. There was no significant group difference in the go condition, supporting the behavioral finding of the children being capable of executing the go trials. Nevertheless, the comparison of the GLM and difference method revealed obvious results. The difference approach has not been able to retrieve significant changes in the motoric regions of the adult subject. This is caused by the overlapping hemodynamics in the fast experimental design. The GLM approach takes the overlapping hemodynamics with a convolution into approach and can, thereby, reveal significant motor related changes. This result shows that a deconvolution process is necessary when analyzing fast experimental design causing overlapping hemodynamics. The higher significance for HbO can be explained with stimulus-locked (extra-cerebral) cardio-vascular responses for which is not corrected in the current way of analysis (like correct for this effect in all channels) and which might overlap with the model of the cortical hemodynamic response (see [Mehnert et al., 2012c]).

During the inhibition condition, however, significant group differences were detected. In line with previous imaging studies [Durston et al., 2002, Rubia et al., 2007], adults showed a stronger increase in task-induced fronto-parietal activation during the no-go condition compared to the go condition. In contrast, the immature activation pattern in children was characterized by higher frontal activation during go trials in comparison to no-go trials. This immature response pattern fits well into the discussion of which cognitive processes are involved in a go no-go task and what improvements are made during development. For example, Cragg and Nation [Cragg and Nation, 2008] studied response inhibition in a group of young children (5-7 years) and older children (9-11 years). They suggested that the higher accuracy during the no-go trials of 9 to 11-year-olds might be more likely due to a higher inhibition speed than a weaker motor preparation and initiation. This means that older children were faster to inhibit the motor response and

therefore did not complete the motor action whereas motor preparation also took place in older children. Thus, Cragg and Nation (2008) differentiated between partial inhibition (response initiation) and successful inhibition (no response initiation) and reported that in 5 to 7-year-olds only one third of correct inhibition trials were a complete successful inhibition, whereas in the remaining no-go trials a go response was at least initiated [Cragg and Nation, 2008]. This mechanism might have played a role in our group of children, too. Reduced fronto-parietal activation pattern in response to no-go trials in our children sample might reflect a delayed inhibition initiation at the onset of the presentation of the no-go target. Instead, they might have initiated a motor response, which they were able to stop before conducting the motor response as seen in behavioral data. Unfortunately, we did not use a paradigm differentiating between partial and successful inhibition, and therefore can only speculate. However, the brain responses seem to indicate similar processes in our study. The higher frontal activation during the go trials in contrast to adults might reflect higher working memory demand for children to keep online on which stimuli they had to react and on which they did not.

In the context of the introduced behavioral discussion about the difference between theoretical understanding of a go/no-go task and the actual behavioral performance [Bell and Livesey, 1985, Livesey and Morgan, 1991, Zelazo et al., 1995, Dowsett and Livesey, 2000], our results suggest immature inhibition skills rather than impaired rule reflection: although we measured signal changes of nearly the whole cortex, we found significant developmental differences only within a fronto-parietal network, commonly associated with executive attention and response inhibition. Following the idea of immature rule reflection one might have expected differences in areas such as medial frontal and cingulate regions (e.g. [Bengtsson et al., 2009]). Furthermore, findings revealed by regression analyses reflect the high plasticity during the ages 4 and 6, which might also explain the training effects of inhibition skills, reported by [Dowsett and Livesey, 2000] and [Rueda et al., 2005].

3.4. Finite Impuls Response to Decode Vigilance

Here we present a study which uses an GLM-like approach without taking the biophysical model of the HRF into account. With finite impulse response (FIR)

analysis, averages of overlapping HRf can be deconvoluted. This study further aims to evaluate the influence of vigilance (a form of attention) on the shape and temporal behavior of the HRF, and will be part of the publication [Bogler et al., 2012].

Experimental Procedure in Decoding Vigilance Experiment
Tasks: 6 blocks of global-local Stroop task (60 trials/block)
Subjects: 9 healthy, right-handed volunteers (aged 20 to 30)
Instrumentation: NIRS: 16 sources, 16 detectors, 44 measurement channels
See Appendix A.3 for a detailed description of the experimental setup

Textbox: Experimental Procedure in Decoding Vigilance Experiment

3.4.1. Methods

To measure changes in vigilance subjects were presented with a global-local Stroop paradigm [Weissman et al., 2006] where the reaction time served as a marker for the actual vigilance of the subjects. See Section A.3 for a full description of the paradigm. The preprocessed NIRS-data was analyzed using custom software. We implemented a general linear model (GLM) that makes no assumptions about the shape of the hemodynamic response. Therefore, according to Equation 3.3 we estimated 15 regressors to model the average stimulus-locked response. The data was recorded with a sampling frequency of 6.25 Hz which is much higher than for fMRI paradigms (typically around 0.5 Hz). Each regressor modeled thereby the average response of 6 consecutive time points with a boxcar function. The 15 regressors each with a length of 6 measured time points corresponded to 90 time points or 14.4 s (90/6.25 s). Furthermore we included a second set of 15 parametric regressors [Friston et al., 1997] which modeled the modulation of the hemodynamic response due to variations in the mean corrected response times. This regression approach was similar to the model used in the study [Weissman et al., 2006]. See also Section 3.1.3 for a short introduction into the mathematical background.

3.4.2. Results

The betas for the set of regressors for the stimulus locked response (SLR) revealed a shape of classical hemodynamic responses with a peak around 7 s and a HRF-like shape in most channels of oxygenated hemoglobin. Also a few channels in deoxygenated hemoglobin showed significant effects. As expected the curve here was in the opposite direction than for HbO (see Figure 3.9).

The second set of regressors (i.e., the parametric regressors), where mean corrected reaction times of the single trial were expressed by the height of the regressors' amplitude, is further referred to as parametric modulation (PM). Here, there are also significant effects in both chromophores. Interestingly, there were also significant effects before trial onsets (see Figure 3.9).

3.4.3. Discussion

Neuronal correlation of variation in reaction times during a global/local Stroop paradigm could be identified using NIRS. Neural correlates of attentional slips have been reported previously using fMRI [Weissman et al., 2006]. However, compared to fMRI, NIRS has a much lower spatial resolution and can only assess the hemodynamic response on the surface of the brain. Using univariate analysis techniques (FIR) variations in reaction times are correlated with HbO changes in frontal and parietal regions. Results of the FIR suggest higher effects in HbO compared to HbR. Although most researchers showed higher reliability for deoxygenated hemoglobin (e.g. [Kirilina et al., 2012]) because HbO is more polluted by peripheral physiological oscillations. The significances in SLR show physiological meaningful results because in frontal and parietal areas we expect a classical hemodynamic response which peaks between 5-8 seconds. The parametric modulation (PM) showed that the time of peak is related to the reaction time of the subject: for a slower reaction time there is also a later peak of the hemodynamic response.

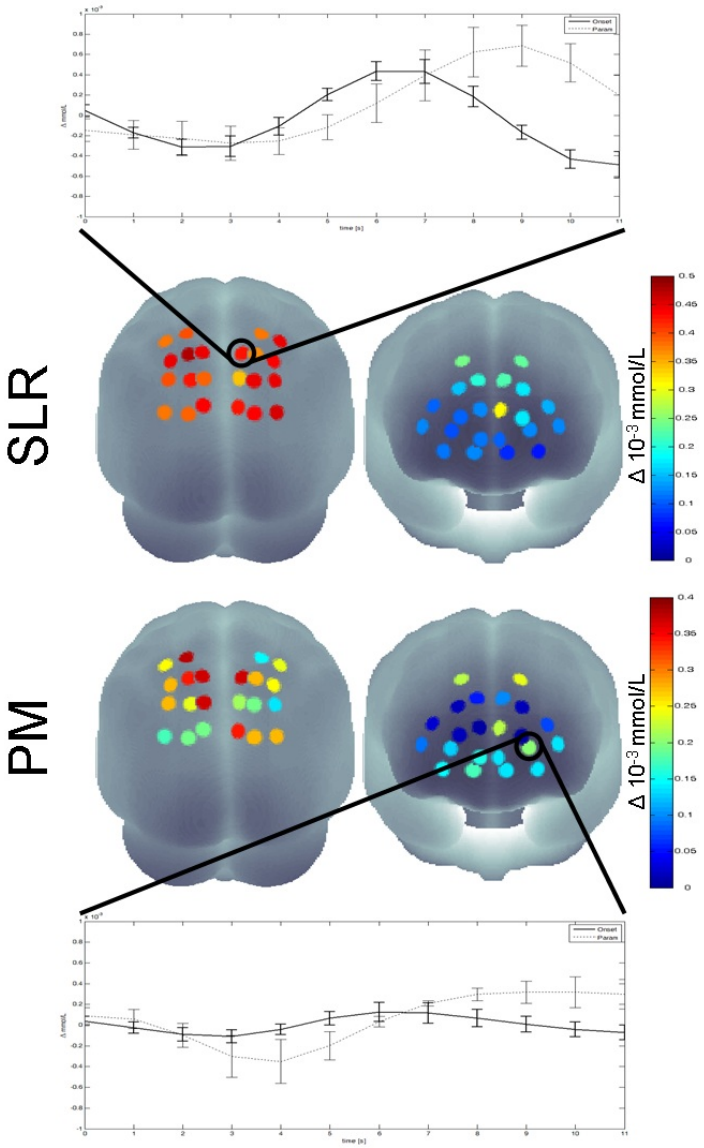

Figure 3.9.: Group average of β-values resulting from Finite Impulse Response (FIR) analysis for stimulus locked response (SLR) and parametric modulation (PM) for the most significant time point on a schematic 3D head surface and time courses of FIR-β for 2 reliable channels.

3.5. Outlook and Discussion

General linear model analysis has shown to gain stable and significant results in fMRI but also in NIRS. While experiments with long inter-trial distances can also be analyzed in different ways, GLM is necessary when analyzing overlapping hemodynamics. This mathematical approach has numerous advantages but suffers from a strong dependency on models and is easy poised by e.g. baseline shifts. With finite impulse response there are even possibilities to analyze data using less a-priori information. It allows to estimate overlapping hemodynamics and the influence of the behavior onto the hemodynamics can be researched. Nevertheless, GLM analysis relies on the assumption that we know the behavior (e.g. peak time, shape) of the hemodynamic response, whereas FIR and other approaches are not dependent on such a model (e.g. [Bießmann et al., 2012]).

4. Analysis with Machine Learning Algorithms

Non-invasive Brain Computer Interfaces (BCI) allow a direct communication between computers and humans without harming the subject. They open a new interface beyond mouse and keyboard to control computers and, thereby, other devices such as robotic arms. Current research focuses on the clinical field. It has been shown that BCI can enable locked-in patients, i.e. patients suffering from whole-body paralysis, to communicate with their environment [Birbaumer et al., 2008]. Further research has been undertaken in neuronal feedback-guided therapies e.g. for stroke patients [Ang et al., 2011]. Possible applications for healthy patients range from assistance in learning to gaming [van Erp et al., 2012]. Current challenges in non-invasive BCI systems are to increase the robustness (e.g. its sensitivity to motion artifacts), the information transfer rate and to enable subjects currently unable to perform BCIs due to several reasons (so called illiterates, [Vidaurre and Blankertz, 2010, Blankertz et al., 2010, Vidaurre et al., 2011]).

Most current BCI systems base on EEG measurements and, thereby, by a single source of the analyzed signal. With a combination of two or more devices *hybrid BCIs* are formed [Müller-Putz et al., 2011]. This approach gains complementary information from a neuronal event, e.g. EEG measures changes in the electric field while NIRS measures the resulting hemodynamics. Combining both types of signals will increase the robustness of a BCI, because they partly have independent information content, and the information transfer rate [Bießmann et al., 2011]. NIRS has the advantages of mobility and a robustness to motion artifacts. Therefore, it is well suited for applications in the growing field of Brain-Computer Interfaces (BCI). A further advantage of NIRS is its capability of artifact-free combination with other devices like EEG, commonly used for non-invasive BCIs.

This chapter introduces the basic concept of BCI and gives a brief overview of the mathematical concepts of the necessary data analysis routines, i.e. machine-learning tools, in Section 4.1. To test the reliability of using NIRS as an optical BCI, we performed a somatomotoric-rhythm based BCI experiment with simultaneous measurements of NIRS and EEG which is presented in Section 4.2. This chapter concludes with an outlook on the suitability of NIRS as an optical BCI in Section 4.3.

4.1. Theory

4.1.1. Brain Computer Interfacing

The idea of Brain Computer-Interfaces (BCI) has been proposed in the early 70's [Vidal, 1973] as a tool to give a subject feedback from analyzing neuronal data. Early approaches used electrophysiological data for *operant conditioning* [Skinner, 1938], where the subject tries to modulate his electrophysiological rhythms in order to control a device. The subject has, for example, to modulate his α-rhythm to gain visual feedback or to control a device. In operant conditioning the learning is done only by the subject. With recent approaches the learning is shifted to the data analysis by means of machine learning algorithms. For BCI, we define classes (also called conditions) and a classifier should detect to which class a current trial belongs. This can for example be the imagination of a movement with the left versus the right hand [Dornhege et al., 2007]. Given some training data, machine learning algorithms can calculate a subject-specific classifiers by maximizing the difference of the classes in the training data set. It therefore calculates in which frequency band and combination of channels left and right hand imagination can most probably be separated and creates a classifier used for the actual feedback. The classifier gives an output to which condition the current trial belongs. This output can be used to control a feedback like a cross on a screen.

Nowadays, BCIs use neuronal signals to control external devices like robotic arms or to give the subject's a feedback on their current neuronal state which is meaningful in therapy of certain diseases (e.g. [Millán et al., 2010, Onose et al., 2012]). Most literature uses EEG signals for non-invasive BCIs. The idea of using NIRS as an optical BCI has been introduced by Coyle in 2004 [Coyle et al., 2004].

Since then a number of groups followed the direction of using NIRS as a basis for optical BCI [Coyle et al., 2007, Sitaram et al., 2007, Wriessnegger et al., 2008, Bauernfeind et al., 2008, Kanoh et al., 2009, Luu and Chau, 2009] by examining the resulting signals for imagery movements.

The continuous prediction of a subjects' performance is another application of machine learning tools. It can be used to analyze the subjects current attentional state in order to prevent eventual mistakes, i.e. when a subject becomes tired. In this kind of application the machine learning algorithm has to solve a regression problem to provide a continuous prediction of the subjects attentional state. Both aims demand real-time analysis of the neuronal data usually done by classification of a current trial. In the next sections I will outline the mathematical concept of Linear Discrimination Analysis and Support Vector Machine used as classifiers for BCIs and Support Vector Regression which is capable to predict continuous changes. Further overview can be found in [Lemm et al., 2011].

4.1.2. Linear Discriminant Analysis

A linear classification technique used to separate two or more classes for a BCI data in real-time is Linear Discriminant Analysis (LDA). Given two conditions (classes) (a and b) in an experiment for which training data D exists, LDA estimates a hyperplane w which separates the space into two subspaces, each belonging to one of the classes. In the 2 dimensional case the hyperplane is a line. Any new data point will lie on one side of this line. The side describes if the new data point is a member of either class a or b. Further assumption made by LDA is that the mean of each class (μ_a and μ_b) might be different but their real (but unknown) covariance matrix Σ is identical, e.g. the distribution of the classes are equal in every direction of the space. The hyperplane w can be computed as:

$$w = \Sigma^{-1}(\mu_a - \mu_b) \tag{4.1}$$

LDA basically describes that new data can be assigned to a class by using a linear combination of the training data. Its main problem is to approximate the unknown covariance matrix and means of the classes from the training data. Given more complex dependencies in the data where the assumption of linearity does not hold anymore, one has to use other machine learning techniques.

4.2. Linear Discriminant Analysis of NIRS Data for Brain-Computer Interfacing

To examine the feasibility of NIRS as a BCI and to study its information content when compared to EEG, we performed an experiment simultaneously measuring EEG and NIRS during an somato-motoric rhythm (SMR) based BCI in comparison to executed movements. Results have already been published [Fazli et al., 2012b]. We exploit the responsiveness of EEG by extracting relevant NIRS features to support and complement high-speed EEG-based BCI and thus forming a hybrid BCI [Pfurtscheller et al., 2010]. We also enhance and robustify overall BCI performance by using information from the hemodynamics, which are not contained within the EEG. Moreover, we evaluate the time delay and spatial information content of the hemodynamic response during a SMR-based BCI paradigm.

Experimental Procedure in Brain Computer Interface Experiment

Tasks: 2 blocks of motor execution (hand gripping, 24 trials/block/condition); 2 blocks of EEG-based feedback (motor imagery, 50 trials/block/condition)

Subjects: 14 healthy, right-handed volunteers (aged 20 to 30)

Instrumentation: NIRS: 8 sources, 16 detectors, 24 measurement channels; EEG: 37 Ag/AgCl electrodes, 2 bipolar EMG, 2 bipolar EOG

See Appendix A.4 for a detailed description of the experimental setup

Textbox: Experimental Procedure in Brain Computer Interface Experiment

4.2.1. Methods

Subjects had to perform 2 separate tasks: executed movements of left and right hand and the imagination of left and right hand movements. One example for this is to imagine lifting a heavy object with the left hand. The data from the executed movement task was used to show the physiological reliability of our approach. Data from motor imagery controlled a real-time feedback, based on the

EEG data. The subject could move a cross to either the left or right side of a screen. NIRS data was simultaneously acquired but analyzed offline.

The online data analysis followed a *co-adaptive calibration* approach as described in [Vidaurre et al., 2011]. Therefore, the experiment is divided into blocks and after each block a new classifier is calculated by integrating the newly measured data. The classifier develops from a subject-independent one to a subject and session specific classifier in an iterative manner. Hereby, not only the algorithm learns about the subject specific data but also the subject learns how to increase the performance.

The user was given instantaneous EEG-based BCI feedback for the two blocks of motor imagery [Vidaurre et al., 2011]. During the first block of 100 trials we used a subject-independent classifier, depending on band power estimates of laplacian filtered and motor-related EEG channels. For the second block subject-dependent spatial and temporal filters were estimated from the data of the first block and combined with some subject-independent features. During the online feedback, features were calculated every 40 ms with a sliding window of 750 ms.

The analysis of NIRS data was performed off-line. A baseline interval was defined from -2 s to 0 s before stimulus onset, and its mean subtracted from each trial. To examine how well the NIRS data classifies the given tasks we analyzed the time courses with the help of a moving window (width 1 s, step size = 500 ms) that we apply from 6 s, prior to stimulus onset and up to 15 s after stimulus onset. We temporally averaged the time courses of HbO and HbR and used them as features for the linear discriminant analysis (LDA). Validation was performed by cross-validation with an 8-fold chronological split. Previous studies have shown that a chronological split maintains non-stationarities of the data and thus represents a relatively conservative measure [Lemm et al., 2011]. Paired t-tests where performed to test whether imagery movements show a significantly earlier peak accuracy as compared to executed movements and in which chromophore accuracy was higher. Trials of the two measured blocks per condition were pooled.

Offline EEG decoding was performed as follows: For both paradigms (real and imagery movements) the two blocks were combined. Subject-dependent band-pass filter coefficients were estimated by means of an established heuristic [Blankertz et al., 2008]. Spatial filters, in form of *Common Spatial Patterns* [Koles and Soong,

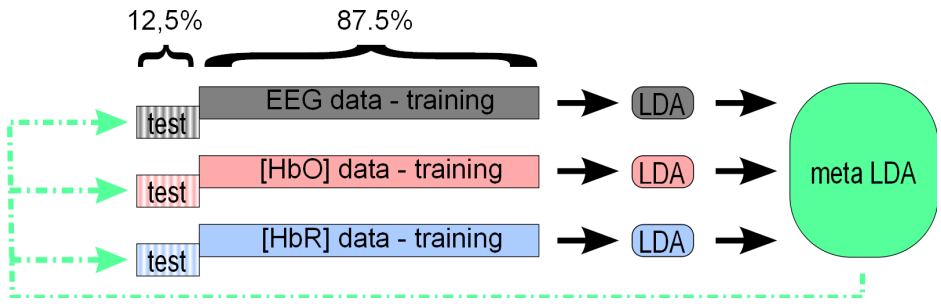

Figure 4.1.: Flowchart of the cross-validation procedure.

1998] filters, and a LDA classifier were estimated. The previously mentioned parameters for subject-dependent temporal filters, spatial filters and linear classifier were estimated solely on the training set of each cross-validation step. The cross-validation followed the same principle as mentioned for the NIRS signals. For the time course of classification accuracy the same moving window was applied as for the NIRS data. Furthermore, to establish a single measure of classification accuracy for each subject and paradigm, the time interval was chosen to be 750-3500 ms after stimulus onset for all subjects.

To examine the possible benefits of combining both signal domains, classification results were calculated for EEG and NIRS separately, but also in combination by estimating a meta-classifier. After estimation of the three individual classifiers (one for the EEG features, one for the HbO features and one for the HbR features) and their performance, we explore a number of possible combinations (such as EEG, HbO or EEG, HbO, HbR etc.). As a meta-classifier we used an LDA, whose weights are re-estimated within each cross-validation step in order to avoid any over-fitting. The general procedure can be seen in Figure 4.1. To investigate the potential improvement of a combination of NIRS and EEG measurements as compared to a BCI, solely dependent on EEG, we show a table comparing EEG classification accuracy and the improvement for EEG in combination with each NIRS chromophore as well as both chromophores. To investigate, whether mostly the same trials are classified wrongly by EEG and by NIRS, we sort the classifier output for all three modalities (EEG, HbO, HbR) of single trials according to their EEG classifier outputs. Hereby we can show the shared and complementary information content of NIRS and EEG.

4.2.2. Results

Our first aim is to show the physiological reliability of NIRS feature classification both in time and location. We performed single trial classification of left and right motor execution (and imagination) with a moving time window after stimulus onset. Classification accuracies for each subject over time can be seen in Figure 4.2 for both chromophores of NIRS (top: HbO, bottom: HbR). The left column shows imagery and the right column executed movements. A classification accuracy of 100% means that the two conditions are perfectly separable. Note that the figure does not reflect the direction of the time course. EEG features are classifiable earlier as compared to HbO and HbR for executed movements ($p < 10^{-4}$ and $p < 10^{-4}$) and for imagined movements ($p < 10^{-5}$ and $p < 10^{-4}$). Furthermore EEG shows a higher accuracy for executed movements versus HbO and HbR ($p < 10^{-3}$ and $p < 0.01$) and also for imagery movements, however here p-values did not reach significance ($p = 0.12$ and $p < 0.05$).

HbR shows a higher average classification accuracy for executed movements than HbO, but we are not able to report a significant relationship here. For imagery movements HbO shows a significantly higher classification accuracy than HbR ($p < 0.001$).

NIRS features are best classifiable at around 3-10 s after stimulus onset. Both NIRS chromophores show in average higher peaks for imagery movements, as compared to executed movements, but we could not find a significant relationship here. To examine the topology of significant NIRS features, Figures 4.3 and 4.4 show $log(p)$ significances of executed and imagery movements, respectively. The time-dependent scalp plots show grand-averages over all subjects, based on the *point-biserial correlation coefficient* $r_{pb} = [(M_1 - M_0)/s_n]\sqrt{(n_1 n_0)/n^2}$, where M_1 and M_0 are the mean values of data points x_i in classes 1 and 0 (i.e., left and right condition), $s_n = \sqrt{(1/n)\sum_{i=1}^{n}(x_i - \bar{x})}$, $n_{1/0}$ the number of examples in classes 1 and 0 and n the total sample size. The point-biserial correlation coefficient is a special case of the Pearson product-moment correlation coefficient and measures the association of a binary random variable and a continuous random variable [Tate, 1954]. The width of the scale on the right indicates the significance level of the individual method. As can be seen for both paradigms EEG as well as NIRS chromophores show highly significant patterns in motor-related cortical areas.

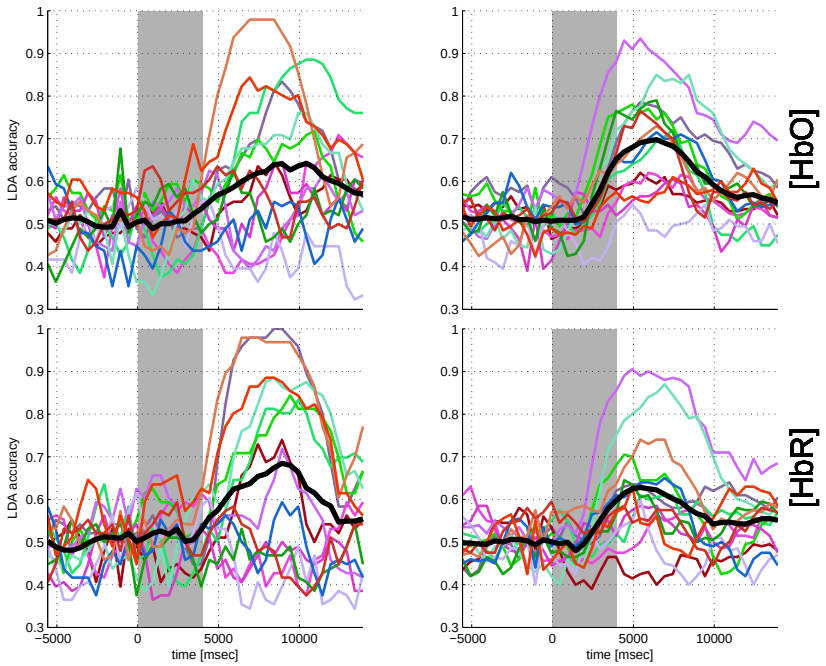

Figure 4.2.: NIRS classification accuracy (LDA) for a 1 s moving time window (top: HbO, bottom: HbR, left: motor execution, right: imagery movements). Colored lines show the accuracy for the single subjects while the black line is the average over subjects. The gray bar indicates the time interval of cue presentation.

Interestingly we find higher significance levels of HbR in both paradigms, as compared to the classification results, where HbO yielded higher accuracies for imagery movements. A second interesting observation is the inverted polarity of HbO for imagery movements. HbO has the expected shape of a hemodynamic response function in the motor execution task, although it ascends in both hemispheres but decrease in the imagery condition. HbR shows the expected time courses for both tasks (imagery/executed) and both conditions (left/right).

While the examination of the NIRS classification itself gave us an idea of the quality and localization of the NIRS features we acquired, our second aim was to actually combine NIRS and EEG features to form a hybrid-BCI. We derived a meta classifier for combining the individual signals. Table 4.1 shows classification accuracies for EEG, HbR and HbO and their combinations for both tasks.

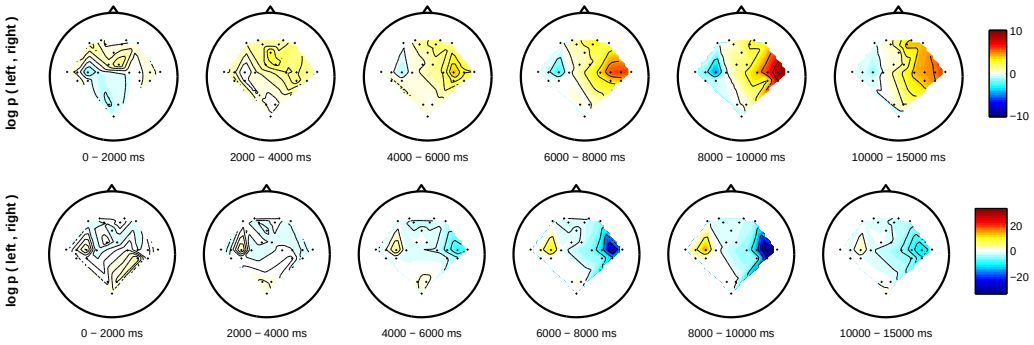

Figure 4.3.: Scalp evolution of grand-average log p values for motor execution in NIRS over all subjects (top: HbO, bottom: HbR).

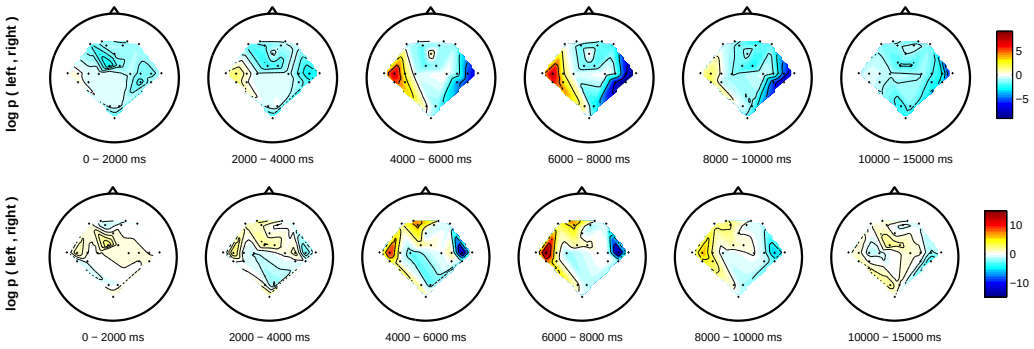

Figure 4.4.: Scalp evolution of grand-average log p values for imagery movements in NIRS over all subjects (top: HbO, bottom: HbR).

While the results in Table 4.1 indicate that combinations of EEG and NIRS are beneficial for average decoding success for both paradigms, only combinations for imagery movements score (highly) significant improvements. By comparing EEG and EEG combined with HbO for imagery movements, we are able to report an average 5% classification accuracy increase over all subjects. This increase is highly significant and the combination scores higher or equal classification rates for 13 out of 14 subjects. Furthermore we would like to note that by our combination two subjects (VPeaa and VPeam) with very bad performance in EEG-BCI are now well classifiable, with rates of 81% and 80.5%, respectively. The two other subjects with very low EEG performance, namely VPeac and VPeal, do not show further improvements.

An impression of shared and complementary information content is given in Figure 4.5. Classifier outputs for single trials sorted according to the outputs for EEG reveal a complementary structure of the information content for both instruments as the positive NIRS outputs do not consistently appear when EEG outputs are high.

subject	executed movements						imagery movements					
	NIRS		EEG	EEG +			NIRS		EEG	EEG +		
	HbO	HbR		HbO	HbR	HbO+R	HbO	HbR		HbO	HbR	HbO+R
VPeaa	84.4	99.0	100.0	99.0	100.0	100.0	77.5	65.0	58.5	78.0	70.0	81.0
VPeab	64.6	75.0	85.4	87.5	89.6	85.4	61.5	50.5	98.0	98.5	98.0	98.5
VPeac	69.8	56.2	99.0	99.0	99.0	96.9	62.0	57.5	65.0	69.5	65.0	72.0
VPead	91.7	79.2	99.0	100.0	96.9	93.8	72.0	58.5	74.5	80.0	75.0	77.5
VPeae	69.8	85.4	97.9	97.9	97.9	94.8	80.0	70.0	82.0	86.5	84.0	85.0
VPeaf	59.4	52.1	94.8	93.8	93.8	82.3	57.0	59.0	58.0	57.5	57.5	57.0
VPeag	58.3	69.8	100.0	100.0	100.0	100.0	91.5	90.0	89.5	97.0	96.0	97.0
VPeah	77.1	90.6	55.2	77.1	90.6	85.4	85.0	85.0	95.5	95.5	96.0	95.0
VPeai	52.1	49.0	76.0	68.8	69.8	63.5	52.5	54.5	55.0	56.5	58.5	48.5
VPeaj	60.4	63.5	90.6	91.7	92.7	77.1	81.5	58.5	89.5	93.0	89.0	92.5
VPeak	59.4	59.4	93.8	94.8	91.7	72.9	70.0	65.5	78.0	82.5	79.0	84.5
VPeal	99.0	99.0	91.7	99.0	99.0	99.0	75.0	74.5	93.5	95.0	96.0	94.0
VPeam	65.6	60.4	89.6	89.6	86.5	75.0	76.0	57.0	58.0	75.5	64.0	80.5
VPean	84.4	87.5	97.9	97.9	97.9	97.9	62.0	64.5	100.0	100.0	100.0	100.0
mean	**71.1**	**73.3**	**90.8**	**92.6**	**93.2**	**87.4**	**71.7**	**65.0**	**78.2**	**83.2****	**80.6***	**83.1***

Table 4.1.: Individual LDA classification accuracies for features of both NIRS chromophores (HbO and HbR) and EEG, and their combinations with a meta-classifier. * marks significant ($p < 0.05$), ** highly significant ($p < 0.01$) improvements for the individual combinations of EEG and NIRS features versus plain EEG decoding.

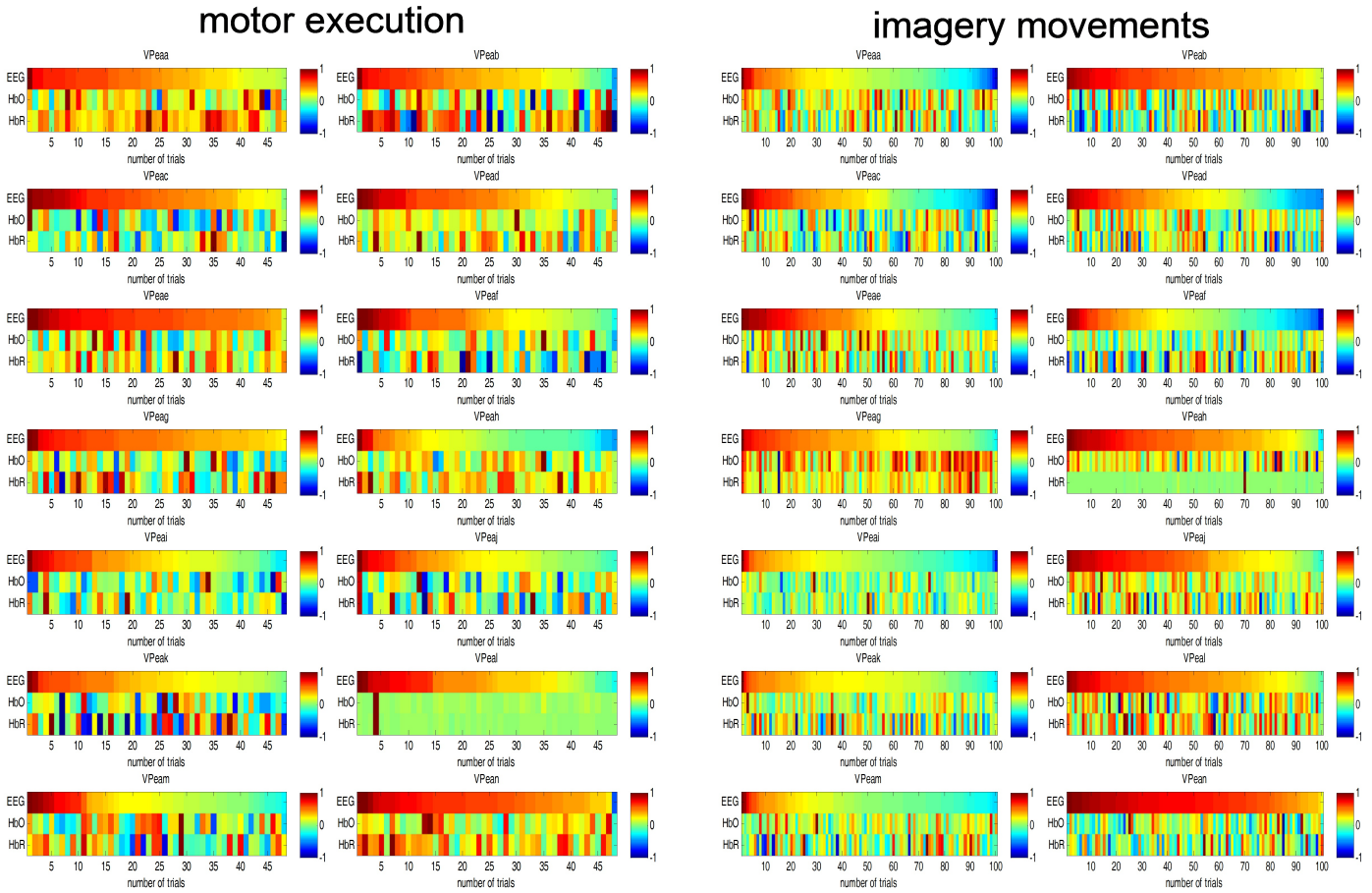

Figure 4.5.: Classifier outputs for execution and imagination of left hand movements for single trials and all three modalities (EEG, HbO, HbR) sorted according the classifier output of EEG. Outputs are normalized to the maximum in each modality and results for all subjects are shown.

4.3. Outlook and Discussion

Recently BCIs that solely rely on NIRS have been realized [Tsubone et al., 2007, Abdelnour and Huppert, 2009]. However, when looking at plain NIRS classification rates it becomes apparent that NIRS cannot be a viable alternative to EEG-based BCIs on its own. This becomes even clearer when taking the long time delay of a hemodynamic response into account. However, in a combination with EEG we find that NIRS is capable of enhancing event related desynchronization (ERD) based BCI performance significantly. Not only does it increase performance for most subjects, but it also allows meaningful classification rates even for those who are not classifiable with solely EEG-based BCI.

In terms of information content, we show that both methods complement each other. If NIRS and EEG had the same or very similar information content, then substantial increases of performance would not be possible by their combination. An increase of combined classification accuracy can be interpreted to be a first hint to their independence. This is further supported by the fact that high classifier outputs of the EEG do not correspond to high classifier outputs of NIRS.

In our study we validated the NIRS data as well as its combinations with EEG in an offline fashion, but our methods could be applied to a real time experiment. In addition, a large number of potential extensions are possible in order to make the combined system faster to set-up. The current (wet) EEG channels could be replaced by dry electrodes [Popescu et al., 2007] and a zero-training classifier [Fazli et al., 2009, Fazli et al., 2011] could be established for NIRS.

While in this contribution we focused on ERD-based BCIs, there is no reason why a NIRS-EEG combination would not also be beneficial for other BCI paradigms, such as event-related potential (ERP)-based BCIs or steady-state visual evoked potential (SSVEP) based BCIs, among others. Future studies will show if this combination will also yield beneficial results there.

The above mentioned studies have shown that machine learning is a technique appropriate for analyzing NIRS data. Furthermore, NIRS data contains complementary information to EEG, which is a good reason for multimodal measurements for BCI applications. This already led to further ways of combining data from NIRS and EEG under BCI conditions [Fazli et al., 2012a].

Furthermore, it was shown that the prediction of reaction times is feasible with

NIRS. Although the results did not reveal significance before the actual trial onset, the approach of analyzing NIRS data with machine learning algorithms looks promising and needs further investigations.

Optical based feedback can be useful for certain therapies where specific areas of the brain should be trained though NIRS has in comparison to EEG a higher spatial resolution. Due to the sluggish hemodynamic response NIRS is not suited for fast feedbacks, but it might provide information about the attentional state of subjects [Fazli et al., 2012a]. Prediction of relative slow changing behavior like vigilance is a good way to think about further research. The general way of analyzing NIRS data has the advantage that it separates given conditions (classes) without any assumption about the hemodynamics and, thereby, is relatively independent of prior knowledge.

5. Analysis of Resting-State Functional Connectivity

In contrast to the analysis of events arising after stimulation as shown in Chapter 3 and 4 (*task-dependent* analysis), *resting-state functional connectivity* (RS-FC) analysis refers to the correlation of time courses during an experiment with a resting condition (subjects are in a *resting-state*). A resting condition is beneficial for subjects which cannot concentrate on attention-demanding tasks. It opens the research to children of any age and for clinical applications in the diagnostics for numerous diseases. The use of correlation analysis on spontaneous low-frequency fluctuations (<0.1 Hz) in fMRI data has been well established for determining functional connectivity in the recent decade. Keeping the disadvantages of fMRI over NIRS in mind, a major benefit of using NIRS for RS-FC would be applications in children (harmless), bed-side monitoring (long-term), but also for patient not suited for fMRI (e.g. with deep-stimulation electrode implants). Only recently, similar methods have been applied to NIRS data [White et al., 2009a, White et al., 2009b, Lu et al., 2010]. In this chapter I report correlation analysis of low-frequency oscillations [Schroeter et al., 2005, Obrig et al., 2000] with the aim of detecting functional connectivity networks. This work establishes the feasibility of NIRS measurements for studying *resting-state networks* (RSN) and, furthermore, the potential to extend this field of research to subject groups ill-suited for fMRI studies, shown here in an example experiment with children at the age of 4-6.

At first I will shortly discuss the biological background and mathematical ideas behind resting-state functional connectivity in Section 5.1. During my work I could show several intrinsic functional networks observed with near-infrared spectroscopy [Mehnert et al., 2009] during the subjects' rest in Section 5.2. Thereafter, an example of analyzing the development of RSNs using partial coherence analy-

sis [Mehnert et al., 2012a] is shown in Section 5.3, I will introduce research on the reliability of resting-state functional connectivity analysis of NIRS data. Therefore, I show results of simultaneous measurements of NIRS and the *golden standard* fMRI (from where this analyzing technique evolved) [Mehnert et al., 2010] in Section 5.4. This is followed by a discussion of further possibilities for RS-FC analysis in the field of near-infrared spectroscopy in the human brain (Section 5.5).

5.1. Theory

Resting-state functional connectivity analysis of brain imaging data has been first reported by Biswal and colleagues in 1995 [Biswal et al., 1995]. Biswal analyzed fMRI data in the somato-motoric areas of subjects during a resting period, i.e. where the subjects did nothing but a visual fixation. By defining a so called *seed voxel* in the motor areas Biswal could show that correlations of this seed voxel in low frequencies (<0.08 Hz) reveal a network, well known from previous task-dependent studies. It consists of voxels in the somatomotoric area of the same and the other hemisphere and also includes other parts of the somatomotoric network like Supplementary Motor Area (SMA). He could also show that this resting-state network has also been involved in a finger tapping task and thereby that resting-state functional connectivity and task-dependent GLM analysis can reveal similar functional networks. This study has open research to a new field not anymore in need of tasks in order to research functional networks. This kind of data analysis is also highly clinical relevant though most patients have show their inability to perform disease-relevant task in a clinical routine [Fox and Greicius, 2010].

A further main milestone was the detection of the so called *default-mode network* (DMN) [Raichle et al., 2001, Greicius et al., 2003, Raichle and Snyder, 2007] which basically deactivates [Shulman et al., 1997] during attentive tasks but activates during resting condition and is associated with *intrinsic thought*, see e.g. [Spreng et al., 2009]. This network has been extensively studied since it is connected to numerous diseases [Buckner et al., 2008]. Nowadays there are at least 5 well-known and reliable RSNs [Shehzad et al., 2009] including visual, somatomotoric, default-mode, attentive (or task-positive as it is anticorrelated to the DMN) and a network in the temporal lobes [Damoiseaux et al., 2006, De Luca et al., 2006, Smith et al., 2009] but not all of them are suitable for NIRS due to the limitation of its

penetration depth. Until now RSN in the motoric [White et al., 2009b, Lu et al., 2010], visual [White et al., 2009b] and temporal [Lu et al., 2010] areas of the brain have been observed with NIRS.

5.1.1. Biological Background

The biological reason for the appearance of spontaneous oscillation in the low frequency range (<0.1 Hz) is widely unknown. There have been numerous reports on resting-state spikes in electrophysiology (see [Buzsaki, 2006] for a review on electrophysological rhythms of the brain and more recently [Deco et al., 2011]) but the link to slow oscillations in hemodynamics is still an open research question. Recent publication have shown a dependency between electrophysiology and hemodynamics [Hoshi et al., 1998, Moosmann et al., 2003, Lu et al., 2007, Mantini et al., 2007, Laufs, 2008] but further research is needed where simultaneous measurements of NIRS and electrophysiology are a promising combination due to their lack of disturbing interaction (no artifacts).

The reliability of RS-FC analysis has been broadly discussed as there are steps in the preprocessing of fMRI data which influence the intensity of correlation (esp. global mean correction, see [Murphy et al., 2009] but also [Fox et al., 2009, Schölvinck et al., 2010]) and numerous extra-cerebral sources of artifacts caused by physiological noise like breathing, heartbeat and blood pressure [Bianciardi et al., 2009, Shmueli et al., 2007, Birn et al., 2008, Nikulin et al., 2012, Birn, 2012]. These are known to influence the hemodynamics (see also Section 2.3).

Furthermore, the term *resting-state* has been criticized though a real rest cannot be obtained in humans, because humans always think about something [Morcom and Fletcher, 2007].

5.1.2. Mathematical Background

Since the early stages of simple correlation analysis enhanced methods for RSN-FC analysis were evolved. It could be shown that data driven methods like Principal Component Analysis (PCA) [Zhong et al., 2009] or more frequently Independent Component Analysis (ICA) (see e.g. [Beckmann et al., 2005]), and numerous similar algorithms enhance the FC-RS analysis. Recent algorithms arise from graph theory [Menon and Uddin, 2008, Wang et al., 2010, Lohmann et al., 2010]. Here,

we focus on correlation and partial coherence analysis. Please see [Margulies et al., 2010] for a current review on post processing tools.

5.1.3. Seed-Voxel Correlation Analysis

The work presented in the following sections is mostly based on seed-voxel correlation analysis which includes two steps: first, one has to define a seed voxel which needs previous knowledge from earlier studies (e.g. a location where a specific task reveals activation). In a second step, one correlates the time course of the seed-voxel (or seed-channel in NIRS) with the remaining resting-state data to retrieve correlation coefficients and, thereby, a dependence of each channel to the seed-channel. This step needs a proper preprocessing of the data, i.e. a denoising of the data to avoid correlations induced by movement of subjects or systemic physiological fluctuations such as the arterial pulsation.

Correlation describes the linear dependence of one time course X_i to another X_j and thereby contains predictive information. For seed-voxel analysis in NIRS we use the Pearson correlation coefficient. Data X is given as $X = C_1, C_2...C_N$ where C are the time courses of the NIRS channels and N is the number of channels. We calculate a Matrix R containing the correlation coefficient between channel i and j as:

$$R_{i,j} = \frac{cov(X_{i,j})}{\sqrt{cov(X_{i,i})cov(X_{j,j})}} \tag{5.1}$$

where *cov* is the covariance. For a seed-channel X_i we gain a vector $r_{i,j} \in R_{i,j}$ containing the correlation coefficient between our seed-channel and the data. In case of comparing X_i with itself the correlation coefficient $r_{i,i}$ equals 1. In case of an inverted time course $X_j = -X_j$ the value will be -1, also called *anticorrelation*. Correlation coefficents do not exceed -1 and 1, where zero means no correlation, and are not arbitrary, i.e. for group comparison (averaging) they have to be normalized by a Fisher's Z-transformation. Though the time courses are normalized by their variance, correlation analysis loses information about the height of amplitude in the single channels.

5.1.4. Partial Coherence Analysis

Analysis of correlation does not look for information of specific frequencies although it is very likely [Sasai et al., 2011] that independent RSNs have specific frequencies in which their spontaneous oscillations occur. By analyzing the coherence between the channels of data, one can extract the frequency specific relations between the brain areas covered by the NIRS setup. In Section 5.3 we introduce results of *partial coherence analysis* to compare connectivity differences between an adult and a children's group which performed the same experimental protocol.

Ordinary coherence K in a multivariate data set X describes the relation between the spectral matrix $S_{i,j}$ of two channels X_i and X_j dependent on the frequency f

$$K\{X_i, X_j, f\} = K_{ij}(f) = \frac{S_{ij}(f)}{\sqrt{S_{ii}(f)S_{jj}(f)}} \tag{5.2}$$

and is thereby very similar to the correlation described in Equation 5.1. In classical analysis of coherence only the absolute value of the coherence, ranging between 0 and 1, is considered. It describes the amount of in-phase components in the two signals compared. Current research has shown that also the imagery part of the coherence contains relevant aspects of brain interaction, at least for EEG data analysis [Nolte et al., 2004] but this idea is not considered in the current work.

Nevertheless, for multivariate data with more than two channels, indirect influence between channels becomes possible (if $X_1 \rightarrow X_2 \rightarrow X_3$, then there is an indirect influence from $X_1 \rightarrow X_3$). To avoid influence of indirect relations *partial coherence* C_{ij} has been introduced [Kamiński, 2007]. Here a linear combination of all other channels but the considered ones is subtracted from the ordinary coherence, leaving only direct influences. We can formulate partial coherence as:

$$C_{ij}(f) = \frac{M_{ij}(f)}{\sqrt{M_{ii}(f)M_{jj}(f)}} \tag{5.3}$$

where M is a decomposition of S from Equation 5.2. More specifically, M_{ij} is a determinant of S with i-th row and j-th column removed. C_{ij} can thereby be expressed by elements of the inverse of $S : d_{ij} = [S^{-1}]_{ij}$.

$$C_{ij}(f) = (-1)^{i+j} \frac{d_{ij}(f)}{\sqrt{d_{ii}(f) d_{jj}(f)}} \tag{5.4}$$

Partial Coherence analysis uses partial coherence to measure the strength of the connection between individual measurement channels.

This section was only a short introduction on measures of connectivity from which only correlation and partial coherence is used in the following sections. It outlines the intense need of work in this field of research.

5.2. Resting-State Networks achieved with Whole-Head Near-Infrared Spectroscopy

Seed-voxel based functional connectivity analysis has recently been applied to NIRS data [Lu et al., 2010, White et al., 2009b] studying the somatomotoric, visual and temporal resting-state networks. One of the limitations of NIRS is the low spatial resolution. To overcome this limitation, dense probe arrays had been used in [White et al., 2009b]. However, full head coverage is desirable in order to avoid that analysis is constrained to specific networks. Therefore I performed a study with nearly whole-head coverage with the aim to show three separate networks simultaneously without changing the setup [Mehnert et al., 2009].

Experimental Procedure in Whole-Head Functional Connectivity
Tasks: 2 blocks of 15 min open-eyes rest
Subjects: 4 healthy, right-handed volunteers
Instrumentation: NIRS: 20 sources, 32 detectors, 80 measurement channels
See Appendix A.5 for a detailed description of the experimental setup

Textbox: Experimental Procedure in Whole-Head Functional Connectivity

5.2.1. Methods

Cortical oxygenation changes of 4 healthy adults (1 female) were measured at rest with eyes-open (2 blocks of 15 min duration) using a near-infrared spectroscopy (NIRS) imaging system (DYNOT 232 by NIRx Medizintechnik GmbH, Berlin, Germany). The sensor array consisted of 52 probes (32 detector fibers, 20 emitter fibers) with an inter-optode distance of approx. 2.5 cm, providing a total of 80 channels. The array covered nearly the whole head, only excluding the occipital areas. The positions of optodes and channels has already been shown earlier in this work in Figure 2.7. For each subject we selected a subset of 5 minutes of data for further analysis, which was not contaminated by movement artifacts. Data were low-pass filtered at 0.01 Hz, and the global mean of all channels was regressed out to reduce the influence of extra-cerebral signal (e.g., oxygenation changes in the skin). Subsequently, correlation analysis was performed for the oxygenated and deoxygenated hemoglobin signal for each channel separately. Three individual regions-of-interest of the temporal, somatomotoric and parietal areas of the cortex were used as the basis for functional connectivity correlation analysis according to the 10-20 EEG system [Koessler et al., 2009].

5.2.2. Results

Our findings indicate the detection of three well-known functional networks: (1) bilateral motor areas, (2) bilateral temporal lobes and (3) a connection between medial-frontal and bilateral parietal cortical areas. Furthermore, we find a high intra-subject consistency for both oxygenated and deoxygenated hemoglobin, as well as high inter-subject reliability. Figure 5.1 shows a z-transformed average of the correlation coefficents for three seed-channels.

5.2.3. Discussion

Since RS-FC analysis has been shown for NIRS, further studies analyzed several RSN [Zhang et al., 2011] and showed reliable results [Zhang et al., 2011] also for different measurement systems [Niu et al., 2011] but also revealed strong dependencies on proper preprocessing [Mesquita et al., 2010], because of the high fraction of extra-cerebral noise in the data. Here we extend recent results to whole-

Figure 5.1.: Three Resting-State Networks measured with whole-head NIRS. Color intensity shows averaged correlation coefficients across subjects for oxygenated (upper row) and deoxygenated (lower row) hemoglobin concentration changes for three separate seed-channels in the left hemisphere: (i) left column: somatomotoric, (ii) middle column: temporal and (iii) right column: parietal area of the cortex.

head measurement and demonstrate the appearance of three distinguished RSN, including a RSN spreading from parietal to frontal areas. NIRS-RS-FC analysis may help to further investigate the developmental effects in children and infants (see Section 5.3), to facilitate bed-side measurements, or to study patients which cannot be examined by fMRI (e.g. deep-brain stimulation).

5.3. Development of Resting-State Functional Connectivity

While RS-FC of neonates has been shown by [White et al., 2012], the age from 4-6 is not well studied with brain imaging methods. In addition to the GLM analysis shown in Section 3.3 we performed a functional connectivity analysis using partial coherence coefficients (P) to study functional patterns age-related with inhibition. This analytical approach uses partial coherence of several frequency bands [Sasai et al., 2011] to investigate relations between brain areas.

Experimental Procedure in Development of Inhibition Experiment

Tasks: 54 trials with 75% go trials and 25% no-go trials (regressed out in this analysis)

Subjects: 51 healthy, right-handed volunteers (21 adults, ranging from 21 to 36; 30 children, ranging from 3-6 years)

Instrumentation: NIRS: 20 sources, 32 detectors, 80 measurement channels

See Appendix A.2 for a detailed description of the experimental setup

Textbox: Experimental Procedure in Development of Inhibition Experiment

5.3.1. Methods

Here we use functional connectivity analysis using partial coherence coefficients (pCC), which performs the correlation analysis in the frequency domain as described in Section 5.1.4. In contrast to conventional correlation analysis, influences of neighboring effects and global physiological artifacts which otherwise are likely to overwhelm any true physiological connectivity effects are thereby attenuated.

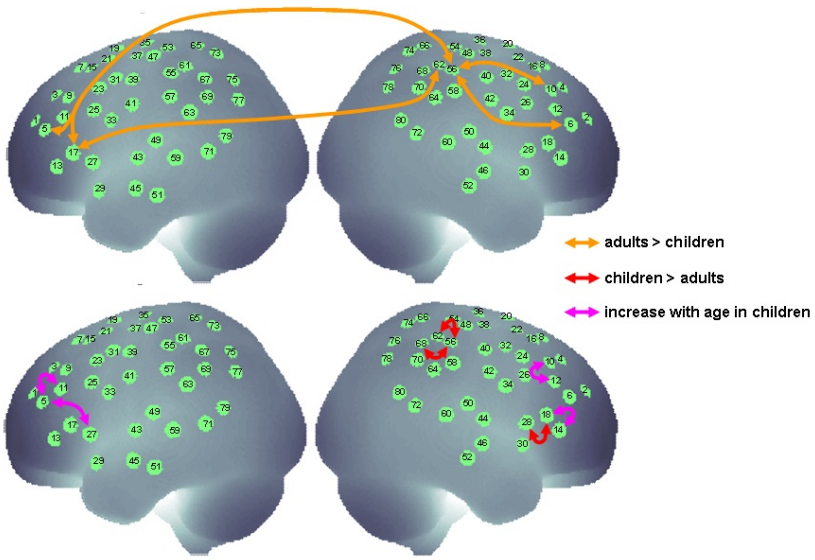

Figure 5.2.: Sketch of developmental effects in network coherence. Top graph: Greater connectivity in adults compared to children are marked in orange. Bottom graph: Greater coherence in children compared to adults, marked in red. Arrows (magenta) represent increasing coherence with age in the children's group.

We suppressed task-related effects from the connectivity analysis by regressing out the task-related HRF model function described above. To evaluate the degree of functional connectivity within the fronto-temporo-parietal network, we generated a coherence matrix with $n^2 = 802^2 = 6400$ entries (where n is the number of channels), each of which contains the bi-regional coherence coefficients for a specific pair of channels, which were then compared between children and adults. For each channel we computed the first eigenvector by singular value decomposition (SVD), yielding the dominant component of the NIRS signal. A Fisher's Z-transformation was applied to produce a normal distribution. The bandwidth of the signals spectra ranged from 0.01 to 0.122 Hz. We combined the frequencies into the bins $<$ 0.03 Hz; $<$ 0.08 Hz, and $<$ 0.12 Hz. See Section A.2 in the appendix for further information of the data processing.

5.3.2. Results

The partial coherence analysis revealed stronger coherence in children compared to adults within the right frontal and the right parietal lobe (see Figure 5.2, top). In contrast, adults showed stronger coherence between bilateral frontal and parietal areas compared to children (see Figure 5.2, bottom).

Likewise, age correlated significantly with pCCs in two channels within the left frontal lobe and two within right frontal areas (Figure 5.2, bottom). However, pCCs in left frontal channels were negatively correlated with age, coherence in the right frontal lobe increased with age (see Figure 5.2, bottom).

5.3.3. Discussion

Using functional connectivity patterns we found stronger partial coherence in short range functional connectivity in the right frontal and right parietal cortex in children compared to adults. We also discovered significantly weaker long range functional connectivity between right frontal and right parietal regions as well as left frontal and right parietal structures. [Fair et al., 2007] and [Supekar et al., 2009] also found weaker fronto-parietal functional connectivity in long range connections in children agree. With regard to their findings of frontal maturation (abundance of short range functional connectivity in childhood, differentiation during adolescence), our results might point towards a developmental pattern in the parietal lobe, which is similar to the frontal pattern: We found inter-parietal (short-range) functional connectivity that was significantly stronger in children compared to adults. Thus, this pattern might be valid not only for the frontal lobe but also for other cortical lobes.

In addition to group differences in partial coherence, we found developmental changes in connectivity between the ages 4 and 6 years. It seemed as if connectivity within the right frontal lobe increased during that time of age, whereas connectivity in the left frontal lobe decreased. These regions of increasing and decreasing partial coherence seem to be similarly located within the frontal lobes to regions of immature brain activation: diffuse, bilateral frontal activation in young children in contrast to a right lateralized fronto-parietal network in the matured brain. This is in accordance with [Zuo et al., 2010] who found weaker homotopic connection with increase of age in higher-order regions of the brain. Furthermore,

changes in connectivity might be rather intrinsically triggered than performance dependent maturation of functional connectivity, as multiple regression showed a significant influence on partial coherence only for age, not for accuracy or reaction time.

We showed that partial coherence analysis of NIRS data can gain new insights into developmental aspects of neuroscience, coinciding with recent findings for fMRI. This supports the reliability of pCC analysis for NIRS and opens numerous fields of research, e.g. for diseases and also for further developmental aspects, without the ability to perform attentive tasks.

5.4. Comparison of Resting-State Functional Connectivity in NIRS and fMRI

While functional connectivity analysis is reliable in fMRI signals, the link of NIRS to fMRI signal during rest remains open. Research is needed to show that the correlations shown in [White et al., 2009a] and [Lu et al., 2010] are truly based on the same signal sources like in RS-FC analysis of fMRI. To determine the source of NIRS signals and their correlation to fMRI during rest and check the reliability of RS-FC analysis in NIRS, we performed a simultaneous measurement with NIRS and the *golden standard* fMRI [Mehnert et al., 2010]. With this measurement it was possible to show the reliability for correlation analysis of slow oscillations in NIRS. Only a small set of optical fibers in a typical grid (2-3 cm inter-optode distance) was used to cover both motor cortices. Such a grid can be extended to whole head coverage (as discussed in Section 5.2), without interfering with the subject's comfort.

5.4.1. Methods

As seed-channel analysis requires prior knowledge of the region of interest, a motor task (see Section A.6) to define the seed-channel was performed by the subjects after the 10 min resting period analyzed here. Maximally activated channels in the motor task were used as seed channels for the correlation analysis. NIRS data was global mean corrected by regressing an z-scored, average time course of all channels from each channel (referred to as *Global Mean Correction*). Seed-channels

Experimental Procedure in Comparison of NIRS and fMRI

Tasks: finger-tapping (25 trials/hand, 10 s tapping, 10 s rest) + open-eyes rest (600 s)

Subjects: 4 healthy, right-handed volunteers

Instrumentation: NIRS: 8 sources, 16 detectors, 26 measurement channels; fMRI: 3 T MAGNETON TIM Trio scanner gradient-echo EPI (TE=30 ms, BW=116 kHz, pixel dimensions 3 mm^2, slice thickness 4 mm / inter-slice gap 1 mm).

See Appendix A.6 for a detailed description of the experimental setup

Textbox: Experimental Procedure in Comparison of NIRS and fMRI

based correlation analysis of task-independent NIRS data provided functional-connectivity maps of the motor network (Figure 5.3, left hand side) and was used as a regressor in statistical analysis of the fMRI data (Figure 5.3, right hand side). Correlations between both methods in the absence of a task and functional structures underlying the NIRS results are drawn.

5.4.2. Results

Functional connectivity analysis shows a compliant pattern in the NIRS data comparing it to the results of [White et al., 2009b] and [Mehnert et al., 2009]. Taking the HbR time course of a right motor seed channel leads to high correlations in bilateral motor cortices (inter-hemispheric correlation) and supplementary motor area (Figure 5.3, left hand side). Furthermore, the same pattern shows up in resting-state fMRI, using the time course of a right motor NIRS channel as a regressor in fMRI data (Figure 5.3 A, right hand side). But the correlation coefficient is smaller than in the finger tapping task shown in Figure A.5 in the appendix.

5.4.3. Discussion

The current study establishes the feasibility of resting-state data analysis for topographical optode arrangements and opens a perspective of whole-head measurements with NIRS. This data set allows the investigation of low frequencies

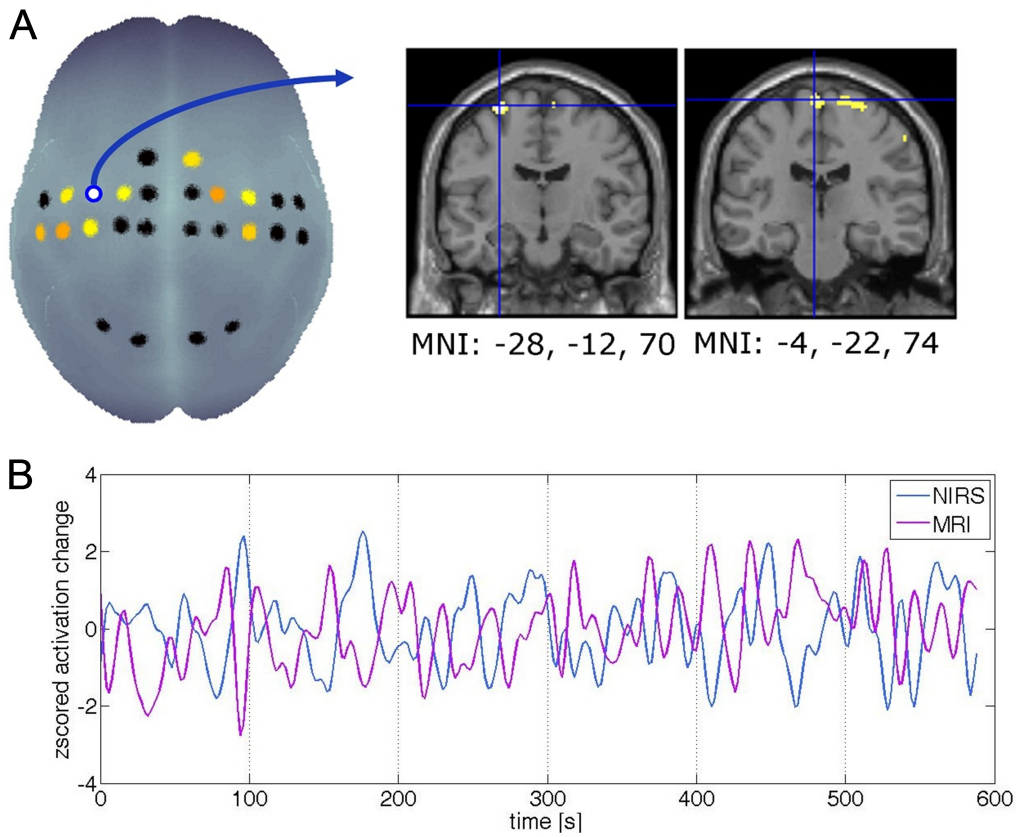

Figure 5.3.: A) Resting-state functional connectivity in simultaneous NIRS and fMRI for a sample subject. Left: Correlation of resting state deoxygenated hemoglobin concentration changes. The peak channel for right finger tapping was used as seed (deep red). Right: Correlation of resting state deoxygenated hemoglobin concentration changes in the right peak channel with fMRI during rest ($p<0.05$, corrected). B) Time courses for the NIRS seed channel (HbR) and the maximal correlated voxel in fMRI. The correlation between the time courses is $r = -0.52$ ($p < 10^{-21}$).

as measured by NIRS and fMRI and attempts to correct the signals for global fluctuations, superficial artifacts and physiological noise. It must be stated that the correlation between fMRI and NIRS in low frequencies of resting state data is lower than for executed movements but it stays significant. Due to its simple applicability, NIRS may develop into a tool for resting-state connectivity studies

in subjects or patients not suited for fMRI experiments. Additionally, one can test advanced analyzing and artifact correction methods like global mean regression or ICA as further questions open to research.

5.5. Outlook and Discussion

We proved reliable resting-state functional connectivity analysis in NIRS data and we gained similar results as in fMRI. Furthermore, the application of RS-FC in a group not suited for fMRI (i.e. children at the age of 3-6) has been shown.With the comparison of simultaneously measured NIRS and fMRI there is a possibility to compare analytical approaches in pre- and post-processing with a *golden standard*. NIRS opens the possibility of artifact-free combinations with electrophysiology and peripheral devices to measure extra-cerebral physiology like heartbeat, breathing and blood pressure to gain deeper insights into remaining extra-cerebral noise, especially relevant for correlation dependent analyzing tools. Even more importantly, insights into the biological origin of slow spontaneous fluctuations of hemodynamic brain imaging data might become feasible.

6. Conclusion and Outlook

In recent years NIRS has gained increased interest of the neuroscience community, but it suffers from analytical and technical limitations, which can only partially be overcome. Especially movement artifacts and extra-cerebral artifacts, caused by the cardio-vascular system, pollute the NIRS data. This work used sophisticated ways to analyze the data. The analysis improved the reliability and overcame relevant limitations of NIRS artifacts. Furthermore, we aimed to show fields where NIRS enhances scientific insights and applications.

6.1. Analyzing Approaches

The straightforward analysis of NIRS data is to calculate the difference between stimulus onset and the peak of the hemodynamic response. But this analysis is not feasible when a task is impossible (e.g. when patient suffering from acute stroke) or the inter-trial intervals are so short that the hemodynamic responses overlap.

The general linear model analysis allows to formulate specific hypotheses about the expected hemodynamic response and, thereby, stabilizes and enhances the statistics. We showed that the GLM analysis allowed to analyze data with overlapping hemodynamics, while it retains similar results as the difference method for non-overlapping hemodynamics. FIR further overcomes GLM's need of a hemodynamic model and allows to analyze the changes in the hemodynamic caused by the subjects attentional state. Artifact reduction is mainly done by proper experimental design, which means to avoid frequency ranges of known extra-cerebral artifacts in the stimulus presentation. Further attenuation of artifacts is done by filtering and interpolation of movement artifact loaded time intervals. General Linear Model analysis is furthermore capable to analyze also overlapping hemodynamics and thus allows faster experiments. This tool seems to become a standard

way of analyzing NIRS data, but it also suffers from its strong dependence on the model of hemodynamic response which has been shown to be highly specific to the subject and brain area of interest. Furthermore, shifts in the baseline, caused e.g. by movement artifacts, are critical for this kind of analysis.

When analyzing NIRS data with machine learning tools there is no need to formulate strong hypotheses or models. The algorithms aim to maximize the difference between conditions (classes) within the data. This is for example done by searching for linear combinations of measurement channels to optimally reduce the artifact related noise. A major advantage of analysis by machine learning routines is their capability of real-time data analysis which makes them well-suited for applications like Brain Computer Interfaces.

Resting-state functional connectivity allows a task-independent way of analysis which is especially for children or patient a fruitful solution. This kind of analysis works in frequency ranges below 0.1 Hz where no extra-cerebral artifact is known. Movement artifact rejection can be done by simply cutting the effected temporal window from the data used for analysis. The analysis of slow frequencies and their correlations between several parts of the brain studies the connectivity of functional networks which might be disturbed in patients. The most critical point, which can be seen here, is the extra-cerebral content of the data. This can produce significant correlations between channels not related on the brains' hemodynamics.

We can conclude:

- General linear model approaches extend NIRS data analysis to overlapping hemodynamics and shorter inter-trial-intervals.
- Machine learning tools open the applications of NIRS for neuronal feedbacks during therapies and in learning environments.
- Functional connectivity analysis achieves neuroscientific insights without the necessity of a task.

An analytical improvement would be to step from correlative analysis to causal ones. There are already numerous tools for EEG and fMRI yielding to analyze the direction of influence from one brain region to the other (e.g. [Stephan et al., 2008, Nolte et al., 2008]) which are also usable for NIRS.

6.2. Application of NIRS

We used NIRS data analysis in studies covering a variety of research fields to exemplary show the further applications of this technique. A major role of NIRS will be in monitoring subjects and patients. One step for a clinical usage of NIRS is that resting-state networks can reliably identified using NIRS. The monitoring of patients becomes thereby independent of a task and ease the application of NIRS in the clinical routine.

To monitor subjects and patients, e.g. during therapies or learning situations, it is furthermore of interest that the shape of the hemodynamic response is significantly different between attentional states. More specific: the peak time increases with lower attention.

Neuronal guided feedbacks might play a crucial role in therapies in the future. Here we conclude that NIRS is suited for brain computer interfaces and can enhance the accuracy of EEG-based feedbacks although the slowness of the hemodynamic response might detain a broader usage.

In the field of clinical application, we showed that the neuronal mechanisms underlying mirror illusion are mediated by the Precuneus and not in the motoric areas which are affected in the case of traumatic limbs after a stroke. A monitoring of mirror therapies with NIRS will therefore enhance the therapies outcome.

In developmental research our results suggest that inhibition in children is mediated by small scale networks while adults use neuronal pathways between parietal and frontal areas. Inhibition plays a major role for children affected by attention deficit hyperactivity disorder. Further research of developmental differences between healthy and affected people is needed to extend our knowledge of this disease.

To summarize:

- NIRS is on the way to become a monitoring tools for attentional states and for therapies.
- NIRS is feasible to provide neuronal feedbacks.
- Research of the development of the brain can benefit using NIRS.

6.3. Technical Improvement

Technical improvement is mostly done by increasing the number of measurement channels and miniaturization of the devices. Whole-head measurements with multiple inter-optode distances can significantly improve the signal quality and spatial resolution [Habermehl et al., 2012,Koch et al., 2010,Zeff et al., 2007], making NIRS a clinical relevant instrument in the near future, while wearable devices will extend the application of NIRS to natural environments and bed-side monitoring of patients [Krüger et al., 2012].

A. Appendix

A.1. Experiment 1: Mirror Illusion

In our study, 20 right-handed healthy subjects (5 female; 21-40 years old; mean age 27.7) without any history of neurological or psychiatric disorders were investigated. Handedness was assessed by the German version of the Edinburgh Handedness Inventory [Oldfield, 1971]. The participants were employees or students of the Charité and participated voluntarily in the experiment with financial compensation. The study was approved by the Ethics Committee of the Charité - Universitätsmedizin Berlin and all subjects gave informed consent prior to the experiment.

In order to allow a systematic and randomized variation of the seen and moved hand without changing other co-factors we implemented the mirror paradigm in accordance with the previous study of Dohle and colleagues [Dohle et al., 2004] by means of a video chain (Figure A.1 A). Subjects either had to hold their hand statically or had to perform a finger-thumb opposition movement sequence under visual control. Subjects could not see their hand directly, it was covered by a black paperboard in front of them. They observed their hand via a video link provided by a webcam (Logitech Webcam Pro 9000). By means of a software package (Logitech Webcam Software v1.1, frame rate: 50 Hz) the image was displayed in real-time on a screen (Acer, 1280x1024 pixel, frame rate: 60 Hz) centered in front of the subjects.

For each hand, a total number of 80 trials under these four conditions were arranged in randomized sequences. Each trial was initiated by an acoustic cue (*start* or *stop*) and lasted 10 s followed by a rest period with an average duration of 15 s (jittered from 10-20 s) in which only a black screen was presented. This rest period served as a baseline for the analysis. Each condition was presented 20 times, yielding in a total experimental time of 38 min per hand. Each

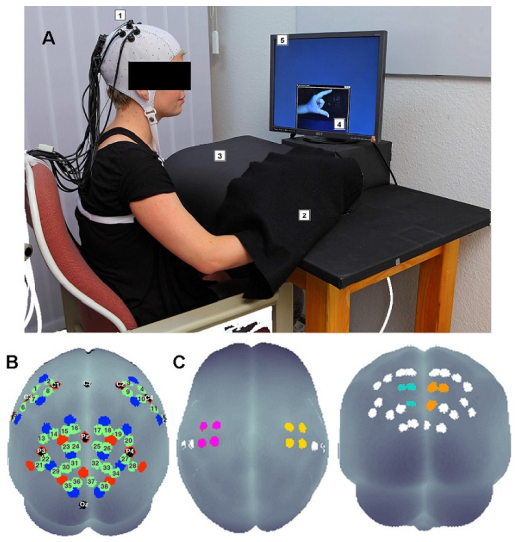

Figure A.1.: A) Photography of the experimental setup: 1) Subject wearing an EEG cap with NIRS detectors and sources; 2) subjects hand inside the black paperboard, covered by a black cloth / drapery being filmed by 3) a web-cam inside the black; 4) visual feedback the subject gets of his hand, in this case MIR and 5) the screen on which the visual feedback is displayed. B) Display of optode positions, measurement channels (numbered in purple), including main EEG positions from the standard 10-20 system (white labels). Note that a number of NIRS sources are at the same location as main standard EEG position and therefore overlap. C) Channels chosen as regions of interest (ROI) for further statistical analysis in the area of somato-motoric areas (left) and the Precuneus (right).

hand was examined separately and the whole experiment lasted approximately an hour and a half. During the whole experiment the subjects were instructed to fixate the screen and to visually focus the hand during the active tasks. The subjects' adherence to the task was ensured by the investigator who was present during the entire experiment. By comparing corresponding channels in both hemispheres, a 2x2x2x2 study design with the four repeated measure factors movement (movement / static), mirror (MIR / NOR), hand (left / right) and hemisphere (ipsilateral / contralateral) was applied.

During the experiment, the blood oxygenation at the surface of the subjects' brain was measured with a NIRS system which offers up to 16 detectors and 16

emitters (NIRScout 16-16, NIRx Medizintechnik GmbH, Berlin, Germany) at two wavelengths (850 and 760 nm). Based on previous publications on the role of the Precuneus during movement mirroring [Dohle et al., 2004, Dohle et al., 2011], we chose fiber optode positions to cover the bilateral occipito-parietal and somato-motoric areas of the subject's head, providing a total of 38 useful channels where source and detector had a distance of 2 to 3 cm. This arrangement is shown in Figure A.1 B. To guarantee optimum safety in optode localization and convenience for the subjects, the emitters and detectors were integrated into a commercially available EEG cap (www.easycap.de) with 128 possible positions. NIRS data were continuously sampled at 3.13 Hz.

NIRS data was corrected for movement artifacts by a semi-automated approach [Koch et al., 2009]. Subsequently, attenuation changes of both wavelengths was transformed to concentration changes of oxy- and deoxygenated hemoglobin (HbO and HbR) using a modified Beer-Lambert law [Cope and Delpy, 1988]. Data were then band-pass filtered between 0.2 and 0.016 Hz to attenuate for heartbeat and breathing-related changes. For the effect estimation of the mirror illusion, we further performed a general linear model (GLM) analysis in the individual subjects. For visual inspection and demonstration we used the approach described in Section 2.6. The two imaging studies by Dohle and colleagues [Dohle et al., 2004, Dohle et al., 2011], which also analyzed the mirror effect, indicated that comparable foci in the region of the Precuneus were activated (Figure A.1 B). Regions of interest (ROI) were defined corresponding to the activation foci of the above-mentioned studies in the Precuneus as the three channels displayed in Figure A.1 B (further referred to as *Precuneus-ROI*) for both hemispheres (i.e. for the left hemisphere (LH) channel numbers: 23, 24 and 31; for right hemisphere (RH): 25, 26 and 32, see also Figure A.1 B). ROIs in somato-motoric area (MA) were defined as the four midsagittal channels on either hemisphere (i.e. for the LH channel numbers: 1, 2, 7 and 8; for RH: 3, 4, 9 and 10, see also Figure A.1 B) as these positions are known to cover somato-motoric areas (see [Koessler et al., 2009]) (further referred to as *MA-ROIs*).

A.2. Experiment 2: Development of Inhibition

Fifty-one healthy subjects completed the study (21 adults, 30 children). Due to either incomplete data sets or motion artifacts (i.e. if more than 30% of the subjects' data contained artifacts, we had to exclude one adult and thirteen children from statistical analysis, resulting in a group of twenty adults (mean age = 26.3±4.3 years, age range 21 - 36 years, 9 males) and 17 children (mean age = 4.7±0.7 years, age range 4-6 years, 11 males). The rejection of the data from about half the group has been reported by other child studies and does not seem to be unusual. Provided a child is willing to perform the task, they are far more prone to causing motion artifacts than are adults. This can not easily be compensated by simply increasing the experiment length because the child's attention level will decrease. It is not possible to counter this effect by reducing the inter-stimulus interval as this would cause subsequent HRF responses to overlap, which would render the analysis impossible.

The NIRS system used in this study (DYNOT 232 by NIRx Medizintechnik GmbH, Berlin, Germany) provides a maximum of 32 sequentially switched illumination positions (emitters) and 32 parallel acquired detector channels (detectors). Fiber optic probes serving as sources and receivers were equidistantly arranged on the head areas of interest (inter-fiber distance of 28±3 mm). Each pair of neighboring emitters and detectors form a measurement channel which probes a subsurface tissue volume centered in between them. The 52 probes (32 detectors + 20 emitters) used result in 80 channels which covered nearly the whole head of the subjects, including the frontal, parietal, and temporal cortices (see Figure 2.7 in the previous chapter). NIRS data was continuously sampled at a rate of 2.44 Hz. To guarantee optimal safety and convenience for the subjects, the fiber-optic bundles (emitter: 1 mm and detector: 3 mm in diameter) were integrated into a commercially available EEG-cap (www.easycap.de). Optode-positions were localized with reference to the EEG 10-20 system with the approach described in Section 2.6.

In a first step we identified channels showing excessive noise level or other interferences caused by imperfect optical coupling of the probes to the head, possible light blockage (e.g. hair) or extra-cranial cross-talk. As a criterion, we excluded all channels whose mean signal was either below or above the known interval of

acceptable detector operation (i.e., between 0.3 V and 4.0 V photovoltaic output). A value below the lower bound signifies low signal-to-noise ratio, while a value exceeding the upper bound risks detector saturation and hence signal distortion.

For the retained channels we converted attenuation changes measured at 760 nm and 830 nm into HbO and HbR concentration changes employing the modified Beer-Lambert law [Cope and Delpy, 1988]. Movement artifacts, a major source of noise in children, were smoothed by a semi-automated procedure which replaces contaminated data segments by linear interpolation [Telkemeyer et al., 2009, Rossi et al., 2011]. This procedure has proven to be capable of attenuating motion artifacts sufficiently so that data sets may be salvaged rather than completely rejected from the analysis. We interpolated an average amount of 17% of the data for the children group and 11% for the adult group. There were no significant differences between groups (comparing groups by a two-sided t-test).

Following data pre-processing a low-pass filter (0.4 Hz, 3^{rd} order Butterworth) was applied to attenuate high frequency noise and the cardiac signal. In addition; a high pass filter of 1/120 Hz was used to reject signal drifts. We removed trials of incorrect responses (i.e., non-responses to go-stimuli and responses to no-go-stimuli) from the data set and excluded these from further statistical analyses. We used the general linear model (e.g. [Nelder and Wedderburn, 1972]) to estimate the statistical fit of a predicted hemodynamic model curve to the measured signals.

We applied GLM analysis separately to both hemoglobin chromophores (HbO and HbR), for each condition, and for each subject. The so obtained statistical fitting parameter β is a measure of the stimulus-related relative change of tissue hemoglobin concentration and the basis of all our further statistical analysis. We generated the hemodynamic model functions, or regressors, by convolving the temporal stimulus profile with a canonical hemodynamic response function (HRF). We used a HRF shape with a peak time of 5 s. Generating the regressors this way accounts for the idiosyncrasy of the sluggish hemodynamic response, which does not reach baseline for some 20 s after stimulus cessation. Results of the GLM analysis are shown in Section 3.3 of this work.

For coherence analysis the full time courses of the oxygenation changes were used after removing the pauses between the two runs. For each subject, we removed these entries in the coherence matrix that did not pass the signal quality criteria

as describe in 2.4 above. We rejected global effects such as caused by cardiac or respiratory pulsation by regressing out the normalized global average of the HbR or HbO signal. For each channel we computed the first eigenvector by singular value decomposition (SCD), yielding the dominant component of the NIRS signal. A Fisher's Z-transformation was applied to produce a normal distribution. The bandwidth of the signals spectra ranged from 0.01 to 0.122 Hz. We combined the frequencies into the bins < 0.03 Hz; < 0.08 Hz, and < 0.12 Hz. Results of the pCC analysis are shown in Section 5.3 of this work.

A.3. Experiment 3: Decoding Vigilance

9 healthy, young subjects (4 female; 22-25 years old) without any history of neurological or psychiatric disorders participated voluntarily in our experiment and gained financial compensation. One subject had to be excluded from all analysis because of technical problems during the measurement. The study was approved by the Ethics Committee of the Universitätsklinikum Leipzig and all subjects gave informed consent prior to the experiment.

The experimental paradigm used to measure changes in vigilance was very similar to the one used in [Weissman et al., 2006]. Subjects were presented with a global-local Stroop paradigm. The visual stimuli consisted of multiple small letters (either S or H) that were arranged so that the shape of either a large S or a large H was formed (see Figure A.2 A). Half of the trials were congruent, i.e. the global and local letters were mapped to the same response, the other half was incongruent. Before the start of each block subjects were instructed to attend either to the local or the global letters. Stimuli were presented for 200 ms. After the visual presentation subjects had to indicate the identity of the attended letter. Inter-trial intervals (ITI) between visual presentations were exponentially distributed with a mean ITI of 7.9 s (ranging from 7 to 12 s). Each subject performed 6 blocks of the experiment during which 60 trials were presented. In the first 3 blocks subjects were instructed to attend to either the global or the local letters. In the subsequent 3 blocks subjects were instructed to attend to the local or global letters, i.e. shift the attention from global to local or vice versa. The subject's single trial performance (i.e., mean corrected reaction time) was used as an indicator for current vigilance for the further analysis.

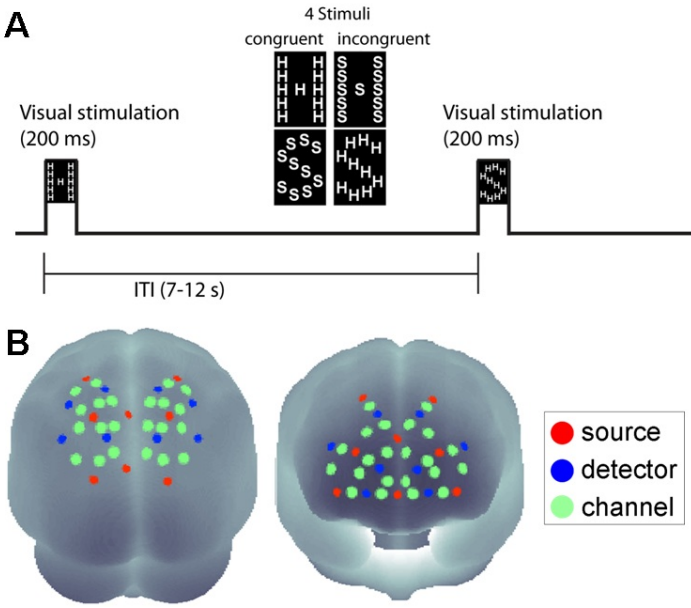

Figure A.2.: A) Sketch of the task including the 4 presented stimuli (middle) and the time line of the task with the length of stimulus presentation and inter-stimulus interval (ITI). B) Display of optode positions (16 sources and 16 detectors) and 44 measurement channels on the surface of a 3D brain (view from the front/back is shown left/right).

During the experiment, the blood oxygenation at the surface of the subjects' brain was measured with a NIRS system which offers up to 16 detectors and 16 emitters (NIRScout 16-16, NIRx Medizintechnik GmbH, Berlin, Germany) at two wavelengths (850 and 760 nm). Based on previous findings, we chose fiber optode positions to cover the frontal and parietal areas of the subject's head, providing a total of 44 useful channels where source and detector were at a distance of between 2 and 3 cm from each other. This arrangement is shown in Figure A.2 B. To guarantee optimal safety in optode localization and convenience for the subjects, the emitters and detectors were integrated into a commercially available EEG cap (www.easycap.de) with 128 possible positions. NIRS data were continuously sampled with 6.25 Hz.

Mapping of statistical results was done using the approach described in Section 2.6 (used for Figure A.2 B and 3.9). Raw data was filtered at 0.25 Hz using a third order digital Butterworth low pass filter. Afterwards attenuation changes

of both wavelengths as measured by the device were transformed to concentration changes of oxy- and deoxygenated hemoglobin (HbO and HbR) using a modified Beer-Lambert law [Delpy et al., 1988]. Data was analyzed using FIR and SVR. Results are shown in Section 3.4.

A.4. Experiment 4: Brain Computer Interface

14 healthy, right-handed volunteers (aged 20 to 30) participated in the study, which lasted approximately 4 hours. The experiment was approved by the local ethics committee (Charité University Medicine, Berlin, Germany), and performed in accordance with the policy of the Declaration of Helsinki. The subjects were seated in a comfortable chair with armrests and were instructed to relax their arms. The experiment consists of 2 blocks of motor execution by means of hand gripping (24 trials per block per condition) and 2 blocks of real-time EEG-based, visual feedback controlled motor imagery (50 trials per block per condition). For all blocks the first 2 s of each trial began with a black fixation cross, that appeared at the center of the screen. A visual cue, in form of an arrow, then appeared pointing to the left or right. For the case of imagery movements, the fixation cross started moving for 4 s, according to the output of an LDA classifier based on the EEG data. The online data analysis followed a *co-adaptive calibration* approach as described in [Vidaurre et al., 2011]. Therefore, the experiment is divided into blocks and after each block a new classifier is calculated by integrating the newly achieved data. The classifier develops from a subject-independent one to a subject and session specific classifier in an iterative manner. Hereby, not only the algorithm learns about the subject specific data but also the subject learns how to increase the performance. For the case of executed movements the fixation cross remained fixed and the subjects were instructed to open and close their hands with an approximate frequency of 1 Hz. After 4s the cross disappeared and the screen remained blank for $10.5 \pm 1.5s$.

During both tasks EEG and NIRS were simultaneously measured. The NIRS-System (NIRScout 8-16, NIRx Medizintechnik GmbH, Germany) was equipped with 24 optical fibers (8 sources with wavelengths of 850 nm and 760 nm, 16 detectors convolving to 24 measurement channels). Frontal, motor and parietal areas of the head were covered as shown in Figure A.3. The sampling frequency

was $f_{\mathrm{NIRS}} = 6.25$ Hz. EEG, electrooculogram (EOG) and electromyogram (EMG) were recorded with a multichannel EEG amplifier (BrainAmp by Brain Products, Munich, Germany) using 37 Ag/AgCl electrodes, 2 bipolar EMG, 2 bipolar EOG (vertical as well as horizontal EOG), sampled at $f_{\mathrm{EEG}} = 5$ kHz and down sampled to 100 Hz by means of a Chebyshev type II digital filter. NIRS probes and EEG electrodes were integrated in a standard EEG cap (extended 10-20 system with a possibility of 256 electrodes) with inter-optode distances between 2-3 cm. The optical probes are constructed to fit into the ring of standard electrodes. This enabled us to situate the NIRS channel positions according to the standard 10-20 system, as shown in Figure A.3.

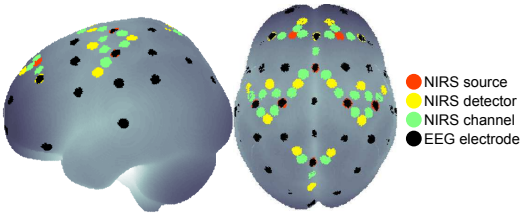

Figure A.3.: Locations of EEG electrodes; sources, detectors and actual measurement channels of NIRS. Note that electrodes and optodes might share a location.

A.5. Experiment 5: Whole-Head Functional Connectivity

Cortical oxygenation changes of 4 healthy adults (1 female) were measured at rest with eyes-open (2 blocks of 15 min duration) using a near-infrared spectroscopy (NIRS) imaging system (DYNOT 232 by NIRx Medizintechnik GmbH, Berlin, Germany). The sensor array consisted of 52 probes (32 detector fibers, 20 emitter fibers) with an inter-optode distance of approx. 2.5 cm, providing a total of 80 channels. The array covered nearly the whole head, only excluding the occipital areas (Figure 2.7). For each subject we selected a subset of 5 minutes of data for further analysis, which was not contaminated by movement artifacts. Data were low-pass filtered at 0.01 Hz, and the global mean of all channels was regressed out to reduce the influence of extra-cerebral signal (e.g., oxygenation changes in the skin). Subsequently, correlation analysis was performed for the oxygenated

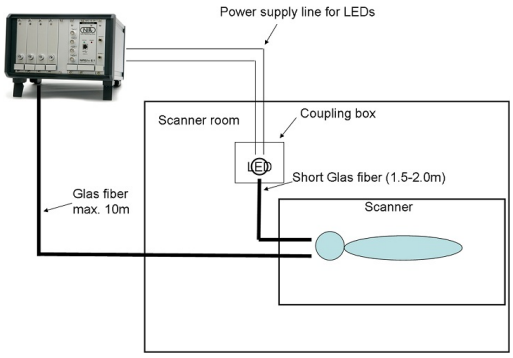

Figure A.4.: Setup for simultaneous measurements of NIRS and fMRI.

and deoxygenated hemoglobin signal for each channel separately. Three individual regions-of-interest of the temporal, somatomotoric and parietal areas of the cortex were used as the basis for functional connectivity correlation analysis according to the 10-20 EEG system [Koessler et al., 2009]. See Section 5.2 for results of this experiment.

A.6. Experiment 6: Comparison of NIRS and fMRI

We tested the reliability of NIRS during task-dependent and task-independent situations in comparison to the *golden standard* fMRI in hemodynamic neuroimaging. The experiment consisted of a block-design finger-tapping task (25 trials, 10 s tapping, 10 s rest, left and right tapping in different sessions) and 10 minutes of open-eyes rest during simultaneous measurement of fMRI and NIRS [Mehnert et al., 2010]. 7 subjects participated in our study but data from 3 subjects had to be discarded from further analysis. In their cases the elaborated experimental procedure led to insufficient fixation of the NIRS optodes on the subjects head. The setup for the simultaneous measurement is shown in Figure A.4. FMRI data acquisition was performed on a whole-body 3 T MAGNETON TIM Trio scanner (Siemens, Erlangen, Germany) equipped with a transmit/receive birdcage head coil. A gradient-echo EPI sequence was used (TE=30 ms, BW=116 kHz, pixel dimensions 3x3 mm^2, slice thickness 4 mm / inter-slice gap 1 mm). 510 volumes were acquired (15 coronal slices through the motor system, TR = 1 s, flip angle 62°).

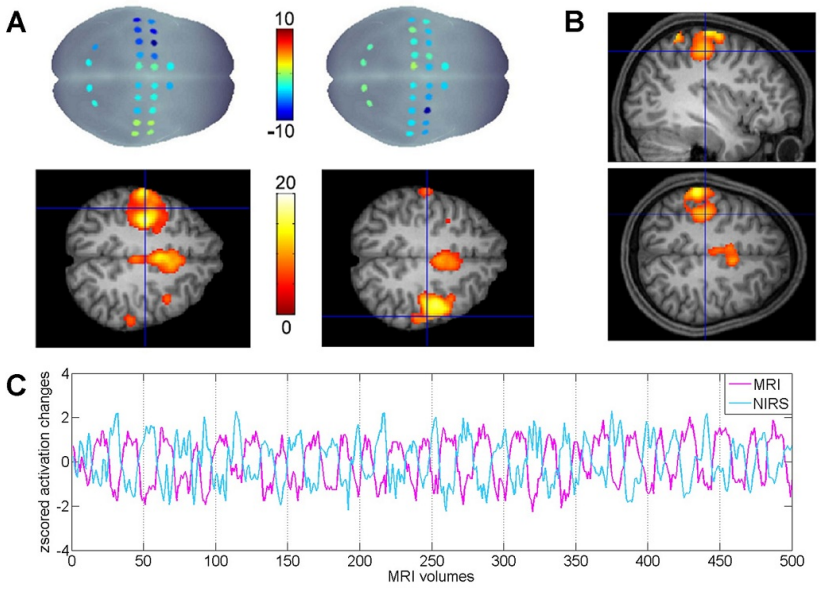

Figure A.5.: Results for simultaneous measurements of NIRS and fMRI in a motor execution task for a sample subject. A) Statistical results for deoxy-hemoglobin in NIRS (top row) and BOLD-fMRI (bottom row) using right and left finger tapping of one subject. Note that high activation is coded in blue (negative t-values) in the NIRS maps. The fMRI results show associated regions of the motor system ($p<0.05$, corrected). B) NIRS peak channel data taken as regressor for fMRI analysis ($p<0.001$, corrected). C) Time courses in the peak voxel / channel for deoxy-hemoglobin in NIRS and fMRI are anti-correlated with a correlation coefficient of -0.8.

NIRS data was recorded with a NIRScout 8-16 (2 wavelengths, 8 sources, 16 detectors, sampling frequency 6.25 Hz), NIRx Medizintechnik GmbH, Berlin, Germany. The optical probes were integrated into a standard EEG cap and were positioned over bilateral motor cortices. Optical data was low-pass filtered (0.2 Hz), and attenuation was transformed to concentration changes of oxy- and deoxygenated hemoglobin using a modified Beer-Lambert law (see Section 2.2.3). A GLM (see Chapter 3) was calculated for fMRI and NIRS data separately. This analysis provided t-values for left and right finger tapping (Figure A.5 A).

The time course for right finger tapping was extracted from the NIRS channel showing maximal activity and used as a regressor for the fMRI data (Figure A.5 B),

Furthermore, the correlation coefficient between this and the time course showing maximal activity in fMRI data (Figure A.5 C) was calculated.

The resting-state experiment consisted of 600 s data acquisition without any task activation (eyes open). For fMRI data acquisition we used a gradient-echo EPI sequence (TE=30 ms, BW=116 kHz, pixel dimensions 3x3 mm^2, slice thickness 4 mm / inter-slice gap 1 mm). 300 volumes (30 axial slices, TR=2 s, flip angle 78°) were acquired. NIRS data was recorded in the same manner as in the motor task and low-pass filtered (0.08 Hz). Attenuation was transformed to concentration changes of oxy- and deoxygenated hemoglobin. Time courses of HbR in channels showing maximal activity in the motor task were used as seed channels for a correlation analysis within the NIRS data. The time courses of the seed channels were also used as a regressor for the simultaneously acquired fMRI data to show the relationship of both devices.

List of Abbreviations

BCI	Brain-Computer Interfacing
BOLD	Blood Oxygenation Level Dependent
DCT	Discrete Cosine Transform
DMN	Default-Mode Network
EEG	Electroencephalography
FC	Functional Connectivity
FIR	Finite Impulse Response
fMRI	Functional Magnetic Resonance Imaging
GLM	General Linear Model
HbO	Oxygenated Hemoglobin
HbR	Deoxygenated Hemoglobin
HRF	Hemodynamic Response Function
ICA	Independent Component Analysis
ITI	Inter-Trial Interval
LDA	Linear Discriminant Analysis
LH	Left Hemisphere
MA	Somato-Motoric Area
ML	Machine Learning
NIRS	Near-Infrared Spectroscopy
PCA	Principal Component Analysis
PCC	Partial Coherence Coefficients

PM	Parametric Modulation
RH	Right Hemisphere
ROI	Region of Interest
RS-FC	Resting-State Functional Connectivity
RSN	Resting-State Networks
SLR	Stimulus Locked Response
SMA	Supplementary Motor Area
SMR	Somato-Motoric Rhythm

List of Equations

List of Figures

List of Tables

Bibliography

[Abdelnour and Huppert, 2009] Abdelnour, A. F. and Huppert, T. (2009). Real-time imaging of human brain function by near-infrared spectroscopy using an adaptive general linear model. *Neuroimage*, 46:133–143.

[Ang et al., 2011] Ang, K. K., Guan, C., Chua, K. S., Ang, B. T., Kuah, C. W., Wang, C., Phua, K. S., Chin, Z. Y., and Zhang, H. (2011). A large clinical study on the ability of stroke patients to use an EEG-based motor imagery brain-computer interface. *Clin EEG Neurosci*, 42(4):253–258.

[Ashburner and Friston, 1999] Ashburner, J. and Friston, K. J. (1999). Nonlinear spatial normalization using basis functions. *Hum Brain Mapp*, 7(4):254–266.

[Bauernfeind et al., 2008] Bauernfeind, G., Leeb, R., Wriessnegger, S. C., and Pfurtscheller, G. (2008). Development, set-up and first results for a one-channel near-infrared spectroscopy system. *Biomedizinische Technik (Biomedical Engineering)*, 53:36–43.

[Beckmann et al., 2005] Beckmann, C. F., DeLuca, M., Devlin, J. T., and Smith, S. M. (2005). Investigations into resting-state connectivity using independent component analysis. *Philosophical Transactions of the Royal Society of London. Series B, Biological Sciences*, 360(1457):1001–1013.

[Beer, 1852] Beer (1852). Bestimmung der absorption des rothen lichts in farbigen flüssigkeiten. *Annalen der Physik*, 162:78–88.

[Bell and Livesey, 1985] Bell, J. and Livesey, P. (1985). Cue significance and response regulation in 3-to 6-year-old children's learning of multiple choice discrimination tasks. *Developmental psychobiology*, 18(3):229–245.

[Bengtsson et al., 2009] Bengtsson, S., Haynes, J., Sakai, K., Buckley, M., and Passingham, R. (2009). The representation of abstract task rules in the human prefrontal cortex. *Cerebral Cortex*, 19(8):1929–1936.

[Bianciardi et al., 2009] Bianciardi, M., Fukunaga, M., van Gelderen, P., Horovitz, S. G., de Zwart, J. A., Shmueli, K., and Duyn, J. H. (2009). Sources of functional magnetic resonance imaging signal fluctuations in the human brain at rest: a 7 t study. *Magnetic Resonance Imaging*, 27(8):1019–1029.

[Bießmann et al., 2012] Bießmann, F., Murayama, Y., Logothetis, N. K., Müller, K.-R., and Meinecke, F. C. (2012). Improved decoding of neural activity from fmri signals using non-separable spatiotemporal deconvolutions. *Neuroimage*, 61(4):1031–1042.

[Bießmann et al., 2011] Bießmann, F., Plis, S., Meinecke, F. C., Eichele, T., and Müller, K.-R. (2011). Analysis of multimodal neuroimaging data. *IEEE Rev Biomed Eng*, 4:26–58.

[Birbaumer et al., 2008] Birbaumer, N., Murguialday, A. R., and Cohen, L. (2008). Brain-computer interface in paralysis. *Curr. Opin. Neurol.*, 21(6):634–638.

[Birn, 2012] Birn, R. M. (2012). The role of physiological noise in resting-state functional connectivity. *Neuroimage*, 62(2):864–870.

[Birn et al., 2008] Birn, R. M., Murphy, K., and Bandettini, P. A. (2008). The effect of respiration variations on independent component analysis results of resting state functional connectivity. *Human Brain Mapping*, 29(7):740–750.

[Biswal et al., 1995] Biswal, B., Zerrin Yetkin, F., Haughton, V., and Hyde, J. (1995). Functional connectivity in the motor cortex of resting human brain using echo-planar mri. *Magnetic resonance in medicine*, 34(4):537–541.

[Blankertz et al., 2010] Blankertz, B., Sannelli, C., Halder, S., Hammer, E. M., Kübler, A., Müller, K.-R., Curio, G., and Dickhaus, T. (2010). Neurophysiological predictor of SMR-based BCI performance. *NeuroImage*, 51(4):1303–1309.

[Blankertz et al., 2008] Blankertz, B., Tomioka, R., Lemm, S., Kawanabe, M., and Müller, K.-R. (2008). Optimizing spatial filters for robust EEG single-trial analysis. *Signal Processing Magazine, IEEE*, 25(1):41–56.

[Bogler et al., 2012] Bogler, C., Mehnert, J., Steinbrink, J., and Haynes, J. (2012). Decoding vigilance with NIRS. *In preparation*.

[Bonferroni, 1935] Bonferroni, C. (1935). *Il calcolo delle assicurazioni su gruppi di teste*. Tipografia del Senato.

[Boynton et al., 1996] Boynton, G. M., Engel, S. A., Glover, G. H., and Heeger, D. J. (1996). Linear systems analysis of functional magnetic resonance imaging in human v1. *Journal of Neuroscience*, 16(13):4207–4221.

[Buckner et al., 2008] Buckner, R. L., Andrews-Hanna, J. R., and Schacter, D. L. (2008). The brain's default network: anatomy, function, and relevance to disease. *Annals of the New York Academy of Sciences*, 1124:1–38.

[Buxton et al., 2004] Buxton, R. B., Uludaĝ, K., Dubowitz, D. J., and Liu, T. T. (2004). Modeling the hemodynamic response to brain activation. *Neuroimage*, 23 Suppl 1:S220–S233.

[Buzsaki, 2006] Buzsaki, G. (2006). *Rhythms of the Brain*. Oxford University Press.

[Cohen-Adad et al., 2007] Cohen-Adad, J., Chapuisat, S., Doyon, J., Rossignol, S., Lina, J., Benali, H., and Lesage, F. (2007). Activation detection in diffuse optical imaging by means of the general linear model. *Medical Image Analysis*, 11(6):616–629.

[Cope and Delpy, 1988] Cope, M. and Delpy, D. T. (1988). System for long-term measurement of cerebral blood and tissue oxygenation on newborn infants by near infra-red transillumination. *Medical and Biological Engineering and Computing*, 26(3):289–294.

[Cope et al., 1988] Cope, M., Delpy, D. T., Reynolds, E. O., Wray, S., Wyatt, J., and van der Zee, P. (1988). Methods of quantitating cerebral near infrared spectroscopy data. *Advances in Experimental Medicine and Biology*, 222:183–189.

[Coyle et al., 2007] Coyle, S., Ward, T., and Markham, C. (2007). Brain-computer interface using a simplified functional near-infrared spectroscopy system. *Journal of Neural Engineering*, 4:219–226.

[Coyle et al., 2004] Coyle, S., Ward, T., Markham, C., and McDarby, G. (2004). On the suitability of near-infrared (NIR) systems for next-generation brain-computer interfaces. *Physiological Measurement*, 25:815–822.

[Cragg and Nation, 2008] Cragg, L. and Nation, K. (2008). Go or no-go? developmental improvements in the efficiency of response inhibition in mid-childhood. *Developmental Science*, 11(6):819–827.

[Damoiseaux et al., 2006] Damoiseaux, J. S., Rombouts, S. A. R. B., Barkhof, F., Scheltens, P., Stam, C. J., Smith, S. M., and Beckmann, C. F. (2006). Consistent resting-state networks across healthy subjects. *Proc Natl Acad Sci U S A*, 103(37):13848–13853.

[De Luca et al., 2006] De Luca, M., Beckmann, C. F., De Stefano, N., Matthews, P. M., and Smith, S. M. (2006). fMRI resting state networks define distinct modes of long-distance interactions in the human brain. *Neuroimage*, 29(4):1359–1367.

[Deco et al., 2011] Deco, G., Buehlmann, A., Masquelier, T., and Hugues, E. (2011). The role of rhythmic neural synchronization in rest and task conditions. *Front Hum Neurosci*, 5(5):1–6.

[Delpy et al., 1988] Delpy, D. T., Cope, M., van der Zee, P., Arridge, S., Wray, S., and Wyatt, J. (1988). Estimation of optical pathlength through tissue from direct time of flight measurement. *Physics in Medicine and Biology*, 33(12):1433–1442.

[Dohle et al., 2004] Dohle, C., Kleiser, R., Seitz, R. J., and Freund, H.-J. (2004). Body scheme gates visual processing. *J Neurophysiol*, 91(5):2376–2379.

[Dohle et al., 2011] Dohle, C., Stephan, K. M., Valvoda, J. T., Hosseiny, O., Tellmann, L., Kuhlen, T., Seitz, R. J., and Freund, H.-J. (2011). Representation of virtual arm movements in precuneus. *Exp Brain Res*, 208(4):543–555.

[Dornhege et al., 2007] Dornhege, G., del R. Millán, J., Hinterberger, T., McFarland, D., and Müller, K.-R., editors (2007). *Toward Brain-Computer Interfacing*. MIT Press, Cambridge, MA.

[Dowsett and Livesey, 2000] Dowsett, S. and Livesey, D. (2000). The development of inhibitory control in preschool children: Effects of 'executive skills' training. *Developmental Psychobiology*, 36(2):161–174.

[Durston et al., 2002] Durston, S., Thomas, K., Worden, M., Yang, Y., and Casey, B. (2002). The effect of preceding context on inhibition: an event-related fmri study. *Neuroimage*, 16(2):449–453.

[Ehlis et al., 2009] Ehlis, A. C., Ringel, T. M., Plichta, M. M., Richter, M. M., Herrmann, M. J., and Fallgatter, A. J. (2009). Cortical correlates of auditory sensory gating: a simultaneous near-infrared spectroscopy event-related potential study. *Neuroscience*, 159:1032–1043.

[Evans et al., 1992] Evans, A., Marrett, S., Neelin, P., Collins, L., Worsley, K., Dai, W., Milot, S., Meyer, E., and Bub, D. (1992). Anatomical mapping of functional activation in stereotactic coordinate space. *Neuroimage*, 1(1):43–53.

[Ezendam et al., 2009] Ezendam, D., Bongers, R. M., and Jannink, M. J. A. (2009). Systematic review of the effectiveness of mirror therapy in upper extremity function. *Disabil Rehabil*, 31(26):2135–2149.

[Fair et al., 2007] Fair, D. A., Dosenbach, N. U. F., Church, J. A., Cohen, A. L., Brahmbhatt, S., Miezin, F. M., Barch, D. M., Raichle, M. E., Petersen, S. E., and Schlaggar, B. L. (2007). Development of distinct control networks through segregation and integration. *Proceedings of the National Academy of Sciences of the United States of America*, 104(33):13507–13512.

[Fazli et al., 2011] Fazli, S., Danóczy, M., Schelldorfer, J., and Müller, K.-R. (2011). $l(1)$-penalized linear mixed-effects models for high dimensional data with application to BCI. *Neuroimage*, 56(4):2100–2108.

[Fazli et al., 2009] Fazli, S., Grozea, C., Danoczy, M., Blankertz, B., Popescu, F., and Müller, K.-R. (2009). Subject independent EEG-based BCI decoding. In Bengio, Y., Schuurmans, D., Lafferty, J., Williams, C. K. I., and Culotta, A., editors, *Advances in Neural Information Processing Systems 22*, pages 513–521. MIT Press.

[Fazli et al., 2012a] Fazli, S., Mehnert, J., Steinbrink, J., and Blankertz, B. (2012a). Using NIRS as a predictor for EEG-based BCI performance. In *34th Annual International IEEE EMBS Conference*.

[Fazli et al., 2012b] Fazli, S., Mehnert, J., Steinbrink, J., Curio, G., Villringer, A., Müller, K. R., and Blankertz, B. (2012b). Enhanced performance by a hybrid NIRS-EEG brain computer interface. *Neuroimage*, 59(1):519–529.

[Fox and Greicius, 2010] Fox, M. D. and Greicius, M. (2010). Clinical applications of resting state functional connectivity. *Front Syst Neurosci*, 4:1–13.

[Fox et al., 2009] Fox, M. D., Zhang, D., Snyder, A. Z., and Raichle, M. E. (2009). The global signal and observed anticorrelated resting state brain networks. *Journal of Neurophysiology*, 101(6):3270–3283.

[Fox and Raichle, 1986] Fox, P. T. and Raichle, M. E. (1986). Focal physiological uncoupling of cerebral blood flow and oxidative metabolism during somatosensory stimulation in human subjects. *Proc. Natl. Acad. Sci. U.S.A.*, 83:1140–1144.

[Friston et al., 2007] Friston, K., Ashburner, J., Kiebel, S., Nichols, T., and Penny, W., editors (2007). *Statistical Parametric Mapping: The Analysis of Functional Brain Images*. Academic Press.

[Friston et al., 1994] Friston, K. J., Holmes, A. P., Worsley, K. J., Poline, J.-P., Frith, C. D., and Frackowiak, R. S. J. (1994). Statistical parametric maps in functional imaging: A general linear approach. *Human Brain Mapping*, 2(4):189–210.

[Friston et al., 2000] Friston, K. J., Mechelli, A., Turner, R., and Price, C. J. (2000). Nonlinear responses in fmri: the balloon model, volterra kernels, and other hemodynamics. *Neuroimage*, 12(4):466–477.

[Friston et al., 1997] Friston, K. J., Price, C. J., Buchel, C., and Frackowiak, R. S. J. (1997). A taxonomy of study design. In Frackowiak, R. S. J., Friston, K. J., Frith, C., Dolan, R., and Mazziotta, J. C., editors, *Human Brain Function*, pages 141–159. Academic Press USA.

[Gregg et al., 2010] Gregg, N. M., White, B. R., Zeff, B. W., Berger, A. J., and Culver, J. P. (2010). Brain specificity of diffuse optical imaging: improvements from superficial signal regression and tomography. *Front Neuroenergetics*, 2(14):1–8.

[Greicius et al., 2003] Greicius, M. D., Krasnow, B., Reiss, A. L., and Menon, V. (2003). Functional connectivity in the resting brain: a network analysis of the default mode hypothesis. *Proc Natl Acad Sci U S A*, 100(1):253–258.

[Grossmann et al., 2010] Grossmann, T., Oberecker, R., Koch, S. P., and Friederici, A. D. (2010). The developmental origins of voice processing in the human brain. *Neuron*, 65:852–858.

[Habermehl et al., 2012] Habermehl, C., Holtze, S., Steinbrink, J., Koch, S. P., Obrig, H., Mehnert, J., and Schmitz, C. H. (2012). Somatosensory activation of two fingers can be discriminated with ultrahigh-density diffuse optical tomography. *Neuroimage*, 59(4):3201–3211.

[Herrmann et al., 2008] Herrmann, M. J., Huter, T., Plichta, M. M., Ehlis, A. C., Alpers, G. W., Muhlberger, A., and Fallgatter, A. J. (2008). Enhancement of activity of the primary visual cortex during processing of emotional stimuli as measured with event-related functional near-infrared spectroscopy and event-related potentials. *Human Brain Mapping*, 29:28–35.

[Hoshi et al., 1998] Hoshi, Y., Kosaka, S., Xie, Y., Kohri, S., and Tamura, M. (1998). Relationship between fluctuations in the cerebral hemoglobin oxygenation state and neuronal activity under resting conditions in man. *Neuroscience Letters*, 245(3):147–150.

[Jasper, 1958] Jasper, H. (1958). The ten-twenty electrode system of the international federation. *Electroencephalography and clinical neurophysiology*, 10(2):371–375.

[Kamiński, 2007] Kamiński, M. (2007). Multichannel data analysis in biomedical research. *Handbook of Brain Connectivity*, pages 327–355.

[Kanoh et al., 2009] Kanoh, S., Murayama, Y. M., Miyamoto, K., Yoshinobu, T., and Kawashima, R. (2009). A NIRS-based brain-computer interface system during motor imagery: system development and online feedback training. *Conf Proc IEEE Eng Med Biol Soc*, 2009:594–597.

[Kirilina et al., 2012] Kirilina, E., Jelzow, A., Heine, A., Niessing, M., Wabnitz, H., Brühl, R., Ittermann, B., Jacobs, A. M., and Tachtsidis, I. (2012). The physiological origin of task-evoked systemic artefacts in functional near infrared spectroscopy. *Neuroimage*, 61(1):70–81.

[Koch et al., 2010] Koch, S. P., Habermehl, C., Mehnert, J., Schmitz, C. H., Holtze, S., Villringer, A., Steinbrink, J., and Obrig, H. (2010). High-resolution optical functional mapping of the human somatosensory cortex. *Frontiers in Neuroenergetics*, 2(12):1–8.

[Koch et al., 2009] Koch, S. P., Werner, P., Steinbrink, J., Fries, P., and Obrig, H. (2009). Stimulus-induced and state-dependent sustained gamma activity is tightly coupled to the hemodynamic response in humans. *Journal of Neuroscience*, 29:13962–13970.

[Kocsis et al., 2006] Kocsis, L., Herman, P., and Eke, A. (2006). The modified Beer-Lambert law revisited. *Physics in Medicine and Biology*, 51:N91–98.

[Koessler et al., 2009] Koessler, L., Maillard, L., Benhadid, A., Vignal, J., Felblinger, J., Vespignani, H., and Braun, M. (2009). Automated cortical projection of eeg sensors: Anatomical correlation via the international 10-10 system. *Neuroimage*, 46(1):64 – 72r.

[Koles and Soong, 1998] Koles, Z. and Soong, A. C. K. (1998). EEG source localization: implementing the spatio-temporal decomposition approach. *Electroencephalogr. Clin Neurophysiol*, 107:343–352.

[Krüger et al., 2012] Krüger, A., Koch, S. P., Mehnert, J., Habermehl, C., Piper, S., Steinbrink, J., Obrig, H., and Schmitz, C. H. (2012). Imaging of motor activity in freely moving subjects using a wearable NIRS imaging system. In *Biomedical Optics*, page BM4A.3. Optical Society of America.

[Laufs, 2008] Laufs, H. (2008). Endogenous brain oscillations and related networks detected by surface eeg-combined fmri. *Human Brain Mapping*, 29(7):762–769.

[Lemm et al., 2011] Lemm, S., Blankertz, B., Dickhaus, T., and Müller, K.-R. (2011). Introduction to machine learning for brain imaging. *Neuroimage*, 56(2):387–399.

[Livesey and Morgan, 1991] Livesey, D. and Morgan, G. (1991). The development of response inhibition in 4-and 5-year-old children. *Australian Journal of Psychology*, 43(3):133–137.

[Logothetis and Wandell, 2004] Logothetis, N. K. and Wandell, B. A. (2004). Interpreting the BOLD signal. *Annual Review of Physiology*, 66:735–769.

[Lohmann et al., 2010] Lohmann, G., Margulies, D. S., Horstmann, A., Pleger, B., Lepsien, J., Goldhahn, D., Schloegl, H., Stumvoll, M., Villringer, A., and Turner, R. (2010). Eigenvector centrality mapping for analyzing connectivity patterns in fmri data of the human brain. *PLoS One*, 5(4):e10232.

[Lu et al., 2010] Lu, C.-M., Zhang, Y.-J., Biswal, B. B., Zang, Y.-F., Peng, D.-L., and Zhu, C.-Z. (2010). Use of fnirs to assess resting state functional connectivity. *Journal of Neuroscience Methods*, 186(2):242–249.

[Lu et al., 2007] Lu, H., Zuo, Y., Gu, H., Waltz, J. A., Zhan, W., Scholl, C. A., Rea, W., Yang, Y., and Stein, E. A. (2007). Synchronized delta oscillations correlate with the resting-state functional mri signal. *Proceedings of the National Academy of Sciences of the United States of America*, 104(46):18265–18269.

[Luu and Chau, 2009] Luu, S. and Chau, T. (2009). Decoding subjective preference from single-trial near-infrared spectroscopy signals. *Journal of Neural Engineering*, 6(016003):1–8.

[Mantini et al., 2007] Mantini, D., Perrucci, M. G., Del Gratta, C., Romani, G. L., and Corbetta, M. (2007). Electrophysiological signatures of resting state networks in the human brain. *Proc. Natl. Acad. Sci. U.S.A.*, 104(32):13170–13175.

[Margulies et al., 2010] Margulies, D. S., Böttger, J., Long, X., Lv, Y., Kelly, C., Schäfer, A., Goldhahn, D., Abbushi, A., Milham, M. P., Lohmann, G., and Villringer, A. (2010). Resting developments: a review of fmri post-processing methodologies for spontaneous brain activity. *MAGMA*, 23(5-6):289–307.

[Matthys et al., 2009] Matthys, K., Smits, M., Van der Geest, J. N., Van der Lugt, A., Seurinck, R., Stam, H. J., and Selles, R. W. (2009). Mirror-induced visual illusion of hand movements: a functional magnetic resonance imaging study. *Arch Phys Med Rehabil*, 90(4):675–681.

[Mehnert et al., 2012a] Mehnert, J., Akhrif, A., Telkemeyer, S., Rossi, S., Schmitz, C. H., Steinbrink, J., Wartenburger, I., Obrig, H., and Neufang, S. (2012a). Developmental changes in brain function and network coherence during response inhibition in the early childhood brain. *Brain & Development*, submitted.

[Mehnert et al., 2012b] Mehnert, J., Brunetti, M., Steinbrink, J., Niedeggen, M., and Dohle, C. (2012b). Effect of the mirror illusion on activation in the precuneus assessed with near-infrared spectroscopy. *In preparation.*

[Mehnert et al., 2009] Mehnert, J., Margulies, D., Schmitz, C., Steinbrink, J., Obrig, H., and Villringer, A. (2009). Resting-state networks revealed with whole-head near-infrared spectroscopy. In *Organization for Human Brain Mapping 2009 Annual Meeting*, volume 47, Supplement 1, page 163.

[Mehnert et al., 2012c] Mehnert, J., Okon-Singer, H., Steinbrink, J., and Villringer, A. (2012c). Modeling event-related blood pressure responses. *In preparation.*

[Mehnert et al., 2010] Mehnert, J., Schmitz, C., Möller, H., Jech, R., Villringer, A., Obrig, H., and Müller, K. (2010). Functional connectivity analysis is reliable in whole-head near-infrared spectroscopy. In *International Society for Magnetic Resonance in Medicine (ISMRM), 18th Scientific Meeting.*

[Menon and Uddin, 2008] Menon, V. and Uddin, L. (2008). Graph-based network analysis of resting-state functional mri. *PLoS Computational Biology*, 3(2):e17.

[Mesquita et al., 2010] Mesquita, R. C., Franceschini, M. A., and Boas, D. A. (2010). Resting state functional connectivity of the whole head with near-infrared spectroscopy. *Biomed Opt Express*, 1(1):324–336.

[Michielsen et al., 2011] Michielsen, M. E., Smits, M., Ribbers, G. M., Stam, H. J., van der Geest, J. N., Bussmann, J. B. J., and Selles, R. W. (2011). The neuronal correlates of mirror therapy: an fmri study on mirror induced visual illusions in patients with stroke. *J Neurol Neurosurg Psychiatry*, 82(4):393–398.

[Millán et al., 2010] Millán, J. d. R., Rupp, R., Müller-Putz, G., Murray-Smith, R., Giugliemma, C., Tangermann, M., Vidaurre, C., Cincotti, F., Kübler, A., Leeb, R., Neuper, C., Müller, K.-R., and Mattia, D. (2010). Combining brain-computer interfaces and assistive technologies: State-of-the-art and challenges. *Frontiers in Neuroprosthetics*, 4(161):1–15.

[Minagawa-Kawai et al., 2011] Minagawa-Kawai, Y., van der Lely, H., Ramus, F., Sato, Y., Mazuka, R., and Dupoux, E. (2011). Optical brain imaging reveals general auditory and language-specific processing in early infant development. *Cerebral Cortex*, 21(2):254–261.

[Moosmann et al., 2003] Moosmann, M., Ritter, P., Krastel, I., Brink, A., Thees, S., Blankenburg, F., Taskin, B., Obrig, H., and Villringer, A. (2003). Correlates of alpha rhythm in functional magnetic resonance imaging and near infrared spectroscopy. *Neuroimage*, 20:145–158.

[Morcom and Fletcher, 2007] Morcom, A. M. and Fletcher, P. C. (2007). Does the brain have a baseline? Why we should be resisting a rest. *Neuroimage*, 37(4):1073–1082.

[Müller-Putz et al., 2011] Müller-Putz, G. R., Breitwieser, C., Cincotti, F., Leeb, R., Schreuder, M., Leotta, F., Tavella, M., Bianchi, L., Kreilinger, A., Ramsay, A., Rohm, M., Sagebaum, M., Tonin, L., Neuper, C., and del. R. Millán, J. (2011). Tools for brain-computer interaction: A general concept for a hybrid BCI (hBCI). *Front Neuroinformatics*, 5(30):1–10.

[Murphy et al., 2009] Murphy, K., Birn, R. M., Handwerker, D. A., Jones, T. B., and Bandettini, P. A. (2009). The impact of global signal regression on resting state correlations: are anti-correlated networks introduced? *Neuroimage*, 44(3):893–905.

[Nelder and Wedderburn, 1972] Nelder, J. and Wedderburn, R. (1972). Generalized linear models. *Journal of the Royal Statistical Society. Series A (General)*, 135(3):370–384.

[Niedermeyer and Da Silva, 2005] Niedermeyer, E. and Da Silva, F. (2005). *Electroencephalography: basic principles, clinical applications, and related fields*. Lippincott Williams & Wilkins.

[Nikulin et al., 2012] Nikulin, V., Fedele, T., Mehnert, J., Noack, C., Lipp, A., Steinbrick, J., and Curio, G. (2012). Monochromatic ultra slow oscillations in the human electroencephalogram . *In preparation*.

[Niu et al., 2011] Niu, H., Khadka, S., Tian, F., Lin, Z.-J., Lu, C., Zhu, C., and Liu, H. (2011). Resting-state functional connectivity assessed with two diffuse optical tomographic systems. *Journal of Biomedical Optics*, 16(4):046006.

[Nolte et al., 2004] Nolte, G., Bai, O., Wheaton, L., Mari, Z., Vorbach, S., and Hallett, M. (2004). Identifying true brain interaction from EEG data using the imaginary part of coherency. *Clin Neurophysiol*, 115(10):2292–2307.

[Nolte et al., 2008] Nolte, G., Ziehe, A., Nikulin, V. V., Schlögl, A., Krämer, N., Brismar, T., and Müller, K.-R. (2008). Robustly estimating the flow direction of information in complex physical systems. *Phys Rev Lett*, 100(23):234101.

[Nyquist, 1928] Nyquist, H. (1928). Certain topics in telegraph transmission theory. *American Institute of Electrical Engineers, Transactions of the*, 47(2):617–644.

[Obrig et al., 2002] Obrig, H., Israel, H., Kohl-Bareis, M., Uludağ, K., Wenzel, R., Müller, B., Arnold, G., and Villringer, A. (2002). Habituation of the visually evoked potential and its vascular response: implications for neurovascular coupling in the healthy adult. *Neuroimage*, 17:1–18.

[Obrig et al., 2000] Obrig, H., Neufang, M., Wenzel, R., Kohl, M., Steinbrink, J., Einhäupl, K., and Villringer, A. (2000). Spontaneous low frequency oscillations of cerebral hemodynamics and metabolism in human adults. *Neuroimage*, 12(6):623–639.

[Obrig and Steinbrink, 2011] Obrig, H. and Steinbrink, J. (2011). Non-invasive optical imaging of stroke. *Philos Transact A Math Phys Eng Sci*, 369(1955):4470–4494.

[Obrig and Villringer, 2003] Obrig, H. and Villringer, A. (2003). Beyond the visible–imaging the human brain with light. *Journal of Cerebral Blood Flow and Metabolism*, 23:1–18.

[Ogawa et al., 1990] Ogawa, S., Lee, T., Nayak, A., and Glynn, P. (1990). Oxygenation-sensitive contrast in magnetic resonance image of rodent brain at high magnetic fields. *Magnetic Resonance in Medicine*, 14(1):68–78.

[Oldfield, 1971] Oldfield, R. C. (1971). The assessment and analysis of handedness: the edinburgh inventory. *Neuropsychologia*, 9(1):97–113.

[Onose et al., 2012] Onose, G., Grozea, C., Anghelescu, A., Daia, C., Sinescu, C., Ciurea, A., Spircu, T., Mirea, A., Andone, I., Spânu, A., Popescu, C., Mihaescu, S., Fazli, S., Danoczy, M., and Popescu, F. (2012). On the feasibility of using motor imagery EEG-based brain–computer interface in chronic tetraplegics for assistive robotic arm control: a clinical test and long-term post-trial follow-up. *Spinal Cord*, 50:599–608.

[Pfurtscheller et al., 2010] Pfurtscheller, G., Allison, B. Z., Brunner, C., Bauernfeind, G., Solis-Escalante, T., Scherer, R., Zander, T. O., Mueller-Putz, G., Neuper, C., and Birbaumer, N. (2010). The Hybrid BCI. *Front Neurosci*, 4(30):1–11.

[Popescu et al., 2007] Popescu, F., Fazli, S., Badower, Y., Blankertz, B., and Müller, K.-R. (2007). Single trial classification of motor imagination using 6 dry EEG electrodes. *PLoS ONE*, 2(7):e637.

[Raichle et al., 2001] Raichle, M. E., MacLeod, A. M., Snyder, A. Z., Powers, W. J., Gusnard, D. A., and Shulman, G. L. (2001). A default mode of brain function. *Proc. Natl. Acad. Sci. U.S.A.*, 98(2):676–682.

[Raichle and Snyder, 2007] Raichle, M. E. and Snyder, A. Z. (2007). A default mode of brain function: a brief history of an evolving idea. *Neuroimage*, 37(4):1083–1090.

[Ramachandran et al., 1995] Ramachandran, V. S., Rogers-Ramachandran, D., and Cobb, S. (1995). Touching the phantom limb. *Nature*, 377(6549):489–490.

[Rossi et al., 2011] Rossi, S., Jürgenson, I. B., Hanulíková, A., Telkemeyer, S., Wartenburger, I., and Obrig, H. (2011). Implicit processing of phonotactic cues: evidence from electrophysiological and vascular responses. *Journal of Cognitive Neuroscience*, 23(7):1752–1764.

[Rothgangel et al., 2011] Rothgangel, A. S., Braun, S. M., Beurskens, A. J., Seitz, R. J., and Wade, D. T. (2011). The clinical aspects of mirror therapy in rehabilitation: a systematic review of the literature. *Int J Rehabil Res*, 34(1):1–13.

[Roy and Sherrington, 1890] Roy, C. S. and Sherrington, C. S. (1890). On the regulation of the blood-supply of the brain. *The Journal of Physiology*, 11(1-2):85–158.

[Rubia et al., 2007] Rubia, K., Smith, A., Taylor, E., and Brammer, M. (2007). Linear age-correlated functional development of right inferior fronto-striato-cerebellar networks during response inhibition and anterior cingulate during error-related processes. *Human brain mapping*, 28(11):1163–1177.

[Rueda et al., 2005] Rueda, M., Posner, M., and Rothbart, M. (2005). The development of executive attention: Contributions to the emergence of self-regulation. *Developmental neuropsychology*, 28(2):573–594.

[Sasai et al., 2011] Sasai, S., Homae, F., Watanabe, H., and Taga, G. (2011). Frequency-specific functional connectivity in the brain during resting state revealed by nirs. *Neuroimage*, 56(1):252–257.

[Schölvinck et al., 2010] Schölvinck, M. L., Maier, A., Ye, F. Q., Duyn, J. H., and Leopold, D. A. (2010). Neural basis of global resting-state fmri activity. *Proceedings of the National Academy of Sciences of the United States of America*, 107(22):10238–10243.

[Schroeter et al., 2005] Schroeter, M. L., Bücheler, M. M., Preul, C., Scheid, R., Schmiedel, O., Guthke, T., and von Cramon, D. Y. (2005). Spontaneous slow hemodynamic oscillations are impaired in cerebral microangiopathy. *Journal of Cerebral Blood Flow and Metabolism*, 25(12):1675–1684.

[Shehzad et al., 2009] Shehzad, Z., Kelly, A. M. C., Reiss, P. T., Gee, D. G., Gotimer, K., Uddin, L. Q., Lee, S. H., Margulies, D. S., Roy, A. K., Biswal, B. B., Petkova, E., Castellanos, F. X., and Milham, M. P. (2009). The resting brain: Unconstrained yet reliable. *Cerebral Cortex*, 19(10):2209–2229.

[Shmueli et al., 2007] Shmueli, K., van Gelderen, P., de Zwart, J. A., Horovitz, S. G., Fukunaga, M., Jansma, J. M., and Duyn, J. H. (2007). Low-frequency fluctuations in the cardiac rate as a source of variance in the resting-state fmri bold signal. *Neuroimage*, 38(2):306–320.

[Shulman et al., 1997] Shulman, G., Fiez, J., Corbetta, M., Buckner, R., Miezin, F., Raichle, M., and Petersen, S. (1997). Common blood flow changes across visual tasks: Ii. decreases in cerebral cortex. *Journal of Cognitive Neuroscience*, 9(5):648–663.

[Singh et al., 2005] Singh, A. K., Okamoto, M., Dan, H., Jurcak, V., and Dan, I. (2005). Spatial registration of multichannel multi-subject fnirs data to mni space without mri. *Neuroimage*, 27(4):842–851.

[Sitaram et al., 2007] Sitaram, R., Zhang, H., Guan, C., Thulasidas, M., Hoshi, Y., Ishikawa, A., Shimizu, K., and Birbaumer, N. (2007). Temporal classification of multichannel near-infrared spectroscopy signals of motor imagery for developing a brain-computer interface. *Neuroimage*, 34:1416–1427.

[Skinner, 1938] Skinner, B. (1938). *The behavior of organisms: an experimental analysis*. Century psychology series. Appleton-Century Company.

[Smith et al., 2009] Smith, S. M., Fox, P. T., Miller, K. L., Glahn, D. C., Fox, P. M., Mackay, C. E., Filippini, N., Watkins, K. E., Toro, R., Laird, A. R., and Beckmann, C. F. (2009). Correspondence of the brain's functional architecture during activation and rest. *Proc Natl Acad Sci U S A*, 106(31):13040–13045.

[Spreng et al., 2009] Spreng, R. N., Mar, R. A., and Kim, A. S. N. (2009). The common neural basis of autobiographical memory, prospection, navigation, theory of mind, and the default mode: a quantitative meta-analysis. *Journal of Cognitive Neuroscience*, 21(3):489–510.

[Stephan et al., 2008] Stephan, K. E., Kasper, L., Harrison, L. M., Daunizeau, J., den Ouden, H. E. M., Breakspear, M., and Friston, K. J. (2008). Nonlinear dynamic causal models for fmri. *Neuroimage*, 42(2):649–662.

[Supekar et al., 2009] Supekar, K., Musen, M., and Menon, V. (2009). Development of large-scale functional brain networks in children. *PLoS Biology*, 7(7):e1000157.

[Talairach and Tournoux, 1988] Talairach, J. and Tournoux, P. (1988). *Co-planar stereotaxic atlas of the human brain: 3-dimensional proportional system: an approach to cerebral imaging*. Thieme.

[Tate, 1954] Tate, R. (1954). Correlation between a discrete and a continuous variable. point-biserial correlation. *The Annals of Mathematical Statistics*, 25(3):603–607.

[Telkemeyer et al., 2009] Telkemeyer, S., Rossi, S., Koch, S. P., Nierhaus, T., Steinbrink, J., Poeppel, D., Obrig, H., and Wartenburger, I. (2009). Sensitivity of newborn auditory cortex to the temporal structure of sounds. *Journal of Neuroscience*, 29:14726–14733.

[Telkemeyer et al., 2011] Telkemeyer, S., Rossi, S., Nierhaus, T., Steinbrink, J., Obrig, H., and Wartenburger, I. (2011). Acoustic processing of temporally modulated sounds in infants: evidence from a combined near-infrared spectroscopy and eeg study. *Frontiers in Psychology*, 2:1–14.

[Thieme et al., 2012] Thieme, H., Mehrholz, J., Pohl, M., Behrens, J., and Dohle, C. (2012). Mirror therapy for improving motor function after stroke. *Cochrane Database Syst Rev*, 3:1–68.

[Tsubone et al., 2007] Tsubone, T., Muroga, T., and Wada, Y. (2007). Application to robot control using brain function measurement by near-infrared spectroscopy. *Conf Proc IEEE Eng Med Biol Soc*, 2007:5342–5345.

[Uludağ et al., 2004] Uludağ, K., Steinbrink, J., Villringer, A., and Obrig, H. (2004). Separability and cross talk: optimizing dual wavelength combinations for near-infrared spectroscopy of the adult head. *Neuroimage*, 22(2):583–589.

[van Erp et al., 2012] van Erp, J., Lotte, F., and Tangermann, M. (2012). Brain-computer interfaces for non-medical applications: How to move forward. *Computer*, 4:26–34.

[Vidal, 1973] Vidal, J. J. (1973). Toward direct brain-computer communication. *Annual Review of Biophysics and Bioengineering*, 2:157–180.

[Vidaurre and Blankertz, 2010] Vidaurre, C. and Blankertz, B. (2010). Towards a cure for BCI illiteracy. *Brain topography*, 23:194–198.

[Vidaurre et al., 2011] Vidaurre, C., Sannelli, C., Müller, K.-R., and Blankertz, B. (2011). Machine-learning-based coadaptive calibration for brain-computer interfaces. *Neural Computation*, 23(3):791–816.

[Villringer et al., 1993] Villringer, A., Planck, J., Hock, C., Schleinkofer, L., and Dirnagl, U. (1993). Near infrared spectroscopy (nirs): a new tool to study hemodynamic changes during activation of brain function in human adults. *Neuroscience letters*, 154(1):101–104.

[Wang et al., 2010] Wang, J., Zuo, X., and He, Y. (2010). Graph-based network analysis of resting-state functional MRI. *Frontiers in systems neuroscience*, 4(16):1–14.

[Wartenburger et al., 2007] Wartenburger, I., Steinbrink, J., Telkemeyer, S., Friedrich, M., Friederici, A. D., and Obrig, H. (2007). The processing of prosody: Evidence of interhemispheric specialization at the age of four. *Neuroimage*, 34:416–425.

[Weissman et al., 2006] Weissman, D. H., Roberts, K. C., Visscher, K. M., and Woldorff, M. G. (2006). The neural bases of momentary lapses in attention. *Nature Neuroscience*, 9(7):971–978.

[White et al., 2012] White, B. R., Liao, S. M., Ferradal, S. L., Inder, T. E., and Culver, J. P. (2012). Bedside optical imaging of occipital resting-state functional connectivity in neonates. *Neuroimage*, 59(3):2529–2538.

[White et al., 2009a] White, B. R., Snyder, A. Z., Cohen, A. L., Petersen, S. E., Raichle, M. E., Schlaggar, B. L., and Culver, J. P. (2009a). Mapping the human brain at rest with diffuse optical tomography. *Conf Proc IEEE Eng Med Biol Soc*, 2009:4070–4072.

[White et al., 2009b] White, B. R., Snyder, A. Z., Cohen, A. L., Petersen, S. E., Raichle, M. E., Schlaggar, B. L., and Culver, J. P. (2009b). Resting-state functional connectivity in the human brain revealed with diffuse optical tomography. *Neuroimage*, 47(1):148–156.

[Wriessnegger et al., 2008] Wriessnegger, S. C., Kurzmann, J., and Neuper, C. (2008). Spatio-temporal differences in brain oxygenation between movement execution and imagery: a multichannel near-infrared spectroscopy study. *International Journal of Psychophysiology*, 67:54–63.

[Ye et al., 2009] Ye, J. C., Tak, S., Jang, K. E., Jung, J., and Jang, J. (2009). Nirs-spm: statistical parametric mapping for near-infrared spectroscopy. *Neuroimage*, 44(2):428–447.

[Zeff et al., 2007] Zeff, B. W., White, B. R., Dehghani, H., Schlaggar, B. L., and Culver, J. P. (2007). Retinotopic mapping of adult human visual cortex with high-density diffuse optical tomography. *Proc. Natl. Acad. Sci. U.S.A.*, 104(29):12169–12174.

[Zelazo et al., 1995] Zelazo, P., Reznick, J., and Piñon, D. (1995). Response control and the execution of verbal rules. *Developmental Psychology*, 31(3):508–517.

[Zhang et al., 2011] Zhang, H., Zhang, Y.-J., Duan, L., Ma, S.-Y., Lu, C.-M., and Zhu, C.-Z. (2011). Is resting-state functional connectivity revealed by functional near-infrared spectroscopy test-retest reliable? *Journal of Biomedical Optics*, 16(6):067008.

[Zhong et al., 2009] Zhong, Y., Wang, H., Lu, G., Zhang, Z., Jiao, Q., and Liu, Y. (2009). Detecting functional connectivity in fmri using pca and regression analysis. *Brain Topography*, 22(2):134–144.

[Zuo et al., 2010] Zuo, X. N., Kelly, C., Di Martino, A., Mennes, M., Margulies, D. S., Bangaru, S., Grzadzinski, R., Evans, A. C., Zang, Y. F., Castellanos, F. X., and Milham, M. P. (2010). Growing together and growing apart: regional and sex differences in the lifespan developmental trajectories of functional homotopy. *J. Neurosci.*, 30(45):15034–15043.